1993

# Fitness for purpose assessment of weld discontinuities in high strength low alloy weldments

George R. Kober
*Lehigh University*

AUTHOR:

Kober, George R.

TITLE:

# Fitness For Purpose Assesment of Weld Discontinuities in High Strength Low Alloy Weldments

DATE: May 30, 1993

# Fitness for Purpose Assesment Of Weld Discontinuities In High Strength Low Alloy Weldments

by

George R. Kober

A Thesis

Presented to the Graduate and Research Committee

of Lehigh University

in Candidacy for the Degree of

Master of Science

in

Civil Engineering

Lehigh University

21 May 1993

## Certificate of Approval

This thesis is accepted and approved in partial fulfillment of the requirements for the Degree of Master of Science in Civil Engineering.

May 19, 1993
Date

Dr. Ben T. Yen
Thesis Advisor

Irwin J. Kugelman
Department Chairperson

## Acknowledgements

The work being reported was accomplished with the support of the U.S. Navy Manufacturing Technology Program under Cooperative Agreement N00014-91-CA-0001. The studies reported here were conducted at the Engineering Research Center for Advanced Technology for Large Structural Systems (ATLSS) at Lehigh University. Dr. John W. Fisher is the director of ATLSS. Dr. Irwin J. Kugelman is chairperson of the Department of Civil Engineering.

Special thanks are due to Dr. Ben T. Yen and Dr. Robert J. Dexter. Dr. Yen is the supervisor of the thesis. Dr. Dexter guided the research and was principle investigator for the Fleet of The Future Program phase 1.3a. Both have offered guidance and suggestions throughout the course of this study.

In addition, many others at Lehigh have contributed to this research. Mark Kaczinski, Ed Tomlinson, and Russel Longenbach setup and maintained the computer controlled testing and data acquisition. Bob Dales, Todd Anthony, Mike Beaky, Steve Leonard, Larry Heffner, and John Hoffner provided technical support in the ATLSS laboratory. Charles Hittinger, Tom Kemmerer, Ray Kromer, Eugene Matlock, John Pinter, and Al Yerger provided technical support in the Fritz laboratory. Photographs were taken and prepared by Richard Sopko. The computer program used in the study was written by Guy Decorges.

Fellow students John Tarquinio, Mike Gentilcore and Alian Nussbaumer all played key roles in the completion of the tests. The author would like to especially thank John Tarquinio for putting up with the trips to New Hampshire, Jenny Deifer for the bowls of popcorn. Also, special thanks are due for Carla Moran, whose presence and constant support in the author's life has made all of this bearable.

# Table of Contents

# List of Tables

# List of Figures

## Abstract

Criteria for acceptance of discontinuities base on fitness-for-purpose are developed for welds in HSLA-80 (A710) steel. Fatigue tests on 66 members with transverse groove welds as well as longitudinal fillet welds are described. The discontinuity at the origin of each fatigue crack is characterized. These welds contained a variety of discontinuities and covered the full range of quality. Fatigue crack growth calculations can accurately predict the observed cycles to failure for the larger internal discontinuities in transverse groove welds, whereas the longitudinal fillet weld fatigue lives were much greater than predicted. Data are then used in a fitness-for -purpose assessment.

# 1. Introduction

## 1.1 Project Overview and Problems with Current Assessment of Discontinuities

Currently, most ships (military and commercial) are not directly designed for fatigue crack control, although there is some underlying consideration of fatigue strength in setting the allowable stress [1,2]. The Navy is considering advanced double-hull surface combatant ships. The multiple load paths (redundancy) and improved stiffness in a double hull design offer potentially improved strength and stability to conventional stiffened panel hull construction [3]. If the allowable primary stress is increased to take advantage of high-strength steel, the magnitude of the stress ranges are also increased. However, results from large-scale fatigue test indicate that the fatigue strength of welded details in air is independent of the type and strength of the steel [4 - 7]. Therefore if the allowable stress range is increased, specific details are more likely to exhibit fatigue problems.

Investigations were made into the fatigue life of common ship details as part of the U.S. Navy - Lehigh University "Fleet of the Future" cooperative program funded by the Office of the Secretary of the Navy Manufacturing Technology Program (MANTECH). The objective of the technical direction letter TDL 91-01 for Phase I.3a was to perform experiments to determine the fatigue failure modes of HSLA-80

cellular members characteristic of the "advanced unidirectional double-hull" surface combatant ships. This objective was met through fatigue tests conducted on over 170 large-scale welded HSLA-80 steel specimens.

One way to reduce the likelihood of fatigue problems is to reduce the size of initial discontinuities that can lead to fatigue cracking. Weld discontinuities are present in all welded structures with ships being no exception. The effect of these discontinuities on the lowering of the fatigue resistance of a structure has been well documented [8 - 16]. The present weld discontinuity assessment standards for military ships [17] as well as bridges [18] for fatigue are based on traditional workmanship standards that maybe conservative and therefore lead to excessive repair. These standards are largely based on shipbuilding experience that has evolved over the years based on the smallest discontinuity that can be detected using non-destructive testing techniques (NDT) [13]. The excessive repair has the disadvantages of increasing fabrication costs as well as the possibility to re-introduce more harmful discontinuities.

One solution to the problem of discontinuity assessment for fatigue is a fitness-for-purpose evaluation. In this approach, the discontinuities are judged against a standard that is related to the intended fatigue performance of the weld. If the discontinuity meets or exceeds the fatigue life required by the standard, it is left in place [15]. The fitness-for-purpose approach is used in Britain to assess weld discontinuities. Procedures for assessing the significance of buried and surface discontinuities found

using NDT are given by the British Standards Institute Published Document 6493 [19]. The British fitness-for-purpose approach uses fracture mechanics principles of fatigue crack growth in assessing the significance of planar discontinuities. For volumetric discontinuities, fracture mechanics theory is not applicable and the fitness-for-purpose approach is based on a very large volume of experimental S-N data published in the literature [11, 12].

## 1.2 Objectives and Scope

The advanced double hull ships are likely to be fabricated from modern high-strength, low alloy (HSLA) steels which offer increased weldability, strength and toughness relative to conventional ship steels. The new design and new materials should lead to safer and more affordable ships [3]. However, since the new design and new materials are outside the scope of existing empirical design bases, fatigue experiments were conducted. Fitness-for-purpose assessment has the potential of reducing the amount of weld repair by the acceptance of innocuous discontinuities that are currently judged rejectable. Fatigue data and initial discontinuity sizes for the large planar and volumetric discontinuities observed in the experiments are used to show that a fitness-for-purpose approach to weld discontinuity assessment can be applied to ship structures.

The British procedure is used as a guide to develop a fitness-for-purpose model for use in evaluating the fatigue performance of large planer and volumetric discontinuities observed in the experiments. The model is then used to predict the fatigue lives for the given experimental variables. The results of the model are then compared to the observed fatigue data and comparisons drawn. Comparisons with the current assessment standards are also made.

It is intended that this method can be used to assess weld discontinuity of all shapes, sizes and locations in the weld as well as in any material. However, data presented refers to HSLA-80 steel. It is hoped that fitness-for-purpose evaluation be incorporated into the advanced double hull concept as well as current hull concepts.

# 2. Background

## 2.1 Existence of Weld Discontinuities

Research has shown that all welds contain internal metallurgical discontinuities [14]. These can be categorized by two groups, planar and volumetric. Planar discontinuities include cracks, lack of penetration and lack of fusion. Volumetric discontinuities include inclusions and porosity. The causes and a general description of these discontinuities can be found in the literature [8, 20].

## 2.2 Current Weld Discontinuity Assessment

Current assessment standards are based on workmanship and have their roots in the capabilities and limitations of the available NDT techniques at the time of the writing of the standard [13]. It has been long recognized that the arbitrary assessment standards have no direct relationship to service conditions of the joint in question. This produces one level of quality. It has been past practice to make the assessment standard more restrictive as the NDT techniques have improved. This is based not on engineering principle but on what past practice has found to be acceptable. There is no rational basis for fixing these limits. As better NDT techniques have developed, smaller and smaller discontinuities have been found and hence the acceptance level lowered. This philosophy of repairing the smallest discontinuity that can be detected

with the available NDT techniques seems unwise when with the aid of hindsight, it is known that welded joints containing the same size of discontinuities have preformed satisfactorily in service. When the discontinuities could not be detected, there was little concern about them [14]. Therefore, the removal of these smaller discontinuities may not be necessary.

## 2.3 Effects of Unnecessary Weld Repair

The removal of discontinuities that would preform satisfactorily leads to the possibility of introducing more harmful discontinuities as well as a higher cost. The removal of a discontinuity can be harmful irrespective of material and welding process. Sandor in his study of discontinuities in the U.S. shipbuilding industry found that weld repair leads to the introduction of new discontinuities, increased residual stress and distortion and the aggravation or extension of pre-existing discontinuities that went undetected during the original inspection [13]. These introduced discontinuities could be more harmful and would also be harder to detect. This also has been reported in the literature [14, 21] Weld repair is usually done under conditions of poor accessibility and high constraint, this leads to the high residual stresses and distortion.

Weld repair also affects the cost of the final product. Additional costs are incurred due to weld repair. These costs include additional welding supplies and personal required, late delivery, interruption of work and schedule and occupation of work

space. Also, weld repair often involves not just welders but other persons from other trades [13].

## 2.4 Current Discontinuity Assessment Standards

The current assessment standards used in Naval shipbuilding and bridge construction are military specification Mil-STD-1689 and the American Welding Society (AWS) Bridge Welding Code respectively. The maximum acceptable discontinuity sizes for the 8 mm longitudinal fillet weld and the 9 mm web and 13 mm transverses groove welds using radiographic test (RT) and magnetic particle test (MT) for both codes are shown in Table 1. For volumetric discontinuities, porosity and inclusions, the AWS assessment is based on the size of the discontinuity and the weld size, thus the increased acceptable discontinuity for the web and flange of the transverse groove welds. The military specification is based only on the size of the discontinuity. Planar discontinuities including cracking, lack of penetration and lack of fusion, are not allowed by both codes. The philosophy of assessment is that all cracks are detrimental.

## 2.5 Fitness-for-Purpose Evaluation

### 2.5.1 Introduction

One solution to the problem of discontinuity acceptance for fatigue is a fitness-for-purpose assessment. In this approach, the discontinuities are judged against a standard that is related to the intended fatigue performance of the weld. If the discontinuity meets the fatigue life required by the standard, it is left in place. This has several advantages over the current approach, even though structures that have been fabricated to these arbitrary standards have preformed well in the past. The major advantage of the fitness-for-purpose approach is the reduction of costs due to weld repair. Millions of dollars each year is spent in removing and replacing discontinuities that would have been acceptable under a fitness-for-purpose standard. A study of weld discontinuities in shipbuilding done by Sandor [13] found that the repair of innocuous discontinuities consisting primarily of porosity and slag that would have been acceptable under a fitness-for-purpose assessment added $0.5 million to $1.0 million (1981 dollars) per ship. Another study cited by Boulton [14] states that 87% of weld metal removed in the repair of pressure vessel seams in the United Kingdom would have been considered acceptable if a fitness-for-purpose approach had been taken.

### 2.5.2 Fitness-for-Purpose Concepts

Fitness-for-purpose's advantage over the current assessment standard is that it is a rational way to look at the discontinuity's effect upon the fatigue performance of the structure in question. Fitness-for-purpose relates the discontinuity size, shape, location as well as stress range and the acceptable final crack size to the expected fatigue life. Thus, a discontinuity can be assessed in a rational way. Fitness-for-purpose uses two methods of relating discontinuity size and fatigue life, fracture mechanics and data from fatigue experiments (S-N data).

Fracture mechanics principles are used to relate the discontinuity size and fatigue life if the following assumptions are valid. These assumptions are that the discontinuity and associated fatigue crack is planar (sharp tipped), the stress around the discontinuity and crack can be determined and that the fatigue crack propagates in a predictable way. Planar discontinuities include cracking, lack of penetration and lack of fusion. Fracture mechanics is used because many factors change from discontinuity to discontinuity. These factors include location, size and shape. It would be impossible to test all combinations so fracture mechanics is used to quantify the effect of the discontinuity [14].

For planar discontinuities, the fracture mechanics fatigue crack propagation law is integrated from the initial discontinuity size to the final crack size that is permissible

in the structure. The permissible crack size is determined by the function of the structure. In pressure vessels, this is usually the crack size that will cause leakage. In bridges, the final crack size is usually the size that will cause local failure.

If the assumptions for the use of fracture mechanics can not be met, a traditional S-N curve approach is used. In this approach the discontinuity is categorized by one simple measurement, usually the length. It is assumed that all other variables remain constant. These variables include location and shape of the discontinuity. Data of stress range and cycles to failure from fatigue test data are grouped for a given set of discontinuity sizes. The S-N data are then analyzed statistically to give a 95% lower confidence limit (mean minus two standard deviations) for the data with the specified discontinuity size. This analysis is usually preformed with a slope equal to the exponent of the fatigue crack propagation law [14]. This approach has been developed by Harrison [11,12] to be used to quantify volumetric discontinuities including inclusions and pores. Fracture mechanics can not be used since volumetric discontinuities are blunt and do not meet the requirement of being sharp tipped. Fracture mechanics has been applied to volumetric discontinuities before [22] but results are usually very conservative [8].

Using the above two methods, quality curves that relate stress range and the number of cycles to failure for a given discontinuity size and final crack size can be determined. The curves are then used to assess the discontinuity based on the expected stress

range, life of the structure and tolerable final crack size. The curves are usually set equal to the fatigue design curves. An examples of these fatigue design curves are the American Association of State Highway and Transportation Officials (AASHTO) fatigue design curves shown in Figure 1 [23].

# 3. Description of Experiments

## 3.1 Test Specimens

An experimental program was conducted on large-scale members to determine the fatigue strength of HSLA-80 weld details used in the advanced double-hull design and to examine crack propagation behavior in cellular structure. Experiments were conducted on large I beams (Figure 2). The beam specimens include longitudinal welds and transverse groove welds.

The fatigue test specimens shown in Figure 2 were constructed at Ingalls Shipbuilding in Pascagoula, Mississippi using materials and fabrication techniques typical of modern surface combatants in accord with Mil-STD-1689. The material is a copper precipitation-hardened steel conforming to Mil-STD-S-24645(SH)-Class 3, commonly referred to as HSLA-80. It is similar to ASTM Specification A710, Grade A, Class 3. The steel was produced by Bethlehem Steel Corporation at their Burns Harbor, Indiana plant. The minimum specified yield strength of the steel is 550 MPa and the actual yield strength was approximately 620 MPa [24]. The weld joint designs are in accord with Mil-STD-22D. The longitudinal fillet welds were made with the submerged arc welding (SAW) process with the MIL 100-S welding wire. The groove welds were done using a semiautomatic carbon-dioxide shielded flux-cored arc weld (FCAW, MIL

100-TC). The welds were visually inspected and a randomly selected 10% of the beams were inspected with a magnetic particle test (MT). Tack welding and repair welding were made with both the FCAW process and the shielded-metal arc welding (SMAW) process using E1018 electrodes.

## 3.2 Design of Experiments

The purpose of the I-beam specimens was to produce S-N curves for weld details typical of the advanced unidirectional double-hull ship design. This design is referred to as the double hull. The double-hull is composed of two shells with continuous web plates or girders fillet welded to the shells. The double-hull ship may be assembled in 12 meter modules, which is approximately the distance between bulkheads. The shells and girders contain butt splices that are generally made without significant restraint before these pieces are joined with fillets welds. A highly-restrained butt splice is made to join two modules. The decks and bulkheads are not examined in this study. The only other welded details relevant to the double hull will be miscellaneous attachments and the attachment to the bulkheads.

As shown in Figure 2, the I-beam cross sections included a 13 mm thick flange which featured the weld details of interest and was subjected to the maximum applied tensile stress. This tension flange will be referred to as the "top" flange, although the actual

orientation of the beam in the test frames varied. These specimens all had a 9.5 mm thick web and had a 25.4 mm thick "bottom" flange. The asymmetric design was used to assure failure in the top flange which contained the weld detail of interest. For all types of specimens, there were only a few unintended failures in the "bottom" flanges. Data associated with unintended failures of the bottom flange or with unintended failures in the shear span could usually be used as longitudinal fillet weld data unless the failures were due to base plate failure. The fatigue test set-up for the I beams (shown schematically in Figure 2 and in the photographs in Figure 3, 4 and 5) allowed for reversed loading and for constant bending moment in the center span (1.2 meters). The use of a large beam with a constant-moment region enables a large volume of the particular weld details to be subjected to a constant stress range.

### 3.2.1 Longitudinal Welds

Thirty-three beams with double sided longitudinal fillet welds were tested. It is important to realize that the "specimen" tested was a 1.2 meter length containing such double sided fillet welds. Since the weld defects are randomly distributed, the fatigue strength could depend on the length of weld under consideration.

### 3.2.2 Transverse Groove Welds

Thirty-three transverse groove welds specimens were fabricated such that the groove welds in the web and flanges were made before these parts were joined with longitudinal fillet welds. Each specimen contained two flange groove welds and two web groove welds, one in line with a flange groove weld and one offset from the other flange groove weld (see Figure 2). Usually, after one groove weld cracked it was "repaired" and the test continued until the other cracked, giving two data per specimen.

## 3.3 Testing Procedures

All specimens were tested on 3.05 m span with two point loading centered on the span. The distance between load points was 1.22 m on all test specimens. To suit available actuators, two types of test frames were used to allow for stress reversal as well as positive loading. Testing was performed at the Fritz and ATLSS Laboratory facilities of Lehigh University. The cyclic waveform was close to a sine wave in all cases. Two types of actuators, Amsler and TSS, were used at Fritz Engineering Laboratory. Two different test stations, with a pair of beams in each station, were used with the two types of equipment. One station had two independent Amsler variable stroke hydraulic pumps each supplying oil pressure to two Amsler jacks on

each beam. The pump used a fixed operating speed of about 4.5 Hertz (264 cpm). Each actuator has a maximum dynamic capacity of 244.6 kN. The jacks are very reliable and quiet but can only be used at positive load ratio.

The other test station used a MTS pump system with one TSS actuator per beam. The actuator was centered on a spreader beam to apply equal load at two load points. The TSS actuator was digitally controlled from a personal computer and allowed a variety of testing frequencies. Frequency was generally limited by the response of the actuator and the framing structure. These computer controlled tests were run at constant frequencies from 2 to 4 Hz. The maximum dynamic capacity of the TSS actuator is 489.3 kN. Figures 3 and 4 show photographs of each Fritz Laboratory test frame.

Only TSS equipment was used at the ATLSS Laboratory facilities. This equipment is capable of reversing the load through zero, i.e. negative load ratio. All of the I beam test stations at the ATLSS Laboratory were constructed to accommodate reversed loading, although some positive load ratio tests were done also. At the ATLSS facility, hydraulic pressure is supplied from a bank of five 120 gpm pumps. A total of three test stations each with two beam specimens were used at ATLSS Laboratory. One TSS actuator was used per beam with a spreader beam to distribute load to two load points, as shown in Figure 5. Each actuator was individually controlled using a

multichannel system on a personal computer using constant frequencies from 2 to 4 Hz. The maximum dynamic capacity of the actuators are 490 kN and 980 kN.

To avoid confounding the effect of uncontrolled variables (such as temperature, humidity, and personnel) with the primary control variables, the order of testing was randomized. Test frames were chosen as they became available which was approximately random. Tests were performed in a load control mode, and the stress range was determined using strain gages in all cases. The Amsler equipment was calibrated according to pressure, while load cells were used in most of the TSS actuators. Displacements were monitored to detect failure. The nominal stress range was determined using strain gages which were monitored periodically to assure that the stress range remained constant. Occasional adjustments in the Amsler equipment were necessary. The strain gage data were generally consistent with the load measured from the load cell and the beam displacements. Each beam was typically visually inspected for cracks every four hours (except 4 a.m.). At first visual observation, the number of cycles, the location, and length along the surface of the crack were recorded. Cycling was continued under load control until failure. As discussed in Section 3.4, failure was defined according to a change in compliance of the beams that caused the displacements to increase by 2.5 mm. This change in displacement was used to automatically shut off the tests. By the time this increase in displacement had occurred, the crack had extended 3/4 to full width of the subject

flange. Beachmarking and fatigue crack growth calculations confirm that more than 90 percent of the life is consumed before a through-thickness crack develops. Therefore, variations in the failure criteria after this point have a relatively small impact on the total fatigue life.

In the case of groove welds tested, specimens were spliced as soon as possible after the first crack was identified in the beam. Figure 6 shows a typical splice. Since the life of the specimen from initial visual detection to total failure was relatively short compared to total life, the small difference in cycles between these data and those which reached the defined failure is insignificant. The welds in each beam were far enough apart so that the nominal stress in the second weld detail was not affected by cracking in the first.

### 3.4 Definition of Failure of Specimens

The accepted Naval definition of fatigue failure is the development of a through-thickness crack, since this might lead to leaking. However, unlike the cellular structural system may have significant damage tolerance and may remain stable for a significant number of cycles after the development of a through-thickness crack. In this program, in order to maintain compatibility with previous fatigue test results, failure was defined as the inability to continue growing the crack in the I beams

without excessive change in specimen compliance. A typical fatigue crack at failure is shown in Figure 7. The compliance does not change significantly until the flange is about 50% cracked and a through-thickness crack is proceeding up the web. The beam displacement increase is about 2.5 mm at this point. Therefore the crack growth and associated change in compliance is very rapid. Therefore, the results are not sensitive to the precise compliance change used as the definition of failure. The number of cycles at which the fatigue crack was first detected and periodic measurements of the crack dimensions have also been recorded in the test log, enabling other definitions of failure to be derived from these tests.

### 3.5 Examination Of Failure Surfaces

After removal from the test frames, the section of the test specimen containing the fatigue crack was removed by flame cutting. The fatigue cracks were opened by first sawing through the surrounding material until the saw cut was within 3 mm of the crack tip. The material containing the crack was then cooled in liquid nitrogen so that the remaining ligaments could be broken by a hammer. After opening, the fracture surfaces were sprayed with a clear lacquer to prevent rusting. The size, shape and location of the initial discontinuity was then recorded along with the final crack length.

# 4. Examination of Discontinuities

Fracture surfaces of most of the fatigue cracks were examined to determine the discontinuity or flaw at the origin of the crack. The final crack size as well as the size and location of the flaw were measured and recorded. This is shown in Tables 2 and 3 for the longitudinal fillet welds and Tables 4 - 7 for the transverse groove welds.

## 4.1 Longitudinal Fillet Welds

A total of 21 cracks in the fillet weld and 9 cracks in the base metal were examined. The cracks in the weld initiated at two distinct weld discontinuities. These discontinuities were pores (Figure 8) and solid inclusions (Figure 9). The initial dimensions are described in Table 2 for solid inclusions and Table 3 for the pores. The solid inclusions were small chunks of metal (similar in chemistry to the weld metal) that were embedded in the fillet weld. The shape of these pores and solid inclusions was typically elliptical. The sizes of the pores ranged from a major axis of 8.5 mm to 1.5 mm. The solid inclusions had major axes that ranged from 10 mm to 2 mm. Fourteen of the twenty one of the pores and solid inclusions were observed to have an elliptical shaped discoloration around the defect as illustrated in Figures 8 and 9. These discolorations are referred to as "fisheyes" or "halos". They extended from the edge of the pore to the point where the circular shaped region intersects the

surface of the specimen. Based on examination in the scanning electron microscope (SEM) [24] and observations in the literature, [25] it is supposed that these halos were caused by quasi-cleavage crack growth. Lundin [25] stated that quasi-cleavage was probably due to the collection of hydrogen within the discontinuity. At a finite level of strain, fracture initiates and propagates assisted by the entrapped hydrogen. It was therefore assumed that this occurred either soon after welding or during the first few load cycles. It was also assumed that after the halos intersect the surface, the hydrogen was released. Therefore, it is presently thought that the initial crack size for growth by fracture mechanics calculations should be taken to be the dimension of the halos. The diameters of the major axis of the halos in the longitudinal fillet welds ranged from 8 mm to 20 mm.

Chemical analysis of the metal in the solid inclusion showed that the chemistry of the inclusion was the same as that of the surrounding weld metal [24]. It is therefore speculated that the inclusions are chunks of the weld wire which fell of after the electrode shorted out momentarily.

### 4.2 Transverse Groove Welds

A total of 46 cracks in the groove welds were examined. Cracks initiated at various types of weld discontinuities. These discontinuities included microcracks along the weld toe (Figure 10), incomplete penetration (Figure 11), cracking with halos believed

to be related to hydrogen (Figure 12), and slag inclusions (Figure 13). Other cracks initiated in the base metal due to inclusions or fretting at splice plates. The initial discontinuity dimensions for each type is shown in Table 4 for the slag inclusions, Table 5 for the microcracks along the weld toe, Table 6 for incomplete penetration and Table 7 for the hydrogen related cracking. The shape of these discontinuities varied greatly. Most of the slag inclusions were either elliptical or trapezoidal in shape. The largest slag inclusions covered a 14 mm x 10 mm rectangle, see Figure 13. The smallest slag inclusions had a major diameter of 7 mm. The lack of penetration on the web welds that cracked ranged from 2 mm to 6 mm. The shape of the hydrogen cracks were shaped like rectangles and triangles. The largest crack was shaped like a triangle with a base of 22 mm and a height of 10 mm. The elliptical halos, observed in the longitudinal welds, were found in some of the groove welds as well. The halos were observed in eleven of twenty one of the welds having incomplete penetration, hydrogen related cracking and slag inclusions. The diameters of the major axis of the halos ranged from 12 mm to 25 mm.

After testing of fifteen beams in this series, it was decided to ultrasonically test (UT) all remaining specimens. Six beams were set aside before the UT and it was decided that these six could be repaired if necessary but all others would be tested as fabricated so the group of test specimens would be consistent. All of the beams had rejectable discontinuities, based on the military UT specification. The discontinuities were typically incomplete penetration. All six of those beams set aside were

rejectable and were arc-gouged and repaired. All but one of the tests on these repaired beams cracked at the weld toe and resulted in very good fatigue life.

# 5. Fitness-for-Purpose Assessment

Fracture mechanics was used to develop a fatigue crack propagation model for the volumetric and planar discontinuities of the longitudinal fillet welds and the transverse groove welds. The weld toe discontinuities in the transverse groove welds were not investigated since numerous fatigue crack models exist [26 - 29].

Normally, fracture mechanics is not applied to volumetric discontinuities like the solid inclusions and pores in the longitudinal fillet welds or the slag inclusions in the transverse groove welds because the discontinuities are blunt. Most of the fatigue life is used to initiate a sharp crack from such a discontinuity. The fracture mechanics model assumes sharp initial discontinuities like the cracking and incomplete penetration in the transverse groove welds, of which all of the fatigue life is used to propagate the crack. The fracture mechanics model is applied to the volumetric discontinuities due to the presence of the halos. The halos are considered to be caused by quasi-cleavage fracture assumed to have occurred in the first few loading cycles. Because the halos formed sharp cracks around the discontinuities, the fracture mechanics model can be applied. This is assumed for all volumetric discontinuities regardless of the presence of a halo.

## 5.1 Fracture Mechanics Calculations Using Discontinuity Size Data

The usefulness of the fracture mechanics model will depend on the accuracy of the data on stress, stress range, size and shape of the initial defect, stress intensity factors as well as others. In linear-elastic fracture mechanics, which is adequate to describe fatigue crack growth, the driving force for fatigue crack growth is characterized in terms of the range in $K_I$, called the mode I stress intensity factor (SIF) [30]. The SIF takes into account the applied stress and the crack size, shape, and orientation. The SIF has the form of :[21]

$$K_I = f(g)\ \sigma\sqrt{\pi a} \tag{5.1}$$

where a = crack length
$\sigma$ = applied stress

and f(g), the correction function, has the form of:

$$f(g) = F_c\, F_s\, F_w\, F_g \tag{5.2}$$

where $F_c$ = correction for the crack shape
$F_s$ = correction for free surface
$F_w$ = correction for finite width
$F_g$ = correction for nonuniform stresses

The factors that make up the correction function, f(g), have been examined by

numerous studies so that solutions exist for the most common crack geometries for fatigue crack propagation. When the stress is cyclic, $\sigma$ becomes $\Delta\sigma$, the stress range, and $K_I$ becomes $\Delta K_I$, the stress intensity factor range. By examining the fracture surface, appropriate correction factors can be chosen.

Fatigue crack propagation can be related to the number of cycles by plotting crack length, a, versus the number of stress cycles, N, for various $\Delta\sigma$'s. A single curve relationship results when the rate of crack growth per cycle of loading, da/dN, is plotted against $\Delta K_I$ in the logarithmic scale. It is hypothesized that $\Delta K_I$ is the controlling parameter for crack propagation and that the relation of the crack growth rates to $\Delta K_I$ is the same for a given material and environment. There are three regions of fatigue crack propagation that can be seen from this representation. Behavior in region I occurs when $\Delta K_I$ is less than $\Delta K_{th}$. $\Delta K_{th}$ is the threshold cyclic stress intensity factor and a property of the material. In this region fatigue cracks do not propagate under constant-amplitude cyclic stress variations [30].
Region II represents the stable fatigue crack propagation behavior above $\Delta K_{th}$, but before rapid crack growth near failure. The relationship can be represented by:

$$\frac{da}{dN}=C(\Delta K_I)^n \tag{5.3}$$

where a = crack length
N = number of cycles
$\Delta K_I$ = stress intensity factor range
C and n are material constants

This equation is commonly called Paris's power law. In this region, fatigue growth is steady and predictable. In region III the fatigue crack growth per cycle is much higher than region II. The cause of this accelerated rate appears to be the superposition of ductile tearing mechanism onto the stable crack growth of region II [30].

The fatigue behavior observed in the tests of this study indicates that the cracks propagated in region II. Therefore, Paris's law can be used to calculate the expected fatigue life. Equation 5.3 is integrated with respect to crack length to predict fatigue life. The equation for calculating the fatigue life is:

$$N = \frac{1}{C}\int_{a_i}^{a_f} \frac{1}{\Delta K_I^{\,n}} da \tag{5.4}$$

where $a_i$ is the initial measured crack size and $a_f$ is the final measured crack size.

Substituting Equations 5.1 and 5.2 into 5.4, N becomes:

$$N = \left(\frac{1}{C}\right)\left(\frac{1}{\alpha f^n(g)\pi^{\frac{n}{2}}\Delta\sigma^n}\right)\left(a_i^{-\alpha} - a_f^{-\alpha}\right) \tag{5.5a}$$

With:

$$\alpha = \left(\frac{n}{2}\right) - 1 \tag{5.5b}$$

This equation is valid only when f(g) is a function of crack size, a, alone. If it is a function of other variables, an iterative method must be used to evaluate Equation 5.4.

The functional form of f(g) is generally so complex that Equation 5.4 must be integrated numerically. By choosing an increment of crack length, Δa, a number of cycles, ΔN can be computed using the following, starting with $N_j$:

$$\Delta N_j = \frac{\Delta a_j}{C(\Delta K_I)^n} \tag{5.6a}$$

$$a_{j+1} = a_j + \Delta a_j \tag{5.6b}$$

Repeating the process until the crack length reaches $a_f$ gives the total number of cycles:

$$N = \sum_{j=1}^{n} \Delta N_j \tag{5.7}$$

$\Delta K_I$ is assumed constant during each step. The selection Δa's should made with care such that this assumption is satisfactory.

## 5.2 Determination of the Parameters of Crack Growth

Perhaps the main uncertainty in fracture mechanics modelling of fatigue crack growth is in modelling the correction function. The correction function has to be modeled to

reflect the crack geometry and shape as well as the specimen geometry and shape. By looking at the fracture surface, an appropriate function can be chosen. The first step is to look at the initial discontinuity and the fatigue crack propagation pattern. Due to the severity of the discontinuities found, it is assumed that the crack initiation time was minimal and all the fatigue life is used in propagating the crack. Therefore, the initial crack length is taken as the measured discontinuity length. In the longitudinal fillet welded specimens the initial discontinuities were either circular or elliptical. In the transverse groove welded test specimens the initial discontinuities were shaped irregularly. For both types of welds, the cracks propagated in a circular or penny shaped manner. This is shown in Figures 14, 15 and 16. The figures show crack growth as a percentage of the total fatigue life of the specimen. It can be seen from all three figures that at least 90% of the fatigue life was spent growing the crack from the initial flaw to breaking the bottom flange surface. Figure 14 shows the penny shaped growth for a circular solid inclusion in a longitudinal weld. The crack grew in a penny shape for 96% of its fatigue life. The crack then assumed a elliptical shape for the remaining 4%. Figure 15 shows a penny shaped growth pattern emanating from an irregularly shaped hydrogen related crack in a transverse groove weld. Figure 16 shows penny shaped growth from an irregular shaped slag inclusion embedded just below the surface in a transverse groove weld. Again the crack was penny shaped until 10% of it's life remained. This pattern of circular growth from an initial defect of assumed elliptical shaped has been observed before [5,6,22].

Based on these observations, five crack growth models based on two correction functions are chosen to model the crack propagation. Both correction functions stem from the stress intensity factor (SIF) for an embedded elliptical crack in an infinite body under uniform stress developed by Irwin [31]. The correction functions assume that only the crack shape effects the correction function and that the free surface correction factor, $F_s$, the finite width correction factor, $F_w$, and the non uniform stress correction factor, $F_g$, are equal to one. This is assumed to simplify the calculations. The first correction function chosen is for the elliptically shaped crack. The second correction function chosen is a simplification of the elliptical model called the penny shaped correction function. These correction functions have been used to model fatigue life accurately before [22].

### 5.2.1 Elliptical Correction Function

The f(g) for an embedded elliptical crack in an infinite body subject to a uniform stress field (Figure 17) is equal to:

$$f(g) = \left(\frac{1}{\Phi}\right)\left(\sin^2\beta + \frac{a^2}{c^2}\cos^2\beta\right)^{.25} \tag{5.8}$$

where: a is half of the minor axis
c is half of the major axis

$\Phi$, the elliptical integral of the second kind and equals:

$$\Phi = \int_0^{\frac{\Pi}{2}} [1-(1-\frac{a^2}{c^2}) \sin^2\theta]^{.5} d\theta \tag{5.9}$$

The stress intensity function for an elliptical crack is largest at the end of the minor axis. For $\beta = \pi/2$, equation 5.6 reduces to:

$$f(g) = \frac{1}{\Phi} \tag{5.10}$$

Reference 19 gives a relationship for $\Phi$ based on the ratio of a/c. This relationship is:

$$\Phi = [1+1.464(\frac{a}{c})^{1.65}]^{0.5} \tag{5.11}$$

### 5.2.2 Penny Shaped Correction Function

The second correction function is called the penny shaped correction function and is a further simplification of the elliptical correction function. When a/b = 1 the solution for $\Phi$ reduces to:

$$\Phi = \frac{\pi}{2} \tag{5.12}$$

It should be noted that as the elliptical crack propagates, it will eventually assume a penny shape. This is caused by the $\Delta K_I$ being higher at the tip of the minor axis than the tip of the major axis.

### 5.2.3 Material Properties

The values of the constants, C and n in Equations 5.3 to 5.6 are determined from laboratory tests. For carbon-manganese steels, Barsom and Rolfe suggests an upper bound using C equal to 6.88 x $10^{-9}$ MPa$\sqrt{m}$ with the exponent equal to 3 [30]. The British code [19] suggests an upper bound using C equal to 9.48 x $10^{-9}$ MPa$\sqrt{m}$ with the exponent equal to 3. Fatigue crack growth rate testing was done as part of the testing program in this study. The upper bound to the observed crack growth rates for the HSLA-80 steel was 9 x $10^{-9}$ MPa$\sqrt{m}$ with an exponent of 3 [24]. The HSLA-80 data fell between the other two upper bounds, and this value is used in the fatigue life calculations.

## 5.3 Fatigue Life Prediction Models

Five fatigue crack growth models are investigated. Three crack growth models used the penny shaped correction function. Based on the observed crack growth pattern, this should be sufficient to predict the fatigue crack growth even though the majority of the initial discontinuities were elliptically shaped. When Equation 5.10 and 5.12 are combined with Equation 5.5 and the material constants are inserted, N is equal to:

$$N = \left(\frac{1}{C}\right)\left(\frac{1}{0.5\left(\frac{2}{\pi}\right)^{3}\pi^{1.5}\Delta\sigma^{3}}\right)\left(a_i^{-0.5} - a_f^{-0.5}\right) \tag{5.13}$$

The elliptical correction function is used in a crack growth model for comparison. This model could not be directly integrated since $\Phi$ is a function of a/c which changed after every increment of growth. In order to calculate the fatigue life, an iterative method is used based on one given in Reference 19. The fifth crack growth model used a combination of the two correction functions.

### 5.3.1 Circumscribed Radius Model

The model uses the penny shaped correction function and assumes the crack grows in a penny shaped fashion even though the initial discontinuity is elliptical in shape. The circumscribed radius model assumes the initial crack size, $a_i$, to be equal to the radius of a circle circumscribing the elliptical discontinuity. This is equal to half of the measured length along major axis, 2c, of the elliptical discontinuity as shown in Figure 18a.

### 5.3.2 Inscribed Radius Model

The model assumes the same correction function and crack growth shape as the circumscribed radius model. The inscribed radius model assumes the initial crack size, $a_i$, is equal to the radius of a circle inscribing the elliptical discontinuity. This is equal to half of the measured length along the minor axis, 2a, of the elliptical discontinuity as shown in Figure 18b.

### 5.3.3 Equivalent Radius Model

For this model, the initial crack size, $a_i$, is calculated by setting the initial value of the stress intensity factor of an elliptical crack with the elliptical correction function to the stress intensity factor of a penny shaped crack with a penny shaped crack correction function. This is done to calculate an $a_i$ for use in the penny shaped model that has the same stress intensity factor as the actual initial elliptical discontinuity. Based on this equality, $a_i$ is equal to:

$$a_i = \left(\frac{\pi}{2\Phi}\right)^2 a_{ie} \tag{5.14}$$

with $a_{ie}$ equal to the measured minor radius of the elliptical discontinuity

The calculated equivalent radius is used with the penny shaped correction function as in the two previous models. The equivalent radius is shown in Figure 18c.

### 5.3.4 Elliptical Crack Model

The elliptical model assumes that the crack propagates in an elliptical shape following the elliptical correction function based on an elliptical discontinuity. As mentioned above, $\Phi$ is a function of a/c, Equation 11, and an iterative process is used to calculate the fatigue life. In this model, $a_i$ and $c_i$ are taken as half of the measured minor and major radii, a and c, respectively. This is shown in Figure 18d.

### 5.3.5 Combination Model

This model combines the elliptical model and the penny shaped model. The elliptical model with the measured $a_i$ and $c_i$ is used to calculate a part of the fatigue life. In the calculation $c_i$ is held constant while $a_i$ is allowed to propagate . Since $\Phi$ is a function of a/c, Equation 11, an iterative process is used to calculate a as the crack propagated. Fatigue life is calculated using the elliptical model until the crack length, a, equaled $c_i$. From this point the crack is treated like a circumscribed crack and the fatigue life calculation is based on the circumscribed radius model. The fatigue life from the elliptical portion is added to the fatigue life from the circumscribed radius model to get the total fatigue life.

## 5.4 Results of Fracture Mechanics Calculations

The dimensions of all initial discontinuities and halos were measured and are listed in Tables 2 - 7. These dimensions are used to calculate the fatigue lives by all five fatigue life prediction models. All five models are applied to both the longitudinal and transverse groove welds Two sets of fatigue life calculations are performed. The first set uses the halo dimensions for discontinuities having halos as the initial crack sizes in the calculations. For the discontinuities without halos, the actual crack size is used as the initial crack size. These dimensions are used since it is assumed that the quasi-cleavage crack growth that formed the halos happened either during fabrication

or in the first few load cycles. These dimensions would then best represent the initial sharp crack. The actual fatigue life and the percentage of calculated to actual fatigue lives are shown in Table 8, for the longitudinal fillet welds with solid inclusions and Table 9 for the longitudinal fillet welds with pores. The calculations for the transverse groove welds with cracking are shown in Table 10, with slag inclusions in Table 11 and with incomplete penetration in Table 12. In this format, a percentage below 100% means that the models under predicted the fatigue life. This set should model the crack growth the best if the quasi-cleavage fracture occurred during the first few loading cycles

In the second set of calculations only the actual crack size are used as the initial crack size. The actual fatigue life and the percentage of calculated to actual fatigue lives are shown in Table 13, for the longitudinal fillet welds with solid inclusions and Table 14 for longitudinal fillet welds with pores. The calculations for the transverse groove welds with cracking are shown in Table 15, with slag inclusions in Table 16 and with incomplete penetration in Table 17. In this format, a percentage below 100% means that the models under predicted the fatigue life.

### 5.4.1 Longitudinal Fillet Weld Fatigue Life

The actual fatigue life is plotted versus the calculated fatigue life using the halos dimensions for the different fatigue life prediction models in Figures 19-23. The line

showing 100% (calculated equals actual life) is shown for reference. Data points below this line conservatively predict the fatigue life. For all of the models, there is a wide scatter of the data points. The width of the scatterband of the calculated fatigue life is approximately a factor of eight of the actual fatigue live. In all but one case, the data fell below the 100% line indicating that the results of the fracture mechanics estimate are conservative. The circumscribed radius model shown in Figure 19 generally predicts the lowest life (most conservative) and the inscribed radius model shown in Figure 20 generally predicts the greatest life (least conservative). The equivalent radius, elliptical and the combination models shown in Figures 21, 22 and 23 respectively are bounded by these extremes.

All models dramatically under-predicted the fatigue life. The average prediction is only 29% of the fatigue life. One possible explanation is that the sharp quasi-cleavage crack growth did not happen instantaneously as was assumed, but grew in a manner described by the models from an initial sharp crack with the dimension of the discontinuity. This would increase the calculated fatigue life by decreasing the initial crack size from the halo to the discontinuity dimensions. The halos surrounding the discontinuities of the longitudinal fillet welds are as much as eight times bigger than the discontinuities themselves. Therefore using the actual discontinuity instead of the halo size as the initial crack length should increase the calculated life. Fatigue life calculations using the actual discontinuity and not the halo size for the initial crack size are shown in Tables 13 and 14. The results are shown in Figures 24-28. When

compared with Figure 19-23, all the figures show an upward shift of the data points and the slight reduction of the scatter . The average prediction increased to 47% of the fatigue life. There is still a significant gap between the calculated and predicted fatigue lives, and the ignoring of the halos does not agree with the results of fractographic examination by a SEM [24] which showed the crack propagating very rapidly. Therefore, other possible explanations are investigated.

Another possibility for the under prediction is that the initial applied stress intensity factor, $\Delta K_I$, is below the threshold value, $\Delta K_{th}$ , for fatigue crack propagation. The fatigue life prediction models assumes the initial $\Delta K_I$ to be above the threshold value and propagate according to Paris's law. If the initial $\Delta K_I$ is below this threshold value, then the models would not account for the fatigue life in this region. This would lead to the under prediction of the fatigue life. The initial $\Delta K_I$ is calculated using the penny shaped correction function with the halo dimensions without considering residual stresses since this gives the lowest possible $\Delta K_I$. The results of the calculations are given in Table 18. The range of $\Delta K_I$ values is from 5 to 29 MPa$\sqrt{m}$ with the average being 17 MPa$\sqrt{m}$. The $\Delta K_I$'s are re-calculated using the discontinuity dimension as the initial crack size. The results of the calculations are given in Table 19. The range of $\Delta K_I$ values is from 4 to 17 MPa$\sqrt{m}$ with the average being 11 MPa$\sqrt{m}$. A recent study on $\Delta K_{th}$ of HSLA steel concluded that the value of $\Delta K_{th}$ is in the range of 3.5 to 5.5 MPa$\sqrt{m}$ [32]. The calculated average values are both above this range. Therefore, it appears that the fatigue crack growth

is in the region modelled by Paris's law and that fatigue crack propagation below in region I is not likely. Therefore the reason of under prediction of the fatigue life is not due to propagation below the threshold. This is true for both assumption of the initial discontinuity size.

A third possibility and the one that seems most reasonable is that the under prediction of the fatigue life was due to development of the sharp crack. The fatigue life prediction models assume an initial sharp crack. If the initial discontinuity is blunt, then the models would under predict the fatigue life by the number of cycles needed to form a sharp crack. This is essentially correspondent to the phenomenon of crack initiation.

Based on the assumption of crack initiation, it is postulated that an unaccounted number of cycles was required to initiate a sharp crack from original discontinuity. It is these unaccounted cycles that are probably responsible for the under prediction of the fatigue life. Once a sharp crack was initiated, it grew to the size of the halos in a very small number of cycles. The fatigue life prediction models using the dimension of the halos predicted the remaining fatigue life from this point.

With this reasoning, it is not recommended that a fracture mechanics approach be use to derive quality curves due to the inability of the models to accurately predict the fatigue life. The S-N curve approach is recommended to assess the volumetric discontinuities instead.

### 5.4.2 Transverse Groove Weld Fatigue Life

The actual fatigue life is plotted versus the calculated fatigue life using the halos dimensions for the fatigue life prediction models in Figures 29-33. In comparison to the results for the longitudinal fillet welds, the predictions for the transverse groove welds appear to be much more accurate, typically exhibiting a scatter of the calculated fatigue life to the actual fatigue live of about three. The data points in Figures 29 - 33 are generally within a band with the 100% line near its center. As was the case for the longitudinal fillet weld calculations, the inscribed radius model shown in Figure 29 predicts the highest fatigue lives and the circumscribed radius model shown in Figure 30 predicts the lowest. The equivalent radius, elliptical and the combination models shown in Figures 31, 32 and 33 respectively are bounded by these extremes.

The actual fatigue life is plotted versus the calculated fatigue life using the actual dimension of the discontinuity for the fatigue life prediction models in Figures 34-38. A comparison between these figures and Figures 29-33 shows that the difference in results using the halo or the actual dimension as the initial crack size is small. This is

due to the condition that the halo dimensions being of the same order as the discontinuity dimensions, a situation different from that of the longitudinal welds probably due to the different type of welded joints and the different welding process.

Due to the models' ability to predict the fatigue life, it appears that the cycles for fatigue crack initiation were small for the transverse groove weld discontinuities. This is assumed since the hydrogen related cracking and incomplete penetration have sharp cracks initially and the volumetric slag inclusions are assumed to have sharp cracks caused by initial quasi-cleavage crack growth. This supports the assumption that the quasi-cleavage crack growth occurred either in fabrication or in the first few loading cycles.

Based on the above results, it is recommended that the circumscribed model be used to calculate quality curves for the transverse groove welds since this model accurately predicts conservative fatigue lives for both the volumetric and planar discontinuities. Use of this recommendation would generally yield safe results.

## 5.5 Quality Curves

Quality curves are derived for the longitudinal fillet weld discontinues and the transverse groove welds. Fracture mechanics using the circumscribed radius model is used to derive the quality curves for the planar and the volumetric in the transverse

groove welds. The S-N curve approach is used to derive the quality curves for the volumetric discontinuities in the longitudinal fillet welds.

### 5.5.1 Transverse Groove Welds

The quality curves are calculated based on initial halo or discontinuity sizes calculated using the circumscribed radius model that are set equal to the AASHTO fatigue design curves. The AASHTO curves provide a stress range at a given number of cycles. Using these values for N and $\Delta\sigma$ from the AASHTO curves along with a acceptable final crack size, $a_f$ , the corresponding initial discontinuity size can be calculated. Since the acceptable finial crack size varies based on the application, $a_f$ can be related to $a_i$ by a size factor, r.

$$r = \frac{a_i}{a_f} \tag{5.15}$$

for a given $\Delta\sigma$ and N, the value of r can be calculated. By re-arranging Equation 5.13 and substituting in Equation 5.15.

$$r = \frac{\left(\frac{N + G a_f^{-5}}{G}\right)^{-2}}{a_f} \tag{5.16}$$

where: N = number of cycles to failure
$a_f$ = final crack length

and

$$G=\frac{1}{C}\ \frac{2}{(\frac{2}{\pi})^{3}\pi^{1.5}\Delta\sigma^{3}} \tag{5.17}$$

where: C = material constant
$\Delta\sigma$ = stress range

From this r value, the initial discontinuity size can be determined based on the acceptable final crack size. Values of r and $a_i$ are calculated for the stress range at 1 x $10^5$ cycles from the AASHTO curves using the final crack length, $2a_f$, equal to 114 mm which is 3/4 of the bottom flange thickness which was used to define failure in the tests. The results of theses calculations are shown in Table 20. Substituting the r ratios into Equation 5.13, quality curves can be drawn for the given r ratios. These quality curves, labeled B through E' are based on the AASHTO design curves with a final crack size of 114 mm and are shown in Figure 39. Based on previous fatigue tests, transverse groove welds are a category B or C detail [23]. The discontinuities have the effect of lowering the fatigue resistance to lower categories.

### 5.5.2 Longitudinal Fillet Welds

Due to fatigue crack initiation, the S-N curve approach is used to determine quality categories. In this approach, S-N data for a given detail and a given r ratio are plotted and a statistical analysis is used to determine the 95% lower confidence limit (mean

minus two standard deviations). The lower confidence bound is then used as the quality curve for the particular detail. In this analysis, the halo or the discontinuity dimension is used to calculate the variable r as in the transverse groove welds.

The fatigue data from the longitudinal fillet weld discontinuities are grouped by their calculated r ratio into quality categories based on the AASHTO fatigue design curves. Discontinuities with an r ratio less 0.060 (category B') are grouped in quality category B'. Discontinuities with an r ratio greater than 0.060 (category B') and less than 0.095 (category C) are grouped in quality category B'-C. Discontinuities with an r ratio greater than 0.095 (category C) are grouped in quality category C-D+. The results are listed in Table 21. A statistical analysis with a fixed slope equal to three is preformed using Dataplot, a program written as part of the project [24]. A fixed slope of three is chosen since three is the exponent of the fatigue crack propagation law. This is also the slope used in the AASHTO curves. The results of the statistical analysis are shown in Table 22 and will be used as quality curves for the longitudinal fillet welds.

### 5.5.3 Comparisons With Actual Data

#### 5.5.3.1 Transverse Groove Welds

The r values for the transverse groove weld discontinuities are calculated. They are then grouped into four quality categories based on the r ratio. Discontinuities with an r ratio less than 0.095 (category C) are grouped in quality category C. Discontinuities with an r ratio greater than 0.095 (category C) and less than 0.226 (category D) are grouped in quality category C-D. Discontinuities with an r ratio greater than 0.226 (category D) and less than 0.421 (category E) are grouped in quality category D-E. Discontinuities with an r ratio greater than 0.421 (category E) and less than 0.697 (category E') are grouped in quality category E-E'. This is shown in Table 23.

When the stress range is plotted against the number of cycles to failure for a given quality category, the data points should fall above the line with r equal to the lower quality curve of the quality category. For example, for quality category C-D, the S-N data should fall above the quality curve for category D.

The data from quality category C ($r < 0.095$) and the C quality curve ($r = 0.095$) are plotted in Figure 40. It can be seen that except at the high stress ranges, the data plots above the category C quality curve, which is expected. The data from quality category C-D ($0.095 < r < 0.226$) and quality curve D ($r = 0.226$) are added to the

data from Figure 40. This is shown in Figure 41. All but one data point falls below this line, showing good agreement with the expected results. The data from category D-E are added and the process is repeated. This is shown in Figure 42. In this figure, all the fatigue data are above the category E quality curve. Again data are added from the next lower quality category and the quality curve plotted, in this case, quality category E'. This is shown in Figure 43. Once again, all the S-N data plots above this quality curve as expected. For all the quality categories, the data agrees well with the predicted quality curves.

#### 5.5.3.2 Longitudinal Fillet Welds

In a similar manner to the transverse groove welds the stress range is plotted against the number of cycles to failure of test specimens of a given quality category along with the quality curve equal to the lower confidence limit. Also plotted are the AASHTO fatigue design curves on either of the lower confidence limit. The data from quality category B' are shown in Figure 44. Data from quality category B'-C are added to the data in quality category B' in Figure 45. Data from quality category C-D+ are added in Figure 46. It can be seen from these three figures, that as the r ratio increases from 0.0102 to 0.4514, the lower bound remains almost constant between the AASHTO B and B' fatigue design categories. Previous test results [5,6] have shown that longitudinal fillet welds are a category B fatigue design detail. Apparently, the initial discontinuity size has the effect of slightly lowering the fatigue resistance to a

B' detail. Since the quality curves for the longitudinal fillet welds are approximately equal to the B' AASHTO fatigue design curve, this more familiar curve can be used as the quality curve.

# 6. Conclusions

1. Fitness-for-purpose assessment can be applied to planar and volumetric discontinuities found in transverse groove welds in full scale HSLA - 80 members.

2. Fracture mechanics fatigue crack growth calculations can be used to assess discontinuities in transverse groove welds since the number of cycles associated with crack initiation is apparently not significant.

3. The circumscribed radius model is simple and produces accurate results for the transverse groove welds. Additional accuracy provided by more complex stress intensity factor models, does not appear to be warranted.

4. Fracture mechanics fatigue crack growth calculations for the longitudinal fillet welds under estimated the cycles to failure. Therefore, the number of cycles associated with crack initiation maybe significant.

5. Due to the over conservatism of the fatigue crack growth calculations a set of lower confidence bound S-N quality curves were developed for a range of discontinuity sizes.

6. In the longitudinal fillet welds, large initial discontinuity size has little effect on the fatigue performance, only lowering the fatigue resistance from B to B'.

7. Planar defects may be acceptable in some circumstances. Therefore an option could be provided to the engineer to omit repairing small planar discontinuities based on a fitness-for-purpose assessment.

## References


1. Petershagen, H.,"Fatigue Problems in Ship Structures", Advances in Marine Structures, Elsevier Applied Science, London, pp. 281-304, 1986.

2. Malakhoff, A., Packard, W.T., Engle, A.H., and Sielski, R.A., "Towards Rational Surface Ship Structural Design Criteria", Advances in Marine Structures - 2, C.S. Smith and R.S. Dow, (eds), Elsevier Applied Science, London, pp. 495-528, 1991.

3. Beach, J.E., "Advanced Surface Ship Hull Technology - Cluster B", ASNE Symposium -1990, Destroyer, Cruiser and Frigate Technology, pp. 89-112, 1990.

4. Hollister, S.C., Garcia, J., and Cuykendall, T.R., Fatigue Tests of Ship Welds, SSC-7, Ship Structure Committee, Washington D.C., 1946.

5. Fisher, J.W., Frank, K.H., Hirt, M.A., and McNamee, B.M., Effect of Weldments on the Fatigue Strength of Steel Beams, National Cooperative Highway Research Program (NCHRP) Report 102, Highway Research Board, Washington, D.C.,1970.

6. Fisher, J.W., Albrecht, P.A., Yen, B.T., Klingerman, D.J., and McNamee, B.M., Fatigue Strength of Steel Beams with Welded Stiffeners and Attachments, National Cooperative Highway Research Program (NCHRP) Report 147, Transportation Research Board, Washington, D.C.,1974.

7. Gurney, T.R., and Maddox, S.J., "A Re-analysis of Fatigue Data for Welded Joints in Steel", Welding Research International, Vol. 3, No. 4, pp. 1-54, 1973.

8. Gurney, T. R., Fatigue of Welded Structures, 2nd ed., Cambridge University Press, Cambridge, 1979.

9. Lundin, C. D., The Significance of Weld Discontinuities - A Review of the Current Literature, Welding Research Council Bulletin 222, Welding Research Council, New York, New York, Dec. 1976.

10. Harrison, J. D., "The Significance of Weld Discontinuities and Their Repair", Proceedings: The 1985 International Engineering Symposium on Structural Steel, American Institute of Steel Construction, Chicago, 1985, pp. 11-1 - 11-9.

11. Harrison, J. D., "Basis for a Proposed Acceptance-standard for Weld Defects. Part 1: Porosity", Metal Construction and British Welding Journal, Vol. 4 No. 3, March 1972, pp. 99 - 107.

12. Harrison, J. D., "Basis for a Proposed Acceptance-standard for Weld Defects. Part 2: Slag Inclusions", Metal Construction and British Welding Journal, Vol. 4 No. 7, July 1972, pp. 262 - 268.

13. Sandor, L.W., Weld Defect Tolerance Study, Available from University of Michigan Transportation Research Institute, NSRP 0107, UMTRI 48968, June 1980.

14. Boulton, C. F., Acceptance Levels of Weld Defects for Fatigue Service, Welding Research Supplement, Jan. 1977, pp. 13-s - 22-s.

15. Maddox, S. J., Assessing the Significance of Flaws in Welds Subject to Fatigue, Welding Research Supplement, Sept. 1974, pp. 401-s - 409-s.

16. Kamath, M. S., Woodley, C. C., Harrison. J. D., The Aplication of Fracture Mechanics to Welded Structures, The Welding Institute, March 1979.

17. Department of Defense, Mil - STD - 1689: Fabrication, Welding and Inspection of Ship Structures, Department of Defense, Washington, D. C., Nov. 1990.

18. American Welding Society, Bridge Welding Code, ANSI/AASHTO/AWS D1.5 - 88, American Welding Society, Miami, 1988

19. British Standards Institution, Guidance On Methods for Assessing the Acceptability of Flaws in Fusion Welded Structures, British Standards Institution Report PD 6493:1991, London, 1991.

20. Lundin, C. D., Fundamentals of Weld Discontinuities And Their significance, Welding Research Council Bulletin 295, Welding Research Council, New York, New York, June 1984.

21. Fisher, J. W., Fatigue and Fracture of Steel Bridges: Case Studies, Wiley Interscience, New York, New York, 1984.

22. Hirt, Manfred A., Fatigue Behavior of Rolled and Welded Beams, Dissertation Presented to Lehigh University, 1971.

23. AASHTO, Standard Specification for Highway Bridges, 14th ed., The American Association of State Highway Transportation Officials, Washington, D.C., 1989.

24. Fisher, J. W., Dexter, R. J., Roberts, R., Yen, B. T., Pessiki, S. P., Decorges, G., Nussbaumer, A. C., Tarquinio, J. E., Kober, G. R., Gentilcore, M. L., Derrah, S. M., Final Report for Cooperative Agreement N00014-91-CA-0001 TDL 91 - 01 Phase I.3 (a) Structural Failure Models for Advanced Double Hull Fatigue and Fracture Failure Modes, Lehigh University, March 1993.

25. Lundin, C. D., Patriarca, C. R., Assessment of the Significance of Weld-Discontinuities: Effects of Micro Structure and Discontinuities Upon Fracture Morphology, Welding Research Council Bulletin 331, Welding Research Council, New York, New York, January 1986.

26. Maddox, S. J., "An Analysis of Fatigue Cracks in Fillet Welded Joints", International Journal of Fracture, Vol 11, No. 2, April 1975, pp. 221 - 243.

27. Smith, I. F. C., Gurney, T. R., Changes in the Fatigue Life of Plates with Attachments Due to Geometrical Effects, Welding Research Supplement, Sept. 1986, pp. 244s - 250s.

28. Frank, K.H., and Fisher, J.W., "Fatigue Strength of Fillet Welded Cruciform Joints, Journal of the Structural Division, ASCE, Vol. 105, No. ST9, pp. 1727-1740, September, 1979.

29. Zettlemoyer, N., Fisher, J. W., Stress Gradient Correction for Stress Intensity at Welded Stiffeners and Cover Plates, Welding Research Supplement, Dec. 1977, pp. 393s - 398s.

30. Barsom, J. M., Rolfe, S. T., Fracture and Fatigue Control In Structures, 2nd ed., Prentice-Hall Inc., Englewood Cliffs, NJ, 1987.

31. Irwin, G.R.,"Crack Extension Force For a Part Through Crack in a Plate", Transaction, ASME, Series E, Vol. 29, December 1962.

32. Todd, J.A., Chen, L., Yankov, E. Y., Tao, H., A Comparison of the Near-Threshold Corrosion Fatigue Crack Propagation Rates in Mil S-24645 HSLA Steel and Its Weld Metal, Journal of Offshore Mechanics and Arctic Engineering, OMAE, October, 1992.

# Appendix A Tables and Figures

Porosity and Slag Inclusions

| | Longitudinal Fillet Welds | Transverse Groove Welds | |
|---|---|---|---|
| | | Flange | Web |
| AWS D1.5-88 | 2.7 mm | 4.2 mm | 3.2 mm |
| Mil-STD-1689 | 2.4 mm | 2.4 mm | 2.4 mm |

Cracks and Incomplete Penetration

| | Longitudinal Fillet Welds | Transverse Groove Welds | |
|---|---|---|---|
| | | Flange | Web |
| AWS D1.5-88 | None Permitted | None Permitted | None Permitted |
| Mil-STD-1689 | None Permitted | None Permitted | None Permitted |

**Table 1:** Maximum Discontinuity Length, $2a_i$, Permitted Using Radiographic (RT) and Magnetic Particle (MT) Inspection for the Tested Welds

| Discontinuity Dimension: mm | | Halo Dimension: mm | | Final Crack Length: mm | Stress Range: MPa | Cycles: x $10^3$ | Crack Number |
|---|---|---|---|---|---|---|---|
| Major Axis | Minor Axis | Major Axis | Minor Axis | | | | |
| 10.0 | 4.0 | 20.0 | 18.0 | 77.8 | 207 | 639.1 | 12 |
| 7.0 | 4.5 | none | none | 67 | 207 | 855.0 | 19 |
| 6.0 | 5.0 | none | none | 69 | 290 | 196.0 | 3 |
| 5.0 | 3.0 | none | none | 78.2 | 207 | 1166.3 | 16 |
| 4.5 | 3.0 | 8.0 | 7.0 | 50.7 | 207 | 817.6 | 18-2 |
| 4.0 | 4.0 | 12.0 | 10.0 | 74.5 | 207 | 559.2 | 9 |
| 4.0 | 3.0 | 10.0 | 7.0 | 75.5 | 290 | 170.0 | 31 |
| 3.5 | 3.5 | 15.0 | 15.0 | 76.5 | 290 | 261.0 | 32 |
| 3.0 | 3.0 | 16.0 | 16.0 | 75.8 | 290 | 139.0 | 29 |
| 3.0 | 2.0 | none | none | 70 | 124 | 4635.1 | 2 |
| 3.0 | 2.0 | 13.0 | 11.0 | 14.4 | 290 | 230.0 | 5-1 |
| 3.0 | 2.0 | 13.0 | 11.0 | 73 | 207 | 636.0 | 28 |
| 2.0 | 1.5 | 20.0 | 19.0 | 74 | 207 | 909.5 | 13 |
| N/A | N/A | N/A | N/A | N\A | 124 | 13190 | 23 |

Note: Major and minor axes refer to ellipses circumscribing the discontinuity and halo. Halo refers to the quasi-cleavage crack growth believed to be caused by hydrogen.

**Table 2:** Description of Longitudinal Fillet Weld Discontinuities: Solid Inclusions

| Discontinuity Dimension: mm | | Halo Dimension: mm | | Final Crack Length: mm | Stress Range: MPa | Cycles: x $10^3$ | Crack Number |
|---|---|---|---|---|---|---|---|
| Major Axis | Minor Axis | Major Axis | Minor Axis | | | | |
| 8.5 | 4.0 | 14.0 | 13.0 | 80 | 117 | 4758.5 | 26 |
| 5.0 | 3.0 | 13.0 | 13.0 | 79.3 | 207 | 1010.0 | 17 |
| 5.0 | 3.0 | 28.0 | 22.0 | 66.5 | 124 | 6940.7 | 30-2 |
| 4.0 | 3.0 | none | none | 24.3 | 290 | 230.0 | 5-3 |
| 3.0 | 3.0 | none | none | 13.2 | 290 | 230.0 | 5-2 |
| 2.5 | 1.5 | 13.0 | 12.0 | 42.3 | 207 | 2811.3 | 24 |
| 2.0 | 1.5 | 16.0 | 14.0 | 42.5 | 124 | 6940.7 | 30-1 |
| 1.5 | 1.5 | none | none | 73.6 | 207 | 470.6 | 18-1 |

Note: Major and minor axes refer to ellipses circumscribing the discontinuity and halo. Halo refers to the quasi-cleavage crack growth believed to be caused by hydrogen.

**Table 3:** Description of Longitudinal Fillet Weld Discontinuities: Pores

| Discontinuity Dimension: mm | | Halo Dimension: mm | | Final Crack Length: mm | Stress Range: MPa | Cycles: x $10^3$ | Crack Number |
|---|---|---|---|---|---|---|---|
| Major Axis | Minor Axis | Major Axis | Minor Axis | | | | |
| 20.0 | 4.0 | 15.0 | 4.0 | 63 | 221 | 142.4 | 16-2 |
| 16.0 | 5.0 | none | none | 138 | 221 | 89.3 | 12-2 |
| 15.0 | 3.0 | 20.0 | 13.0 | 86 | 221 | 147.5 | 15-2 |
| 14.0 | 10.0 | 15.0 | 13.0 | 130 | 165 | 524.0 | 10-1 |
| 14.0 | 5.0 | none | none | 140 | 110 | 7842.5 | 2-1 |
| 12.0 | 4.0 | none | none | 90 | 165 | 606.3 | 9-2 |
| 9.0 | 7.0 | 16.0 | 11.0 | 44 | 221 | 83.0 | 14-1 |

Note: Major and minor axes refer to ellipses circumscribing the discontinuity if it is elliptical in shape, to the length and width of the discontinuity if it is rectangular in shape and to the base and height of the discontinuity if it is triangular in shape. Halo refers to the quasi-cleavage crack growth believed to be caused by hydrogen.

**Table 4:** Description Of Transverse Groove Weld Discontinuities: Slag Inclusions

| Number of Occurrences: | Dimension: mm |
|---|---|
| 26 | < 0.1 |

**Table 5:** Description Of Transverse Groove Weld Discontinuities: Weld Toe

| Discontinuity Dimension: mm | | Halo Dimension: mm | | Final Crack Length: mm | Stress Range: MPa | Cycles: x $10^3$ | Crack Number |
|---|---|---|---|---|---|---|---|
| Major Axis | Minor Axis | Major Axis | Minor Axis | | | | |
| 6.0 | 6.0 | 23.0 | 12.0 | 22 | 221 | 89 | 15-3 |
| 5.0 | 2.0 | none | none | 76 | 110 | 3491.5 | 28-3 |
| 3.0 | 3.0 | none | none | 20 | 55 | 11066.1 | 6-3 |
| 3.0 | 3.0 | none | none | 78 | 165 | 583.8 | 20-3 |
| 3.0 | 3.0 | none | none | 32 | 165 | 792.6 | 19-3 |
| 2.0 | 2.0 | none | none | 83 | 221 | 121.9 | 16-1 |

Note: Major and minor axes refer to ellipses circumscribing the discontinuity if it is elliptical in shape, to the length and width of the discontinuity if it is rectangular in shape and to the base and height of the discontinuity if it is triangular in shape. Halo refers to the quasi-cleavage crack growth believed to be caused by hydrogen.

**Table 6:** Description Of Transverse Groove Weld Discontinuities: Incomplete Penetration

| Discontinuity Dimension: mm | | Halo Dimension: mm | | Final Crack Length: mm | Stress Range: MPa | Cycles: x $10^3$ | Crack Number |
|---|---|---|---|---|---|---|---|
| Major Axis | Minor Axis | Major Axis | Minor Axis | | | | |
| 22.0 | 10.0 | 15.0 | 10.0 | 71 | 165 | 190.0 | 18-1 |
| 20.0 | 10.0 | 25.0 | 20.0 | 28 | 110 | 1462.0 | 29-2 |
| 16.0 | 8.0 | none | none | 74 | 165 | 233.4 | 20-1 |
| 15.0 | 11.0 | none | none | 77 | 110 | 1532.2 | 32-1 |
| 14.0 | 11.0 | 13.0 | 12.0 | 80 | 221 | 87.6 | 17-1 |
| 14.0 | 9.0 | 22.0 | 14.0 | 31.3 | 165 | 55.0 | 13-1 |
| 13.0 | 10.0 | 17.0 | 15.0 | 75 | 221 | 67.0 | 17-2 |
| 7.0 | 2.0 | 18.0 | 15.0 | 60 | 165 | 122.6 | 13-2 |

Note: Major and minor axes refer to ellipses circumscribing the discontinuity if it is elliptical in shape, to the length and width of the discontinuity if it is rectangular in shape and to the base and height of the discontinuity if it is triangular in shape. Halo refers to the quasi-cleavage crack growth believed to be caused by hydrogen.

**Table 7:** Description Of Transverse Groove Weld Discontinuities: Cracking

% of calculated life / actual life

| Actual Life x $10^3$ | Circum-scribed Radius Model | Inscribed Radius Model | Equiv. Radius Model | Com-bination Model | Elliptical Model | Crack Number |
|---|---|---|---|---|---|---|
| 639.1 | 16.14 | 17.50 | 16.19 | 16.14 | 16.81 | 12 |
| 559.2 | 28.83 | 32.67 | 29.10 | 28.84 | 30.74 | 9 |
| 817.6 | 24.25 | 26.58 | 24.37 | 24.28 | 25.46 | 18-2 |
| 909.5 | 12.12 | 12.63 | 12.13 | 12.12 | 12.37 | 13 |
| 1163.9 | 24.60 | 33.32 | 26.08 | 24.93 | 28.65 | 16 * |
| 855 | 26.59 | 35.11 | 27.87 | 26.71 | 30.59 | 19 * |
| 636 | 23.86 | 26.82 | 24.05 | 23.87 | 25.341 | 28 |
| 139 | 34.44 | 34.44 | 34.40 | 34.44 | 34.30 | 29 |
| 170 | 39.18 | 49.48 | 40.47 | 39.23 | 44.071 | 31 |
| 261 | 19.27 | 19.27 | 19.25 | 19.27 | 19.19 | 32 |
| 196 | 46.76 | 52.39 | 47.15 | 46.92 | 49.66 | 3 * |
| 230 | 11.22 | 14.20 | 11.41 | 11.23 | 12.82 | 5-1 |
| 4635.1 | 38.87 | 48.73 | 39.99 | 10.30 | 43.57 | 2 * |

* = No Halo Around Discontinuity, Actual Discontinuity Dimension Used in Calculations

**Table 8:** Fatigue Life Calculations For Longitudinal Weld with Halos: Solid Inclusions

% of calculated life / actual life

| Actual Life x $10^3$ | Circum-scribed Radius Model | Inscribed Radius Model | Equiv. Radius Model | Com-bination Model | Elliptical Model | Crack Number |
|---|---|---|---|---|---|---|
| 1010 | 15.28 | 15.28 | 15.27 | 15.28 | 15.21 | 17 |
| 2811.3 | 4.67 | 4.99 | 4.68 | 4.67 | 4.84 | 24 |
| 407.6 | 140.45 | 140.45 | 140.34 | 140.45 | 137.6 | 18-1 * |
| 230 | 47.19 | 47.19 | 47.15 | 47.19 | 46.52 | 5-2 * |
| 230 | 46.97 | 53.51 | 44.96 | 44.70 | 48.81 | 5-3 * |
| 6940.7 | 7.39 | 8.30 | 7.44 | 7.40 | 7.85 | 30-1 |
| 6940.7 | 5.34 | 6.61 | 5.46 | 5.34 | 5.95 | 30-2 |
| 4758.5 | 17.08 | 17.99 | 17.10 | 17.08 | 17.55 | 26 |

* = No Halo Around Discontinuity, Actual Discontinuity Dimension Used in Calculations

**Table 9:** Fatigue Life Calculations For Longitudinal Fillet Welds with Halos: Pores

% of calculated life / actual life

| Actual Life x $10^3$ | Circum-scribed Radius Model | Inscribed Radius Model | Equiv. Radius Model | Com-bination Model | Elliptical Model | Crack Number |
|---|---|---|---|---|---|---|
| 16532.2 | 60.24 | 74.93 | 61.88 | 60.26 | 67.24 | 32-1 * |
| 1462 | 23.59 | 31.99 | 24.29 | 23.59 | 27.93 | 29-2 |
| 190 | 141.25 | 188.28 | 147.82 | 141.31 | 163.16 | 18-1 |
| 233.4 | 110.71 | 179.03 | 125.60 | 110.79 | 140.46 | 20-1 * |
| 55 | 101.15 | 164.14 | 110.80 | 101.18 | 130.83 | 13-1 |
| 122.6 | 75.49 | 87.25 | 76.31 | 75.50 | 81.27 | 13-2 |
| 143 | 88.86 | 93.94 | 89.01 | 88.89 | 91.47 | 17-1 |
| 124 | 83.15 | 91.24 | 83.54 | 83.16 | 87.19 | 17-2 |

* = No Halo Around Discontinuity, Actual Discontinuity Dimension Used in Calculations

**Table 10:** Fatigue Life Calculations For Transverse Groove Welds with Halos: Cracking

% of calculated life / actual life

| Actual Life x $10^3$ | Circum-scribed Radius Model | Inscribed Radius Model | Equiv. Radius Model | Com-bination Model | Elliptical Model | Crack Number |
|---|---|---|---|---|---|---|
| 7842.5 | 13.75 | 25.67 | 17.28 | 13.78 | 18.55 | 2-1 * |
| 606.3 | 54.38 | 108.06 | 71.05 | 54.64 | 75.09 | 9-2 * |
| 109.6 | 275.63 | 302.55 | 277.14 | 275.70 | 245.66 | 10-1 |
| 89.3 | 136.21 | 277.75 | 182.00 | 136.52 | 179.74 | 12-2 * |
| 83 | 110.72 | 150.50 | 115.92 | 110.76 | 129.46 | 14-1 |
| 147.5 | 35.57 | 87.37 | 51.93 | 35.57 | 74.80 | 15-2 |
| 112 | 96.76 | 235.12 | 145.64 | 97.23 | 149.53 | 16-2 |

* = No Halo Around Discontinuity, Actual Discontinuity Dimension Used in Calculations

**Table 11:** Fatigue Life Calculations For Transverse Groove Welds with Halos: Slag Inclusions

% of calculated life / actual life

| Actual Life x $10^3$ | Circum-scribed Radius Model | Inscribed Radius Model | Equiv. Radius Model | Com-bination Model | Elliptical Model | Crack Number |
|---|---|---|---|---|---|---|
| 11066 | 157.51 | 157.51 | 157.36 | 157.51 | 155.44 | 6-3 * |
| 3491.5 | 54.49 | 93.18 | 64.99 | 56.50 | 70.72 | 28-3 * |
| 792.6 | 30.66 | 87.88 | 51.92 | 31.07 | 52.12 | 19-3 * |
| 583.8 | 131.17 | 131.17 | 131.06 | 131.17 | 129.69 | 20-3 * |
| 89 | 41.59 | 99.31 | 53.54 | 41.61 | 68.54 | 15-3 |
| 131 | 307.95 | 307.95 | 307.71 | 307.95 | 303.09 | 16-1 * |

* = No Halo Around Discontinuity, Actual Discontinuity Dimension Used in Calculations

**Table 12:** Fatigue Life Calculations For Transverse Groove Welds with Halos: Incomplete Penetration

% of calculated life / actual life

| Actual Life x $10^3$ | Circum-scribed Radius Model | Inscribed Radius Model | Equiv. Radius Model | Com-bination Model | Elliptical Model | Crack Number |
|---|---|---|---|---|---|---|
| 639.1 | 26.56 | 47.24 | 32.17 | 26.69 | 35.16 | 12 |
| 4635.1 | 38.57 | 48.73 | 40 | 40.29 | 43.58 | 2 |
| 559.2 | 58.30 | 58.30 | 58.25 | 58.30 | 57.77 | 9 |
| 817.6 | 35.49 | 45.59 | 36.91 | 36.00 | 40.36 | 18-2 |
| 909.5 | 53.58 | 62.96 | 54.56 | 59.35 | 58.70 | 13 |
| 1163.9 | 24.60 | 33.32 | 26.09 | 24.93 | 28.65 | 16 |
| 855 | 26.59 | 35.11 | 27.87 | 26.70 | 30.59 | 19 |
| 636 | 60.64 | 76.56 | 62.87 | 63.34 | 68.48 | 28 |
| 139 | 101.23 | 101.23 | 101.15 | 101.23 | 100.08 | 29 |
| 170 | 69.84 | 82.74 | 71.18 | 70.83 | 76.37 | 31 |
| 261 | 49.30 | 49.30 | 49.26 | 49.30 | 48.81 | 32 |
| 196 | 46.75 | 52.39 | 47.15 | 46.91 | 49.67 | 3 |
| 230 | 48.21 | 64.21 | 50.45 | 50.92 | 56.12 | 5-1 |

**Table 13:** Fatigue Life Calculations Using Actual Dimensions For Longitudinal Welds: Solid Inclusions

% of calculated life / actual life

| Actual Life x $10^3$ | Circum-scribed Radius Model | Inscribed Radius Model | Equiv. Radius Model | Com-bination Model | Elliptical Model | Crack Number |
|---|---|---|---|---|---|---|
| 1010 | 28.40 | 38.44 | 30.15 | 28.77 | 33.07 | 17 |
| 2811.3 | 14.52 | 19.63 | 15.39 | 16.03 | 16.98 | 24 |
| 407.6 | 140.45 | 140.45 | 140.34 | 140.45 | 137.61 | 18-1 |
| 230 | 47.19 | 47.19 | 47.14 | 47.19 | 46.52 | 5-2 |
| 230 | 43.96 | 53.50 | 44.96 | 44.70 | 48.81 | 5-3 |
| 6940.7 | 31.29 | 37.01 | 31.89 | 34.81 | 34.41 | 30-1 |
| 6940.7 | 18.84 | 25.64 | 19.99 | 19.09 | 22.00 | 30-2 |
| 4758.5 | 23.95 | 38.20 | 27.27 | 24.08 | 30.11 | 26 |

**Table 14:** Fatigue Life Calculations Using Actual Dimensions For Longitudinal Welds: Pores

% of calculated life / actual life

| Actual Life x $10^3$ | Circum-scribed Radius Model | Inscribed Radius Model | Equiv. Radius Model | Com-bination Model | Elliptical Model | Crack Number |
|---|---|---|---|---|---|---|
| 1532.2 | 60.24 | 74.93 | 61.88 | 60.27 | 62.25 | 32-1 |
| 1462 | 31.98 | 64.91 | 39.16 | 32.00 | 46.61 | 29-2 |
| 190 | 104.78 | 188.28 | 124.96 | 104.82 | 140.36 | 18-1 |
| 233.4 | 110.71 | 179.03 | 125.60 | 110.80 | 140.46 | 20-1 |
| 55 | 164.16 | 241.13 | 175.71 | 164.28 | 200.02 | 13-1 |
| 143 | 84.34 | 99.69 | 85.71 | 84.37 | 91.79 | 17-1 |
| 124 | 101.14 | 121.23 | 103.07 | 101.19 | 110.86 | 17-2 |

**Table 15:** Fatigue Life Calculations Using Actual Dimensions For Transverse Groove Welds: Cracking

% of calculated life / actual life

| Actual Life x $10^3$ | Circum-scribed Radius Model | Inscribed Radius Model | Equiv. Radius Model | Com-bination Model | Elliptical Model | Crack Number |
|---|---|---|---|---|---|---|
| 11066 | 157.51 | 157.51 | 157.36 | 157.51 | 155.44 | 6-3 |
| 3491.5 | 54.49 | 93.18 | 64.99 | 56.50 | 70.72 | 28-3 |
| 792.6 | 30.66 | 87.88 | 51.94 | 31.06 | 52.12 | 19-3 |
| 583.8 | 131.17 | 131.17 | 131.06 | 131.17 | 129.69 | 20-3 |
| 89 | 185.41 | 195.41 | 185.21 | 185.41 | 183.87 | 15-3 |
| 131 | 307.95 | 307.95 | 307.71 | 307.95 | 303.09 | 16-1 |

**Table 16:** Fatigue Life Calculations Using Actual Dimensions For Transverse Groove Welds: Incomplete Penetration

% of calculated life / actual life

| Actual Life x $10^3$ | Circum-scribed Radius Model | Inscribed Radius Model | Equiv. Radius Model | Com-bination Model | Elliptical Model | Crack Number |
|---|---|---|---|---|---|---|
| 7842.5 | 13.75 | 25.67 | 17.28 | 13.78 | 18.54 | 2-1 |
| 606.3 | 54.38 | 108.06 | 71.06 | 54.64 | 75.09 | 9-2 |
| 109.6 | 199.37 | 357.17 | 296.58 | 288.49 | 301.28 | 10-1 |
| 89.3 | 83.66 | 277.75 | 182.00 | 83.84 | 179.74 | 12-2 |
| 122.6 | 149.85 | 321.90 | 208.46 | 155.03 | 216.68 | 13-2 |
| 83 | 175.06 | 209.52 | 178.26 | 175.31 | 192.01 | 14-1 |
| 147.5 | 79.05 | 217.72 | 134.58 | 79.83 | 128.64 | 15-2 |
| 112 | 76.97 | 235.12 | 140.30 | 77.34 | 134.21 | 16-2 |

**Table 17:** Fatigue Life Calculations Using Actual Dimensions For Transverse Groove Welds: Slag Inclusions

Pores

| Crack Number | $\Delta K_I$: MPa$\sqrt{m}$ |
|---|---|
| 5-2 | 12.67 |
| 5-3 | 14.63 |
| 17 | 18.83 |
| 18-1 | 6.40 |
| 24 | 18.83 |
| 26 | 11.04 |
| 30-1 | 12.51 |
| 30-2 | 16.56 |

Solid Inclusions

| Crack Number | $\Delta K_I$: MPa$\sqrt{m}$ |
|---|---|
| 2 | 5.41 |
| 3 | 17.92 |
| 5-1 | 26.38 |
| 9 | 18.09 |
| 12 | 23.36 |
| 13 | 23.36 |
| 16 | 11.67 |
| 18-2 | 14.77 |
| 19 | 13.81 |
| 28 | 18.83 |
| 29 | 29.26 |
| 31 | 23.13 |
| 32 | 28.34 |

**Table 18:** Initial $\Delta K_I$ of Longitudinal Fillet Weld Discontinuities Using Circumscribed Radius Model and Halo Dimensions

Pores

| Crack Number | $\Delta K_I$: MPa$\sqrt{m}$ |
|---|---|
| 5-2 | 12.67 |
| 5-3 | 14.63 |
| 17 | 11.67 |
| 18-1 | 6.40 |
| 24 | 8.26 |
| 26 | 8.61 |
| 30-1 | 4.42 |
| 30-2 | 7.00 |

Solid Inclusions

| Crack Number | $\Delta K_I$: MPa$\sqrt{m}$ |
|---|---|
| 2 | 5.42 |
| 3 | 17.92 |
| 5-1 | 12.67 |
| 9 | 10.44 |
| 12 | 16.52 |
| 13 | 7.38 |
| 16 | 11.68 |
| 18-2 | 11.08 |
| 19 | 13.81 |
| 28 | 9.04 |
| 29 | 12.67 |
| 31 | 14.63 |
| 32 | 13.69 |

**Table 19:** Initial $\Delta K_I$ of Longitudinal Fillet Weld Discontinuities Using Circumscribed Radius Model and Actual Dimensions

| AASHTO Category | Stress Range, MPa, At N = 1 x $10^5$ Cycles | Assumed Final Crack Length, $a_f$: mm | Calculated Initial Discont. Length, $a_i$: mm | r |
|---|---|---|---|---|
| A | 434 | 57 | 0.31 | 0.005 |
| B | 339 | 57 | 1.15 | 0.022 |
| B' | 271 | 57 | 3.41 | 0.060 |
| C | 244 | 57 | 5.40 | 0.095 |
| D | 193 | 57 | 12.87 | 0.226 |
| E | 152 | 57 | 23.97 | 0.421 |
| E' | 109 | 57 | 39.74 | 0.697 |

**Table 20:** Initial Discontinuity Size Calculations and Ratio of Initial Discontinuity Size over Final Crack Size, r, Based on AASHTO S-N Curves Using Circumscribed Radius Model

| Quality Category | Crack Number | Circum-scribed Radius, $a_i$: mm | Final Crack Size, $a_f$: mm | r | Cycles | Stress Range: MPa |
|---|---|---|---|---|---|---|
| < B' | 18-1 | 0.75 | 73.6 | 0.0102 | 407600 | 207 |
| | 2 | 1.5 | 70 | 0.0214 | 4635100 | 124 |
| | 16 | 2.5 | 78.2 | 0.032 | 1163900 | 207 |
| | 3 | 3 | 69 | 0.0435 | 196000 | 290 |
| | 19 | 3.5 | 67 | 0.0522 | 855000 | 207 |
| B' - C | 31 | 5 | 75.5 | 0.0662 | 170000 | 290 |
| | 18-2 | 4 | 50.7 | 0.0789 | 817600 | 207 |
| | 9 | 6 | 74.5 | 0.0805 | 559200 | 207 |
| | 17 | 6.5 | 79.3 | 0.082 | 1010000 | 207 |
| | 5-3 | 2 | 24.3 | 0.0823 | 230000 | 290 |
| | 26 | 7 | 80 | 0.0875 | 4758500 | 117 |
| | 28 | 6.5 | 73 | 0.089 | 636000 | 207 |
| C - D + | 32 | 7.5 | 76.5 | 0.098 | 261000 | 290 |
| | 29 | 8 | 75.8 | 0.1055 | 139000 | 290 |
| | 5-2 | 1.5 | 13.2 | 0.1136 | 230000 | 290 |
| | 12 | 10 | 77.8 | 0.1285 | 693100 | 207 |
| | 13 | 10 | 74 | 0.1351 | 909500 | 207 |
| | 24 | 6.5 | 42.3 | 0.1537 | 2811300 | 207 |
| | 30-1 | 8 | 42.5 | 0.1882 | 6940700 | 124 |
| | 30-2 | 14 | 66.5 | 0.2105 | 6940700 | 124 |
| | 5 | 6.5 | 14.4 | 0.4514 | 230000 | 290 |

**Table 21:** Quality Categories of Longitudinal Fillet Weld Discontinuities by the Ratio of Initial Discontinuity Size over Final Crack Size, r, by AASHTO Criteria

| Quality Category | Equation of Lower 95% Confidence Bound ($\mu - 2\sigma$) |
|---|---|
| < B' | Log (N) = 12.4 + -3 Log (SR) |
| B' - C | Log (N) = 12.5 + -3 Log (SR) |
| C - D+ | Log (N) = 12.4 + -3 Log (SR) |

**Table 22:** Results of Statistical Analysis of Longitudinal Fillet Weld Quality Categories

| Quality Category | Crack Number | Circum-scribed Radius, $a_i$: mm | Final Crack Size, $a_f$: mm | r | Cycles | Stress Range: MPa |
|---|---|---|---|---|---|---|
| < C | 16-1 | 1 | 83 | 0.012 | 131000 | 221 |
| | 20-3 | 1.5 | 78 | 0.0192 | 583800 | 165 |
| | 28-3 | 2.5 | 76 | 0.0329 | 3491500 | 110 |
| | 2-1 | 7 | 140 | 0.05 | 7842500 | 110 |
| | 10-1 | 7.5 | 130 | 0.0577 | 109600 | 165 |
| | 12-2 | 8 | 138 | 0.058 | 89300 | 221 |
| | 9-2 | 6 | 90 | 0.0667 | 606300 | 165 |
| | 6-3 | 1.5 | 20 | 0.075 | 11066100 | 55 |
| | 17-1 | 6.5 | 80 | 0.0813 | 143000 | 221 |
| C - D | 32-1 | 7.5 | 77 | 0.0974 | 1532200 | 110 |
| | 18-1 | 7.5 | 71 | 0.1056 | 190000 | 165 |
| | 20-1 | 8 | 74 | 0.1081 | 266400 | 165 |
| | 17-2 | 8.5 | 75 | 0.1133 | 124000 | 221 |
| | 16-2 | 7.5 | 63 | 0.119 | 112000 | 221 |
| | 13-2 | 9 | 60 | 0.15 | 122600 | 221 |
| | 14-1 | 8 | 44 | 0.1818 | 83000 | 221 |
| | 19-3 | 6.25 | 32 | 0.1953 | 792600 | 165 |
| D - E | 15-2 | 20 | 86 | 0.2326 | 147500 | 221 |
| | 13-1 | 11 | 31.3 | 0.3514 | 5500 | 221 |
| E - E' | 29-2 | 12.5 | 28 | 0.4464 | 1462000 | 110 |
| | 15-3 | 11.5 | 22 | 0.5227 | 89000 | 221 |

**Table 23:** Quality Categories of Transverse Groove Weld Discontinuities by the Ratio of Initial Discontinuity Size over Final Crack Size, r, by AASHTO Criteria

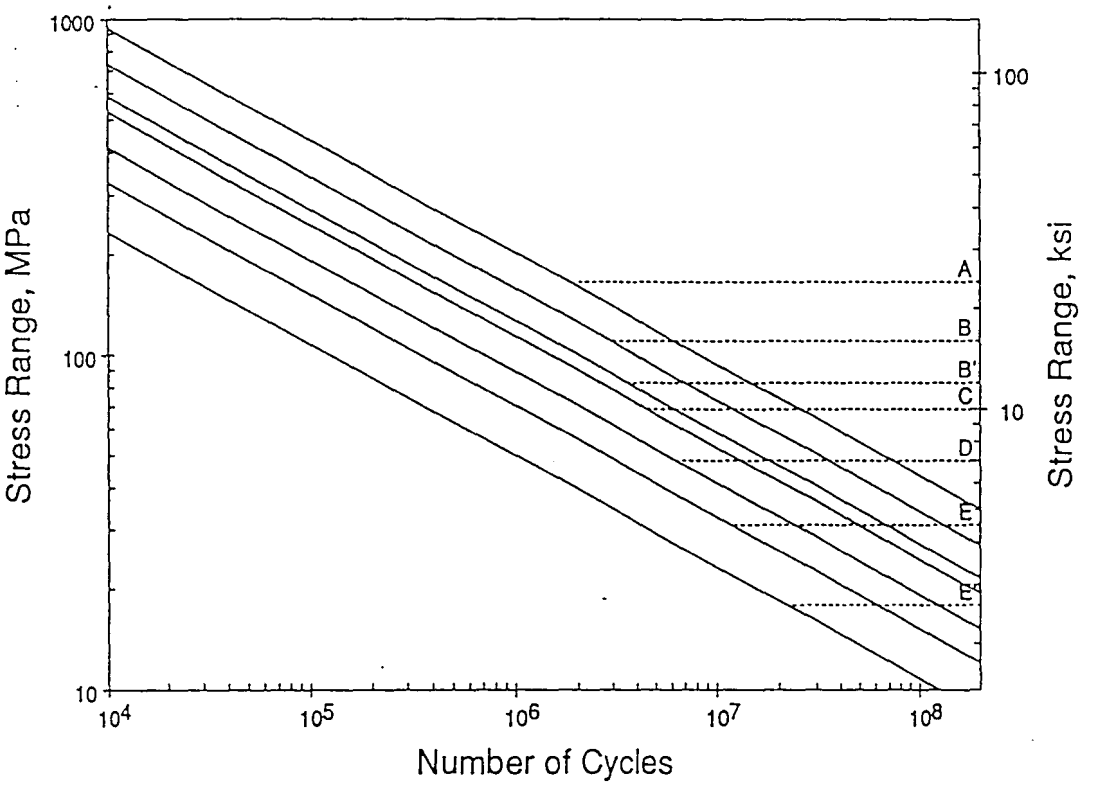


**Figure 1:** AASHTO Fatigue Design Curves.

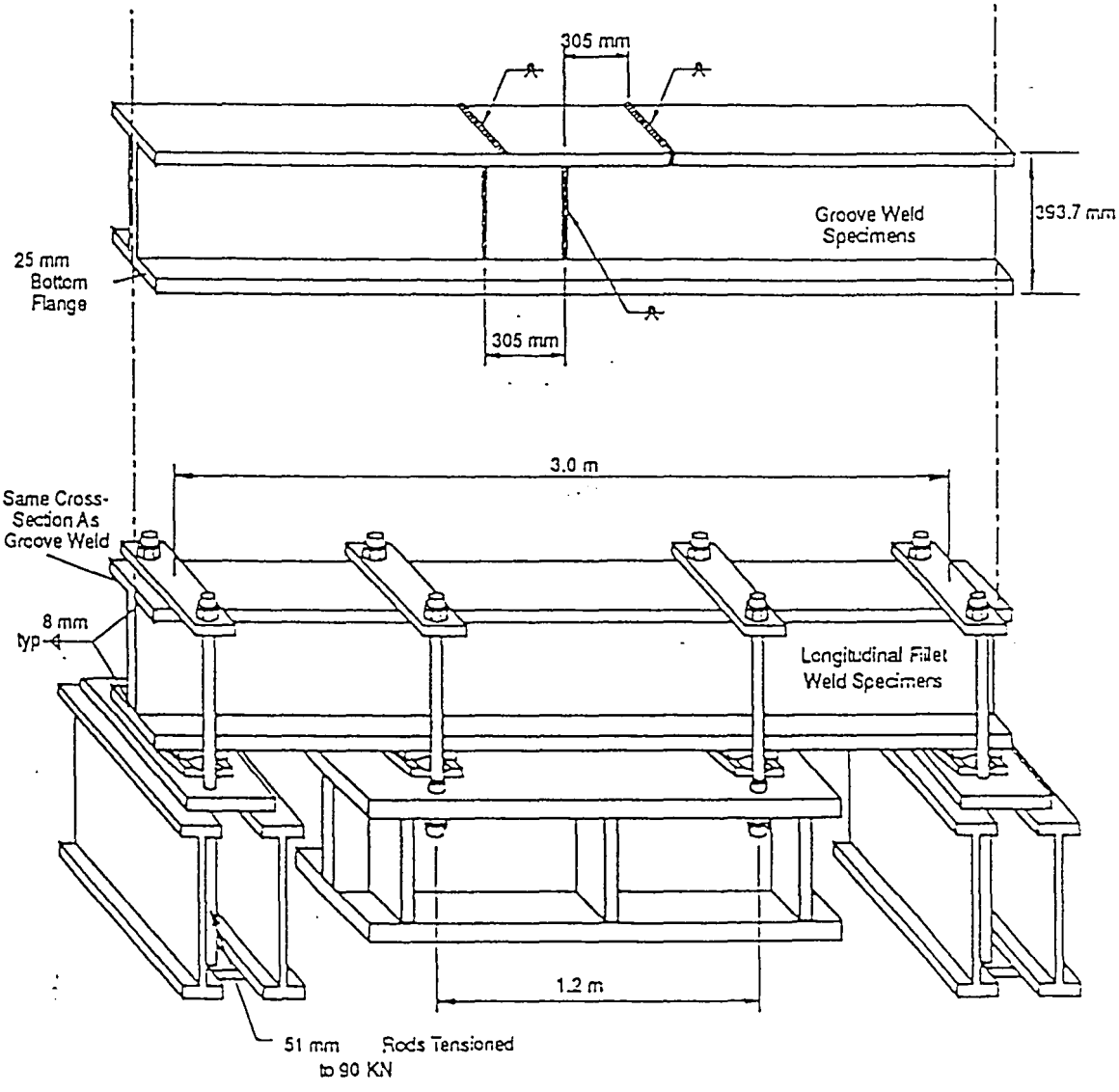


**Figure 2:** Fatigue Test Setup and Specimens. Longitudinal Fillet Weld Specimen Shown With Typical Test Fixture.

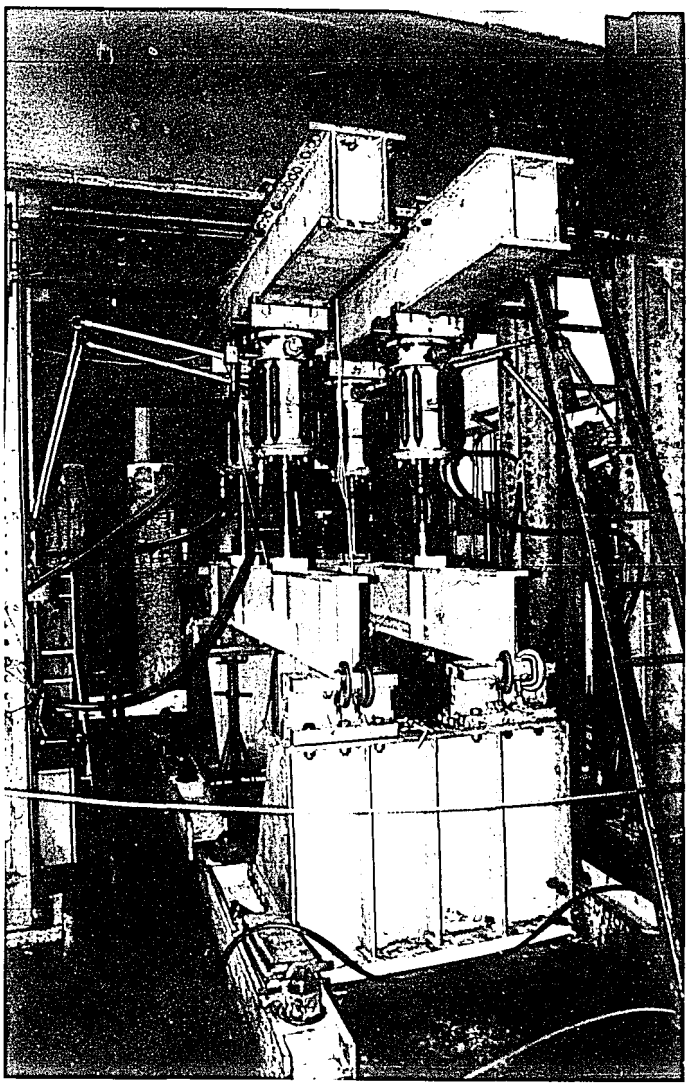

**Figure 3:** Fritz Laboratory Test Setup Utilizing Amsler Jacks. Positive Loading Ratio Only.

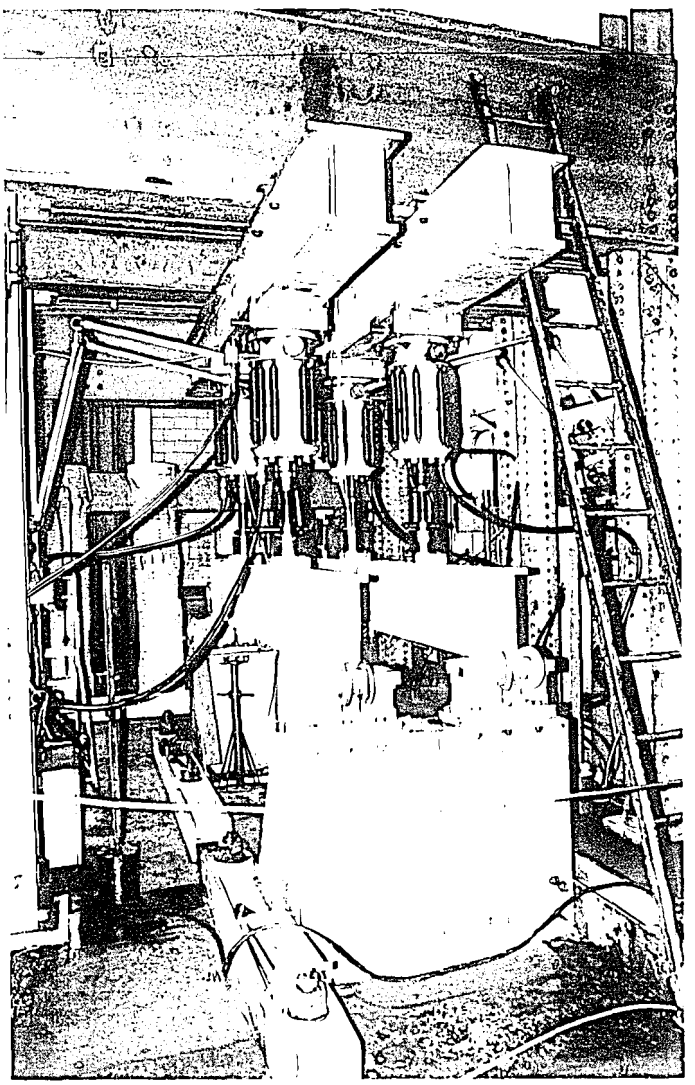

**Figure 3:** Fritz Laboratory Test Setup Utilizing Amsler Jacks. Positive Loading Ratio Only.

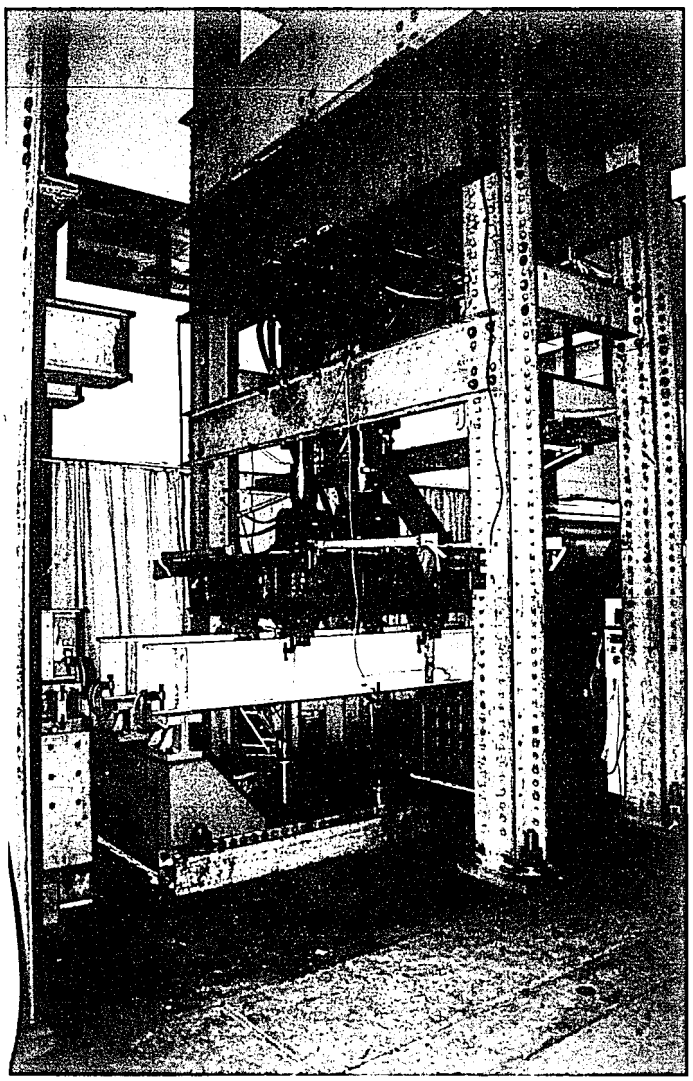

**Figure 4:** Fritz Laboratory Test Setup Utilizing TSS Jacks. Positive Loading Ratio Only.

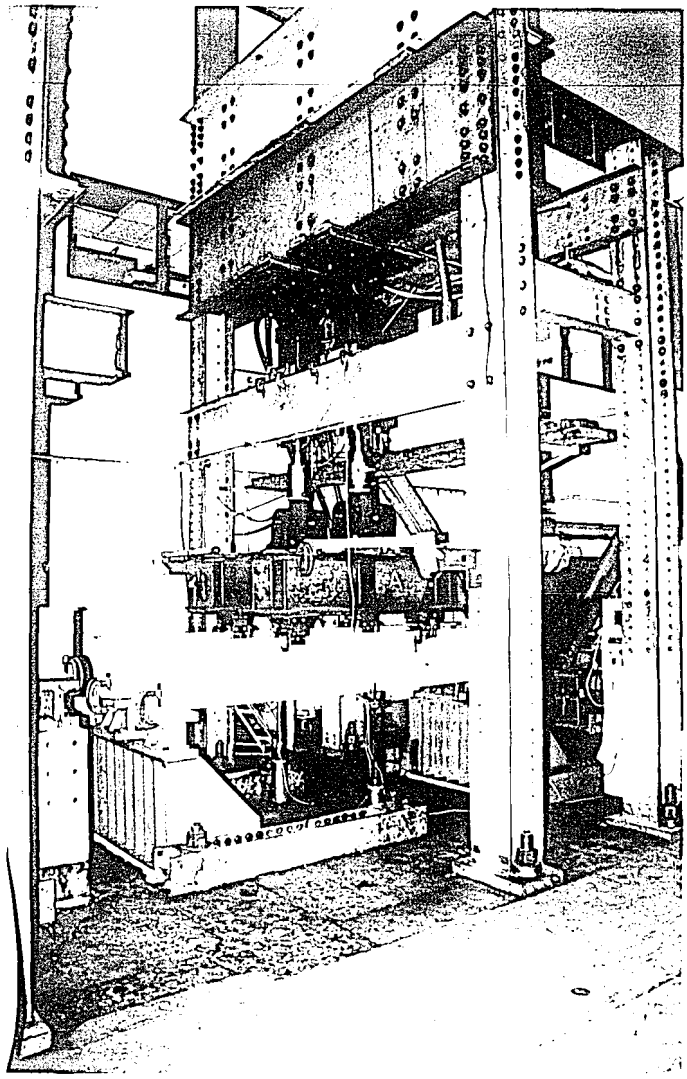

**Figure 4:** Fritz Laboratory Test Setup Utilizing TSS Jacks. Positive Loading Ratio Only.

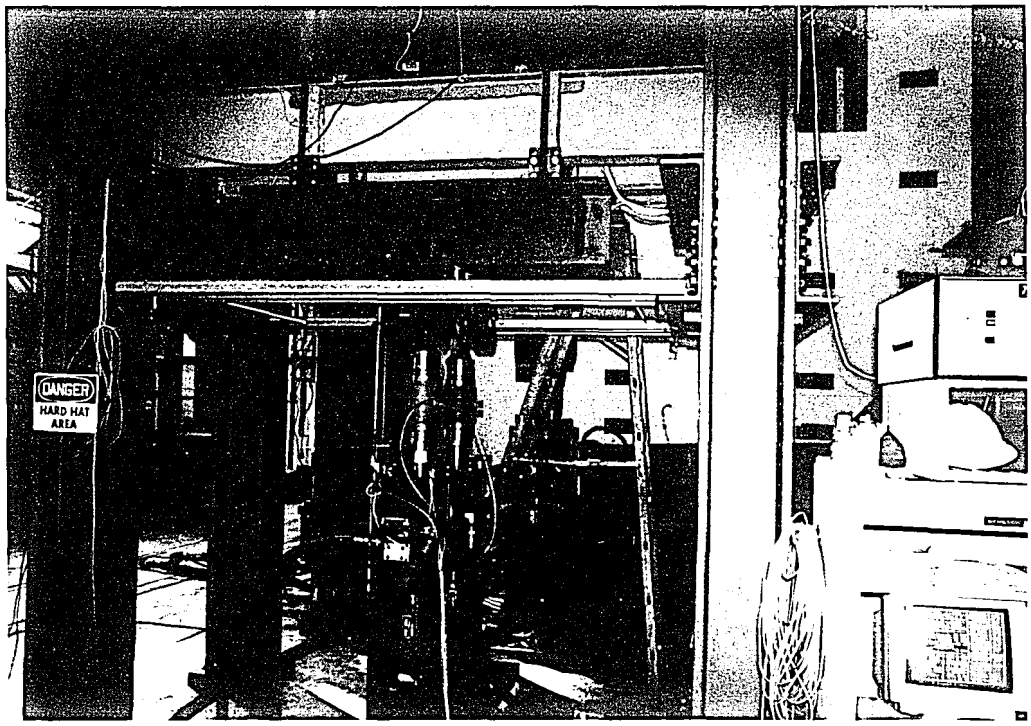


**Figure 5:** ATLSS Laboratory Test Setup Utilizing TSS Jacks With Typical I-beam Fatigue Test Setup That Allows for Reverse Loading.

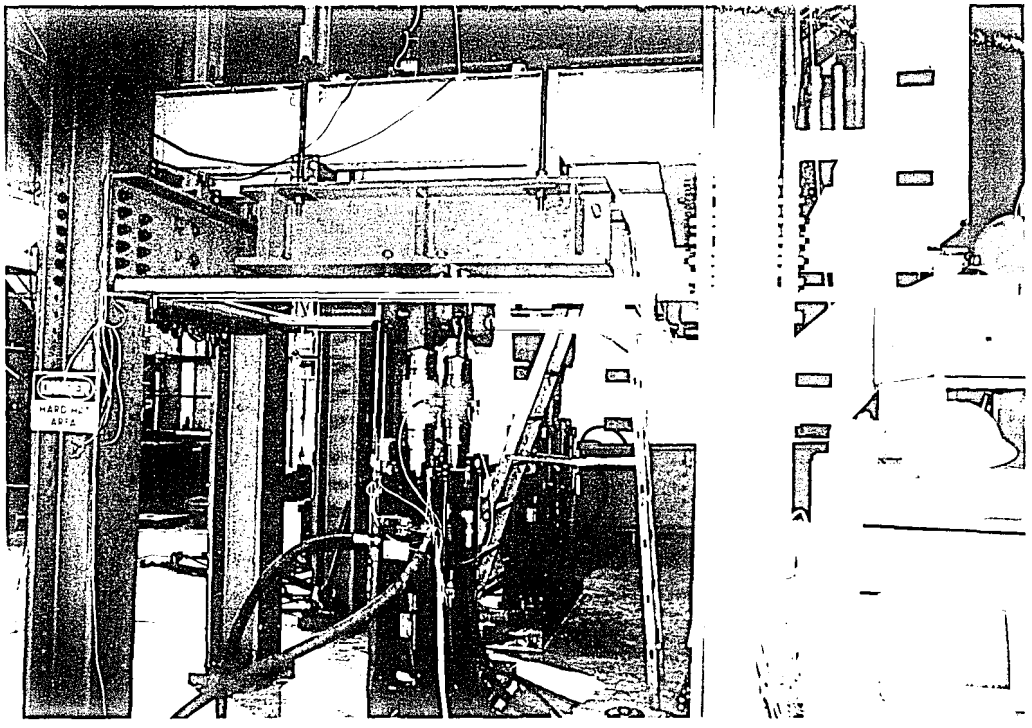

**Figure 5:** ATLSS Laboratory Test Setup Utilizing TSS Jacks With Typical I-beam Fatigue Test Setup That Allows for Reverse Loading.

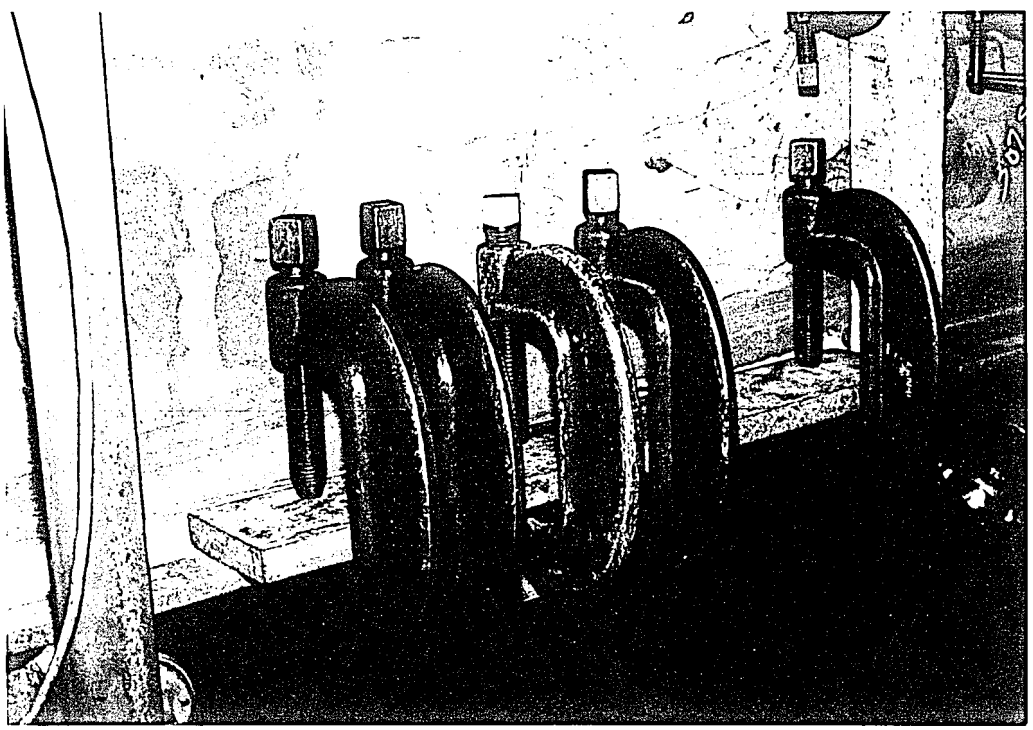

**Figure 6:** Typical Splice of Groove Welded Test Beam. This Allowed for Continued Testing of Other Details on the Beam.

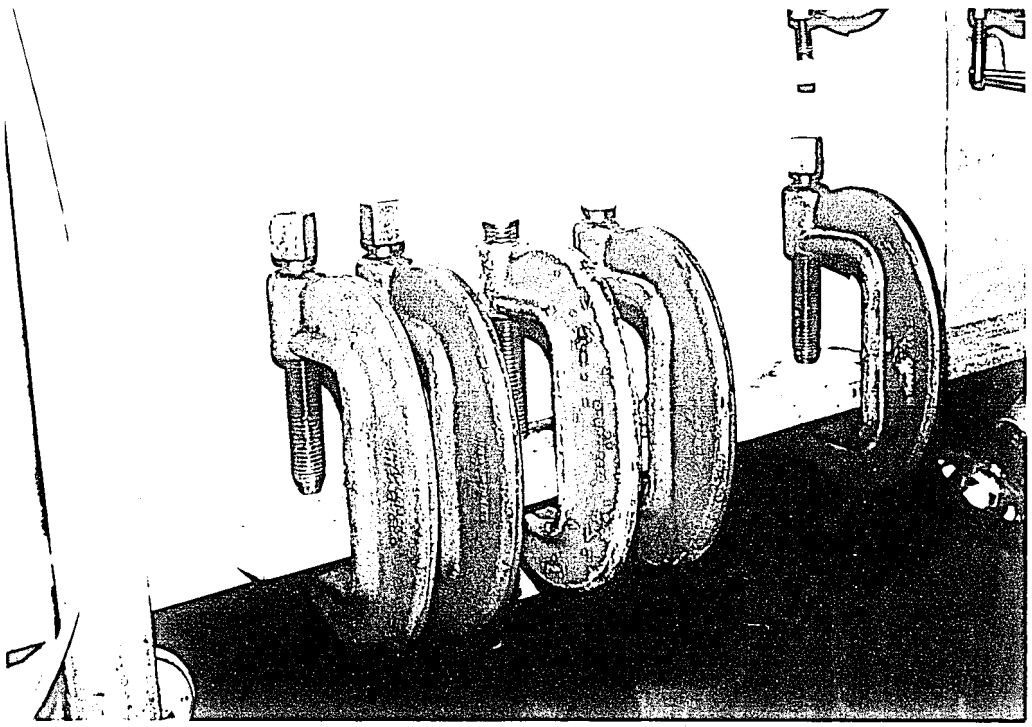

**Figure 6:** Typical Splice of Groove Welded Test Beam. This Allowed for Continued Testing of Other Details on the Beam.

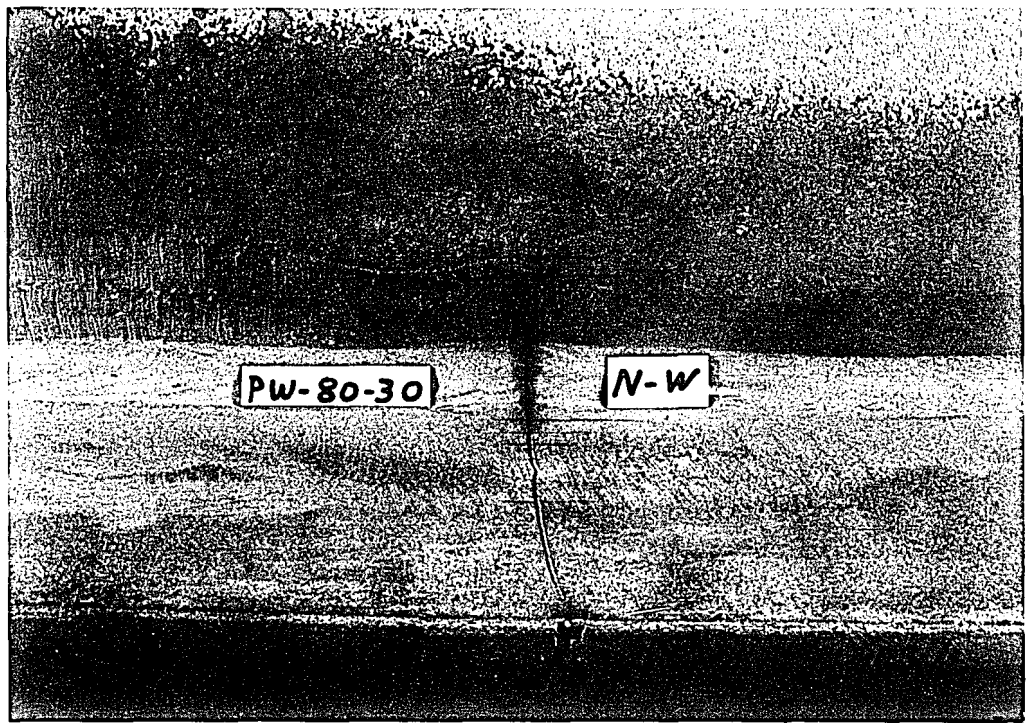


**Figure 7:** Typical Fatigue Crack at Failure.

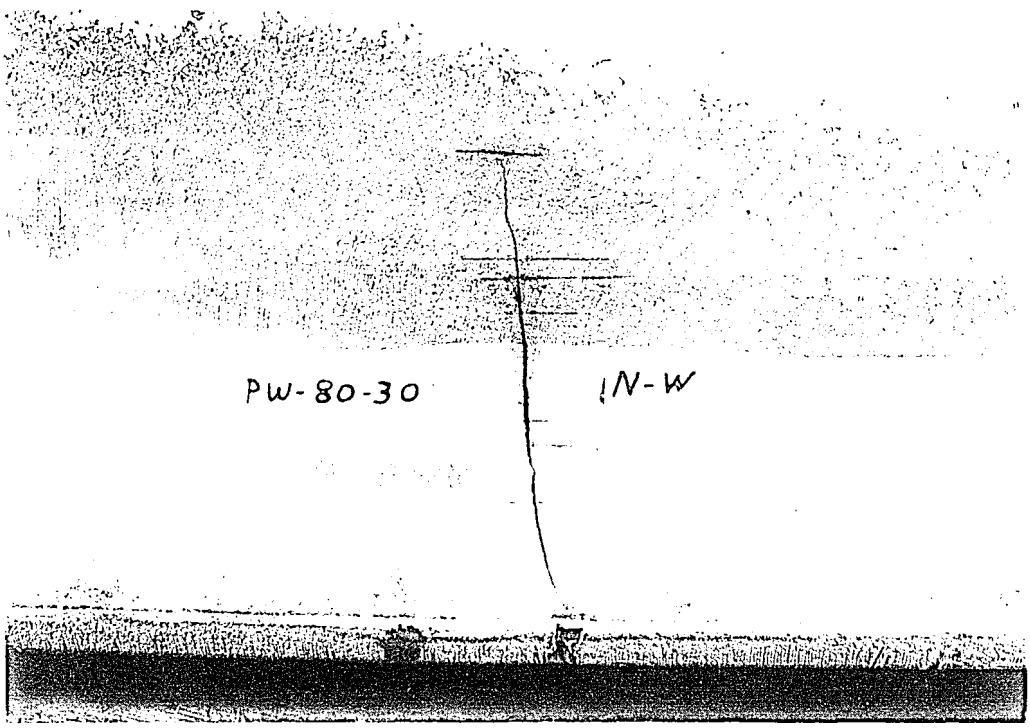


**Figure 7:** Typical Fatigue Crack at Failure.

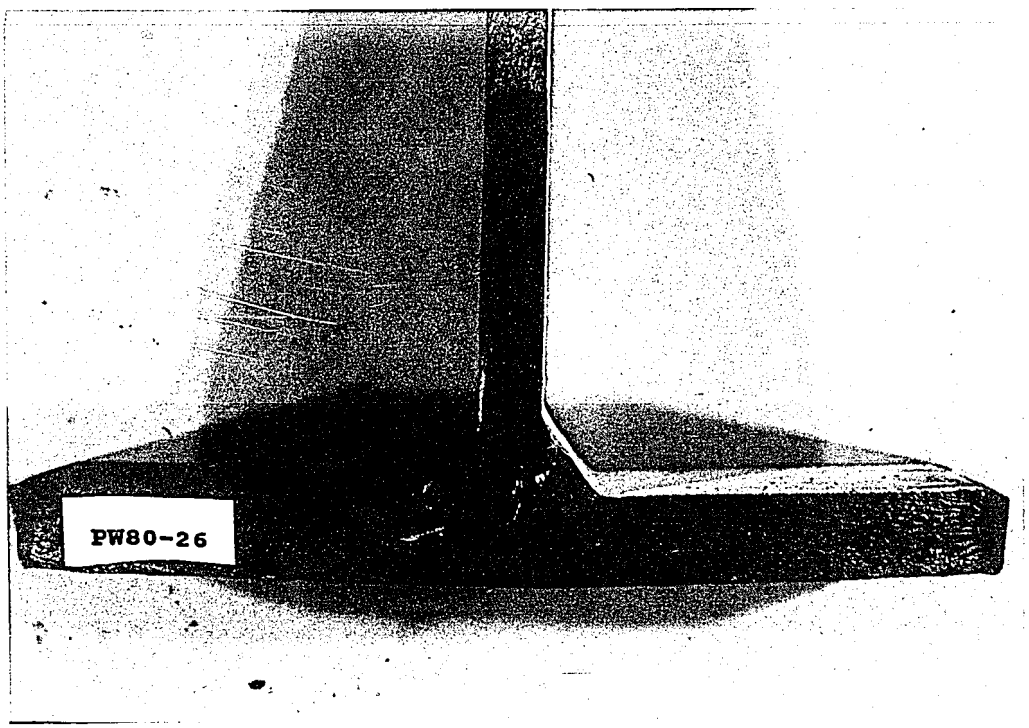


**Figure 8:** Typical Pore in Longitudinal Fillet Weld Surrounded By "Halo" or Region of Quasi-cleavage Crack Growth Possibly Associated With Hydrogen.

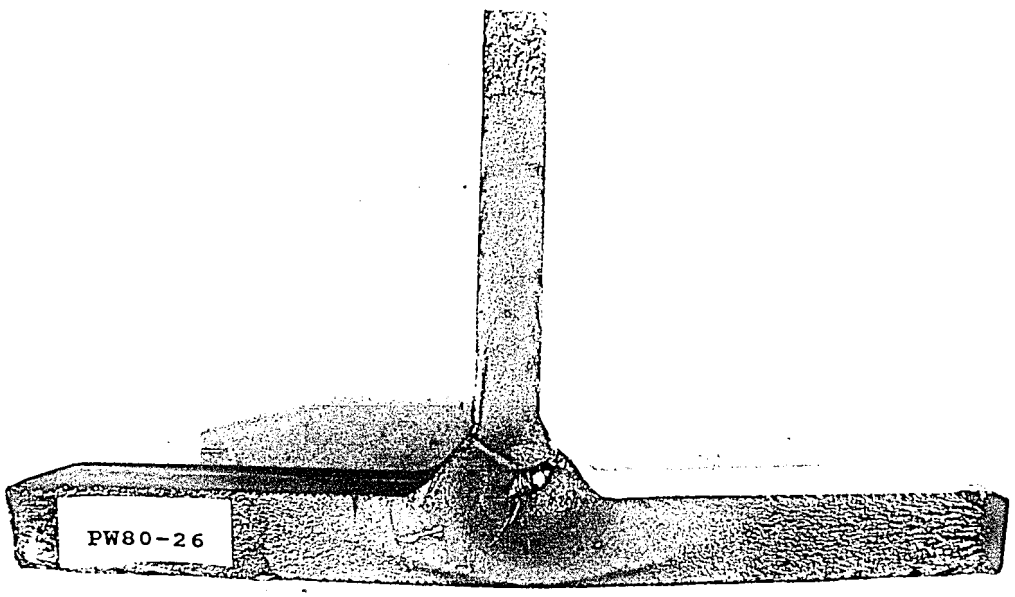


**Figure 8:** Typical Pore in Longitudinal Fillet Weld Surrounded By "Halo" or Region of Quasi-cleavage Crack Growth Possibly Associated With Hydrogen.

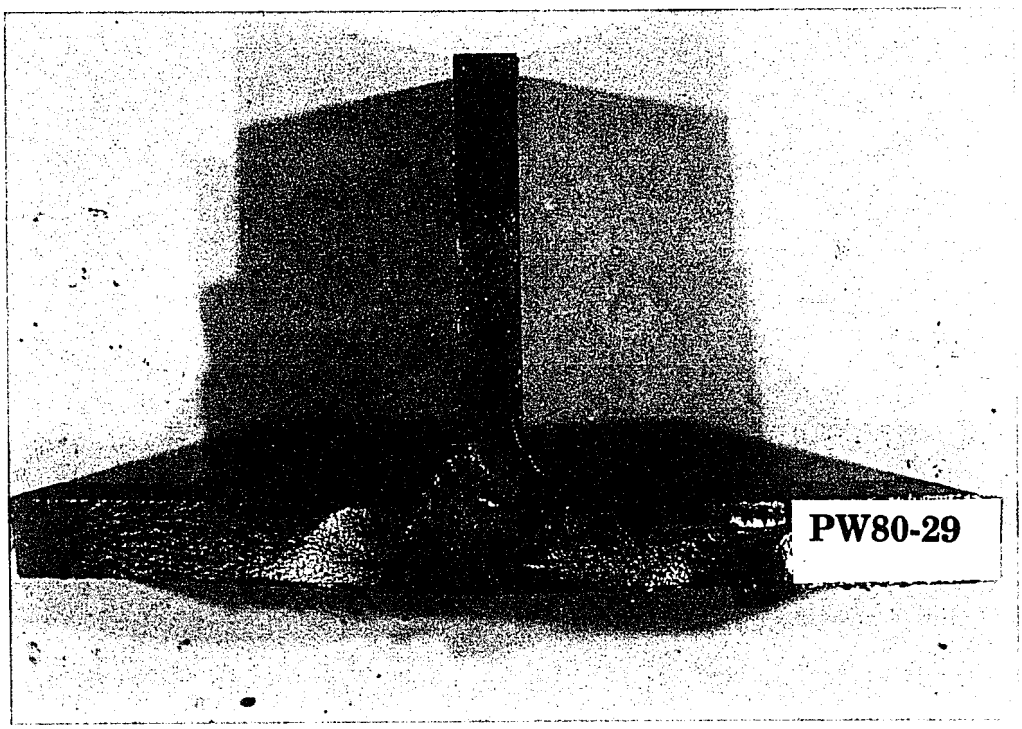


**Figure 9:** Typical Solid Inclusion in Longitudinal Fillet Weld Surrounded by "Halo" or Region of Quasi-cleavage Crack Growth Possibly Associated With Hydrogen.

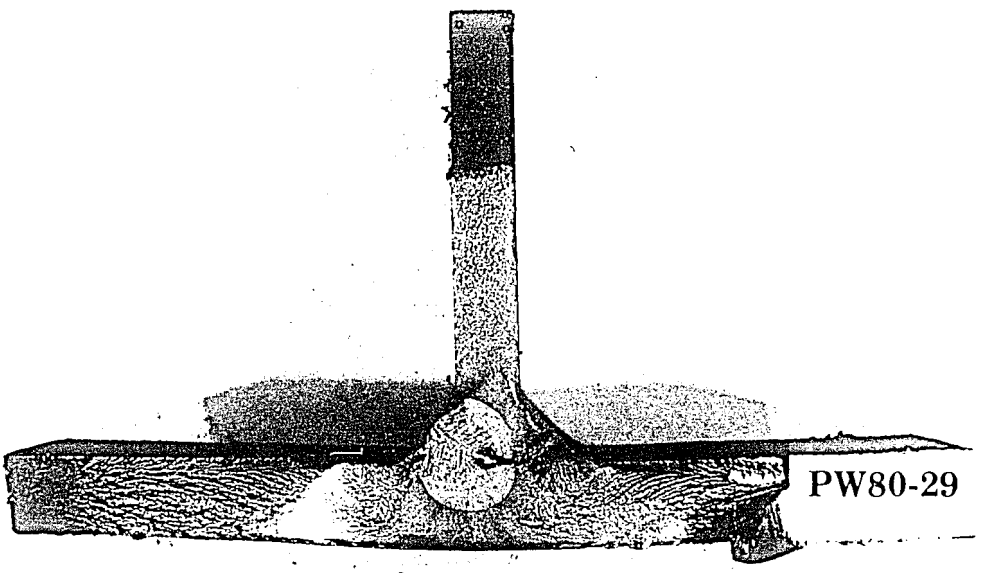


**Figure 9:** Typical Solid Inclusion in Longitudinal Fillet Weld Surrounded by "Halo" or Region of Quasi-cleavage Crack Growth Possibly Associated With Hydrogen.

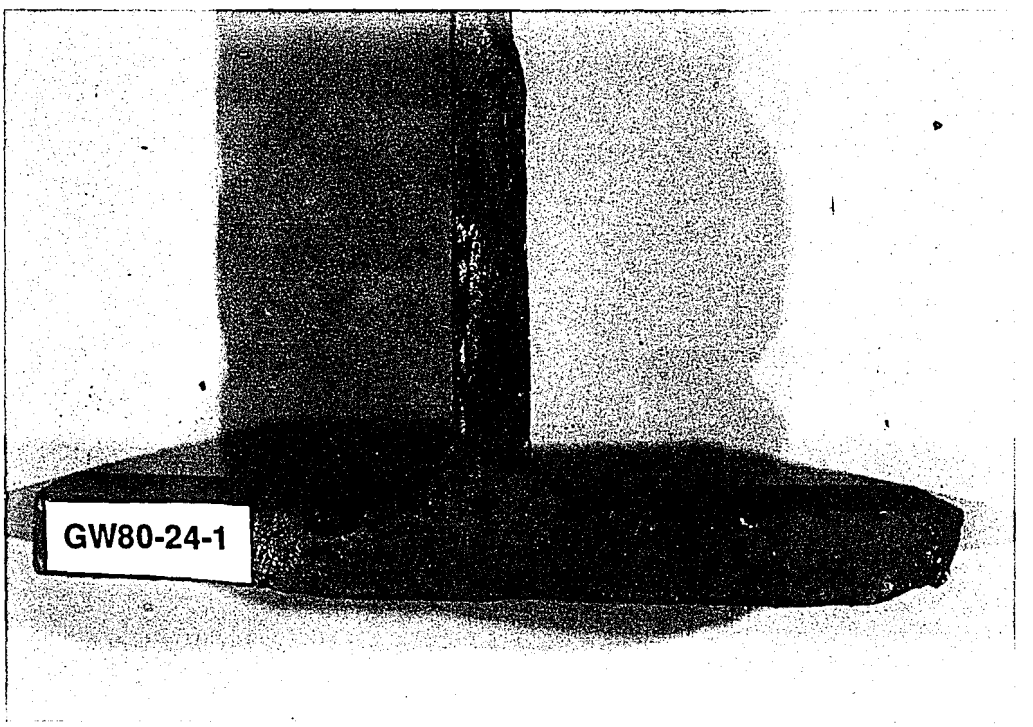


**Figure 10:** Typical Microcrack Along the Weld Toe.

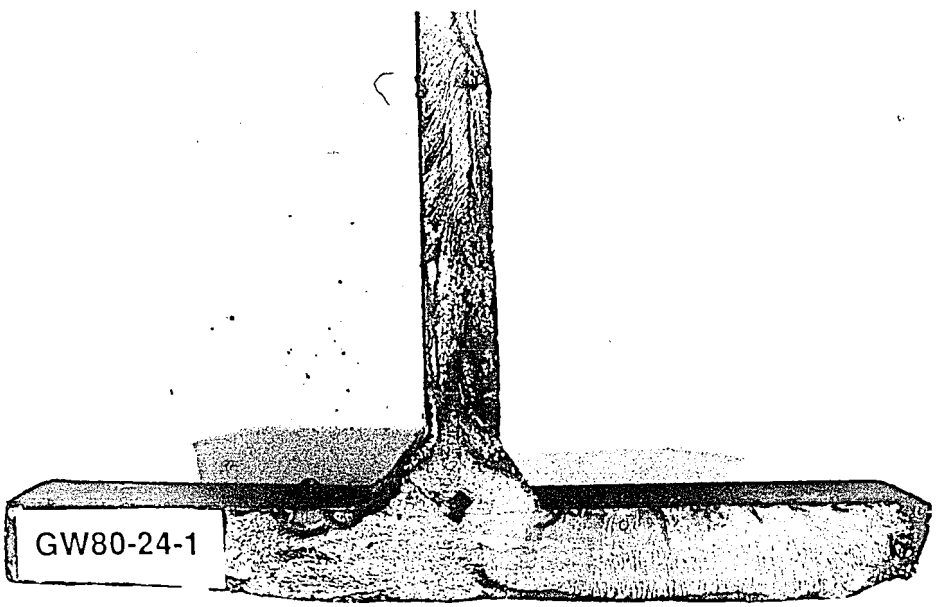


**Figure 10:** Typical Microcrack Along the Weld Toe.

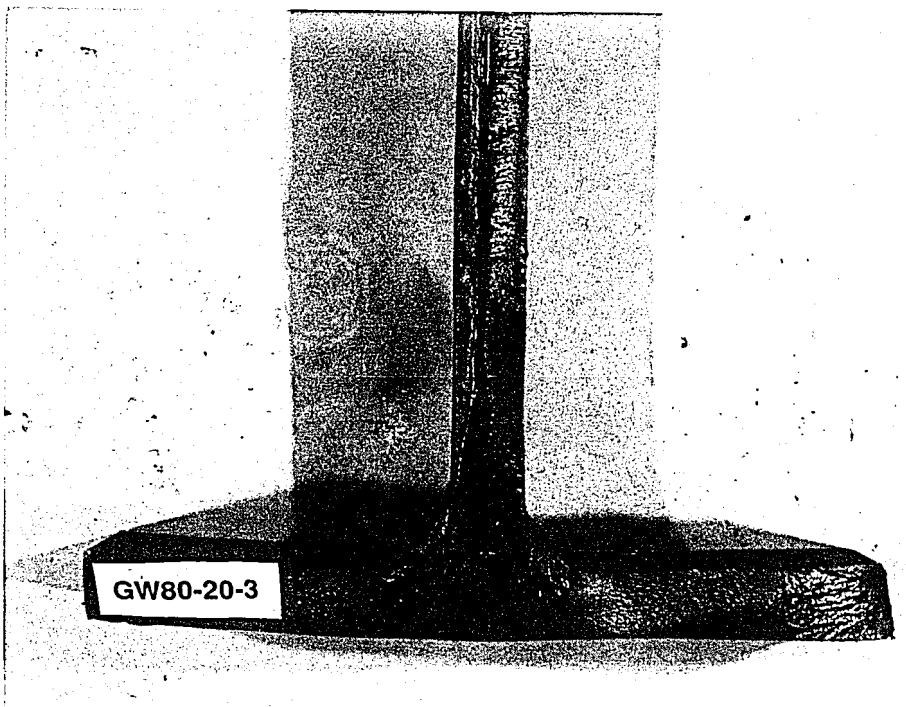


**Figure 11:** Typical Incomplete Penetration of Two-sided Groove Weld in 9.5mm Thick Web.

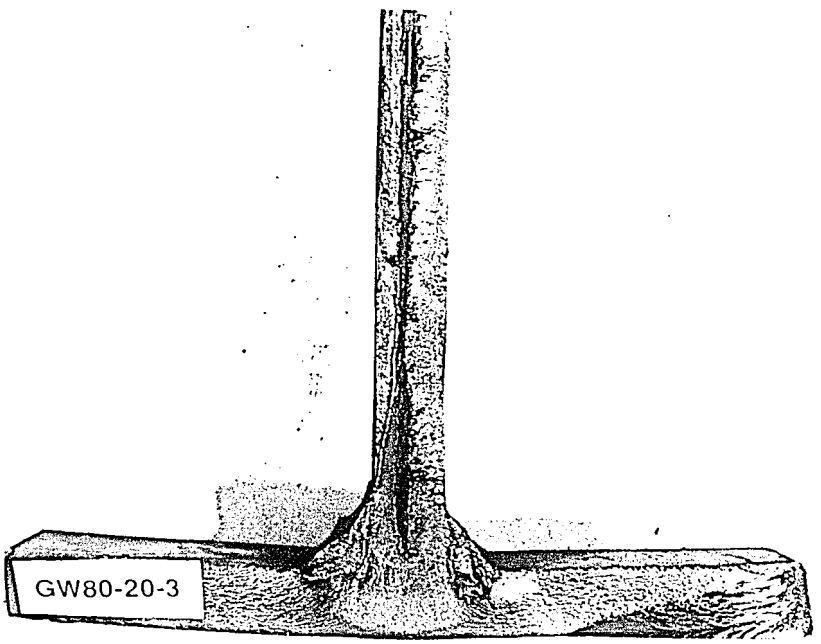


**Figure 11:** Typical Incomplete Penetration of Two-sided Groove Weld in 9.5mm Thick Web.

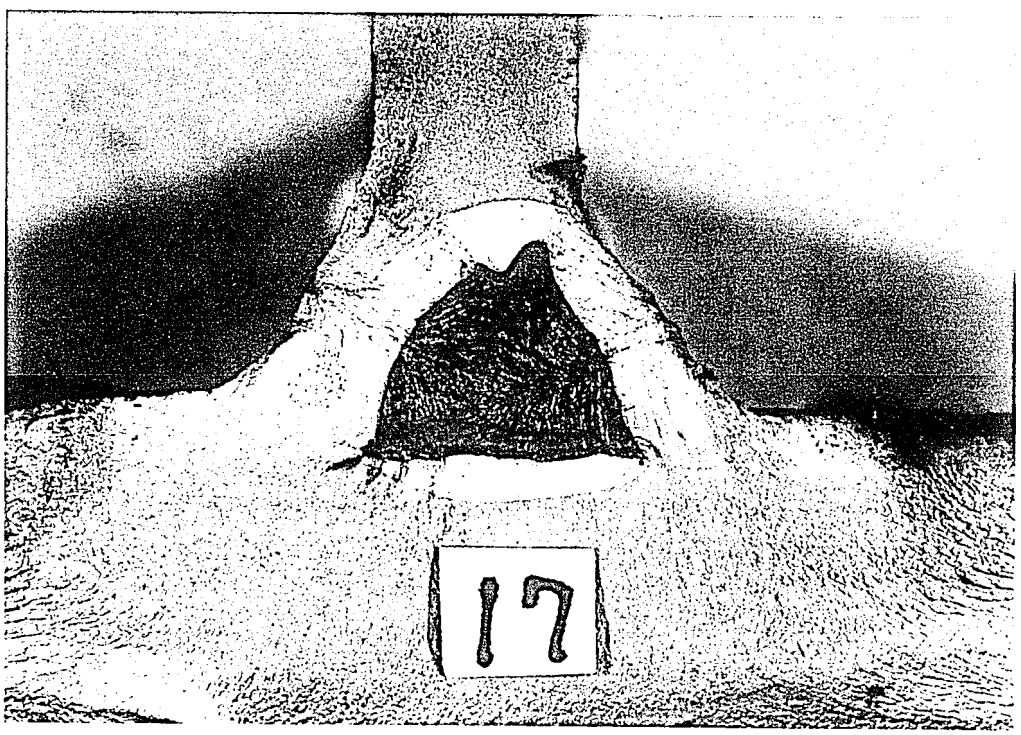


**Figure 12:** Typical Hydrogen Crack Observed on Fatigue Crack Surface at Intersection of Longitudinal Fillet Welds and Transverse Groove Weld.

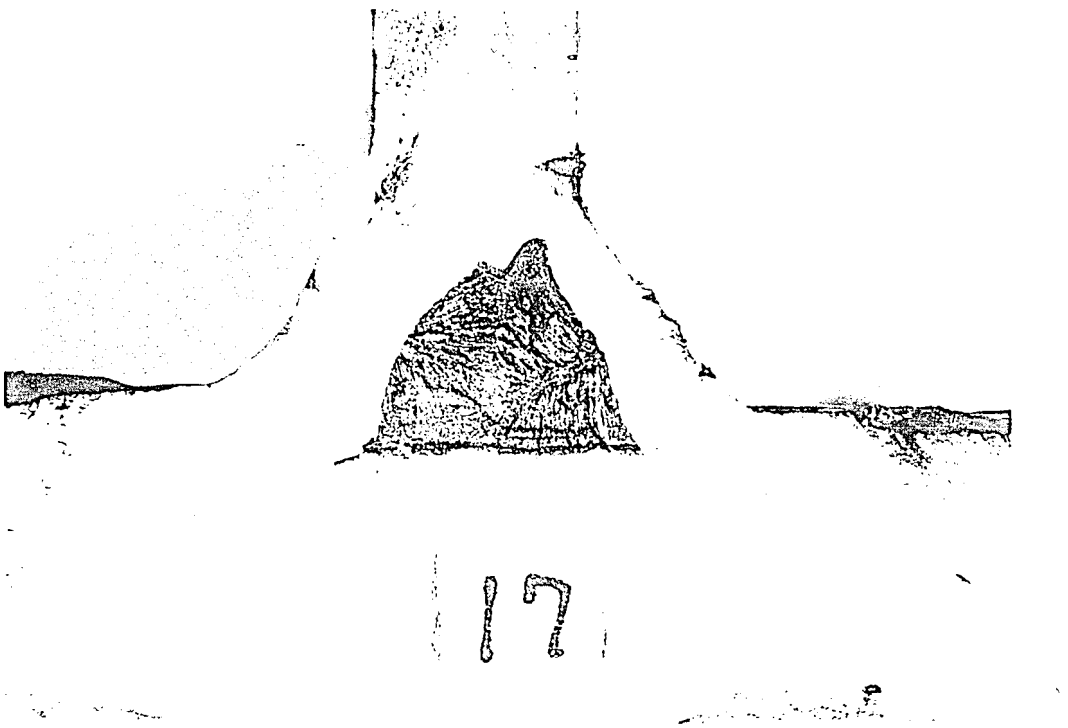


**Figure 12:** Typical Hydrogen Crack Observed on Fatigue Crack Surface at Intersection of Longitudinal Fillet Welds and Transverse Groove Weld.

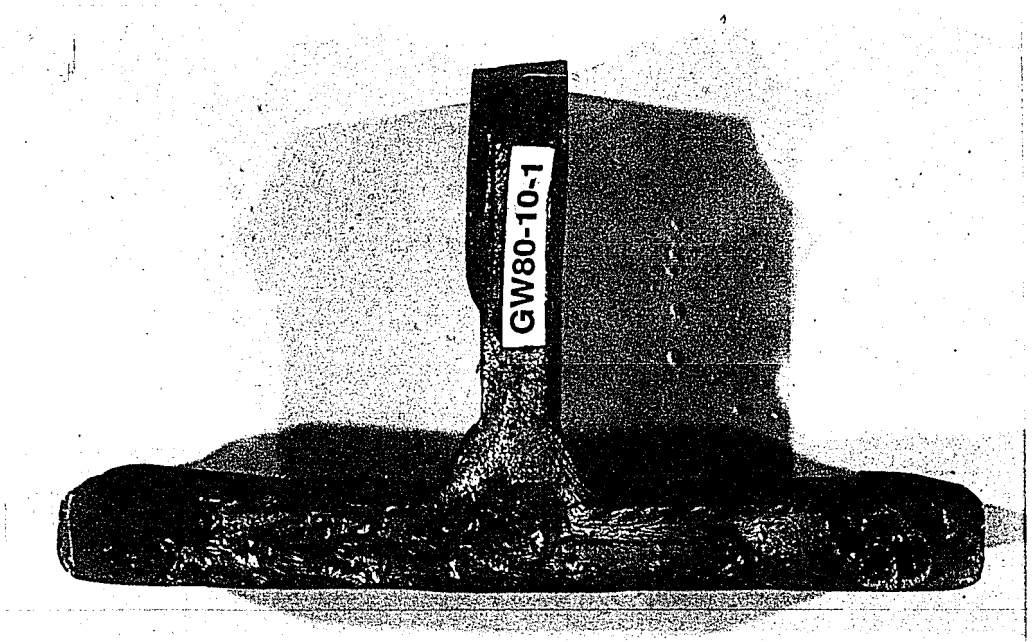


**Figure 13:** Typical Slag Inclusion in Transverse Groove Weld.

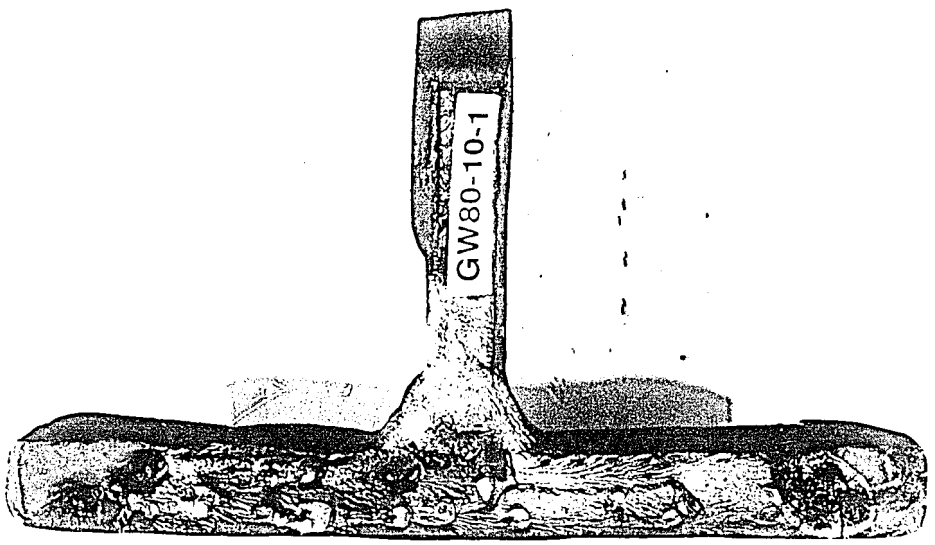


**Figure 13:** Typical Slag Inclusion in Transverse Groove Weld.

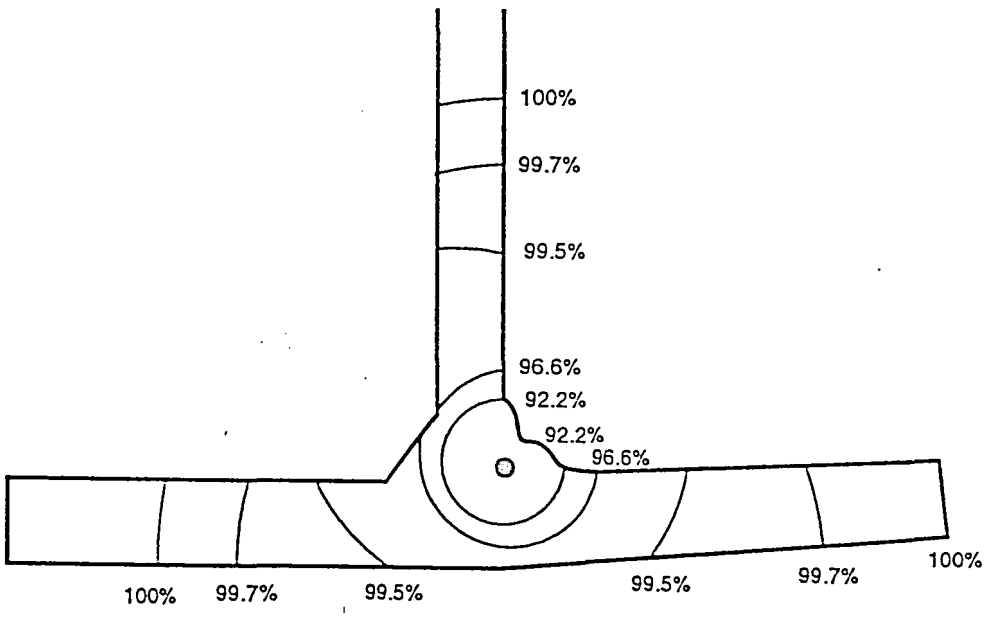


**Figure 14:** Penny Shaped Crack Growth From a Circular Solid Inclusion in a Longitudinal Fillet Weld Showing Crack Fronts As a Percentage of Total Fatigue Life.

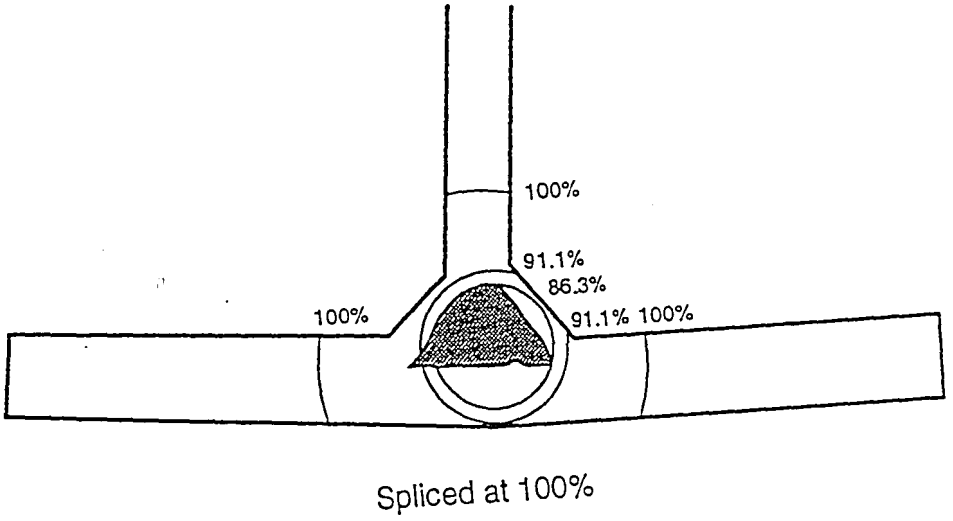


**Figure 15:** Penny Shaped Crack Growth From an Irregularly Shaped Hydrogen Related Crack in a Transverse Groove Weld Showing Crack Fronts As a Percentage of Total Fatigue Life.

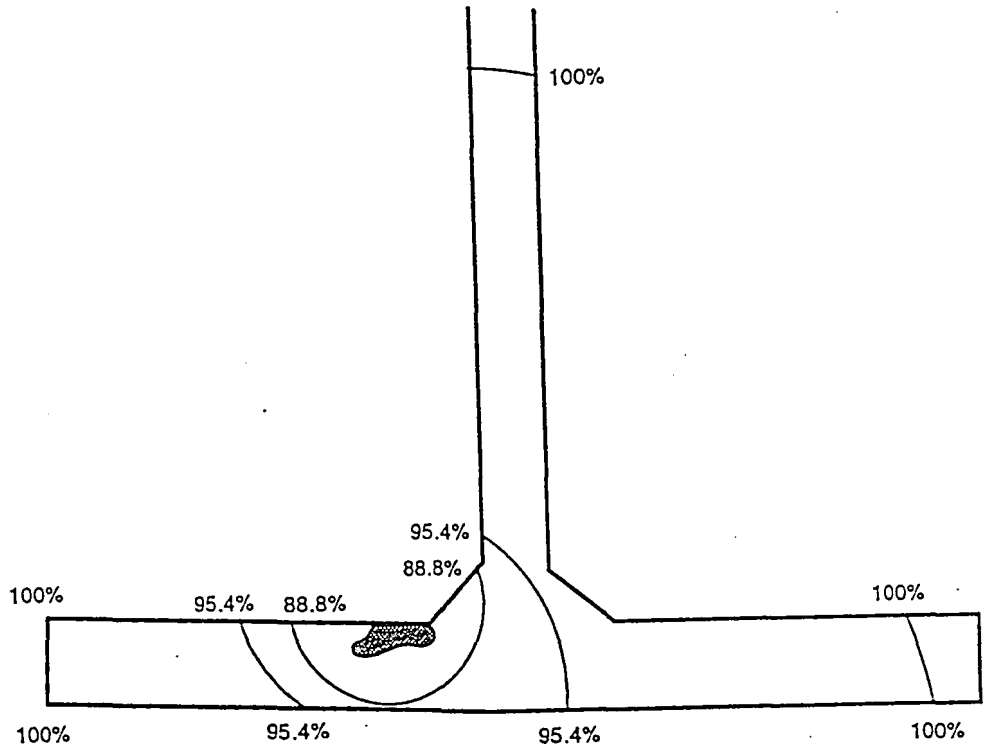


**Figure 16:** Penny Shaped Crack Growth From an Irregularly Shaped Slag Inclusion in a Transverse Groove Weld Showing Crack Fronts as a Percentage of Total Fatigue Life.

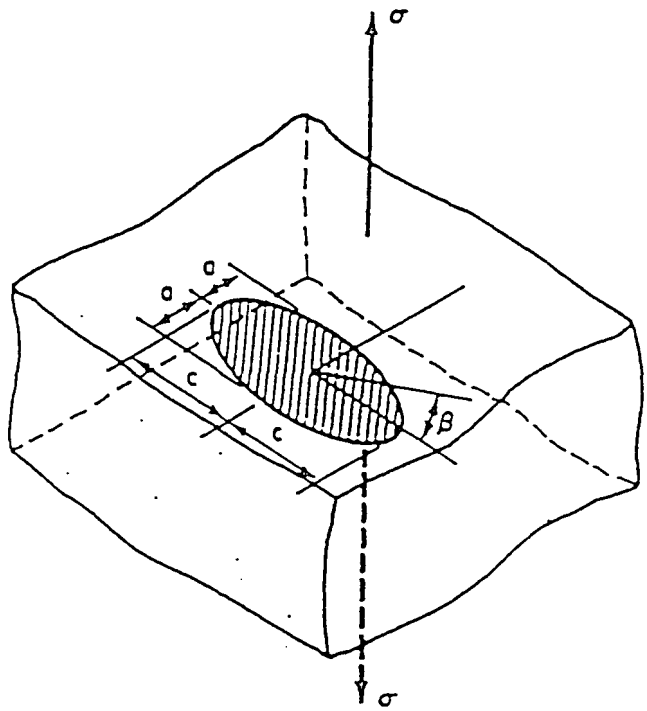


**Figure 17:** Elliptical Crack in an Infinite Body Subjected to Uniform Tension (Ref. 31).

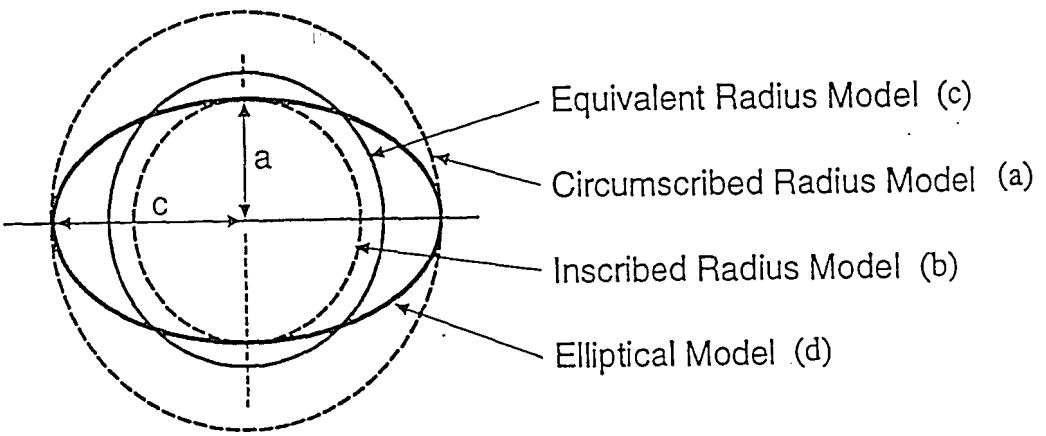


**Figure 18:** Initial Crack Size for Fatigue Life Prediction Models.
a) Circumscribed Radius Model
b) Inscribed Radius Model
c) Equivalent Radius Model
d) Elliptical Model

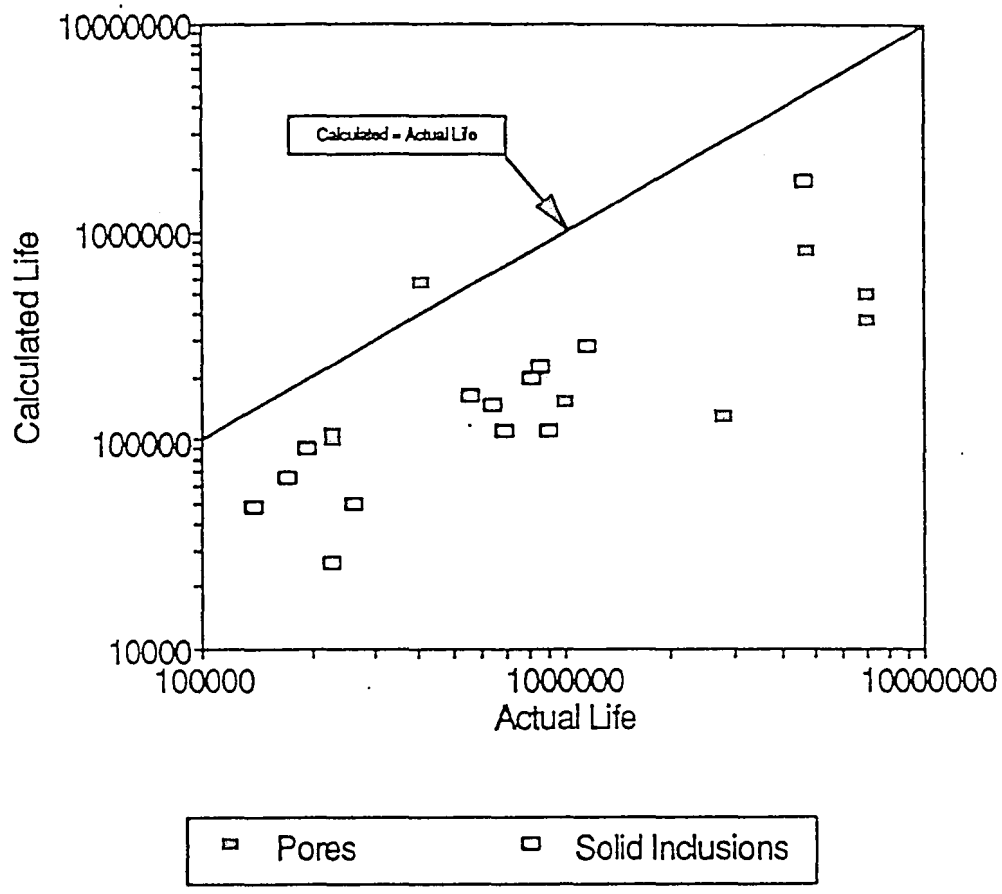


**Figure 19:** Fatigue Life of Longitudinal Fillet Weld Calculated Using the Circumscribed Radius Model with Initial Discontinuity Size Determined From Halo Dimensions.

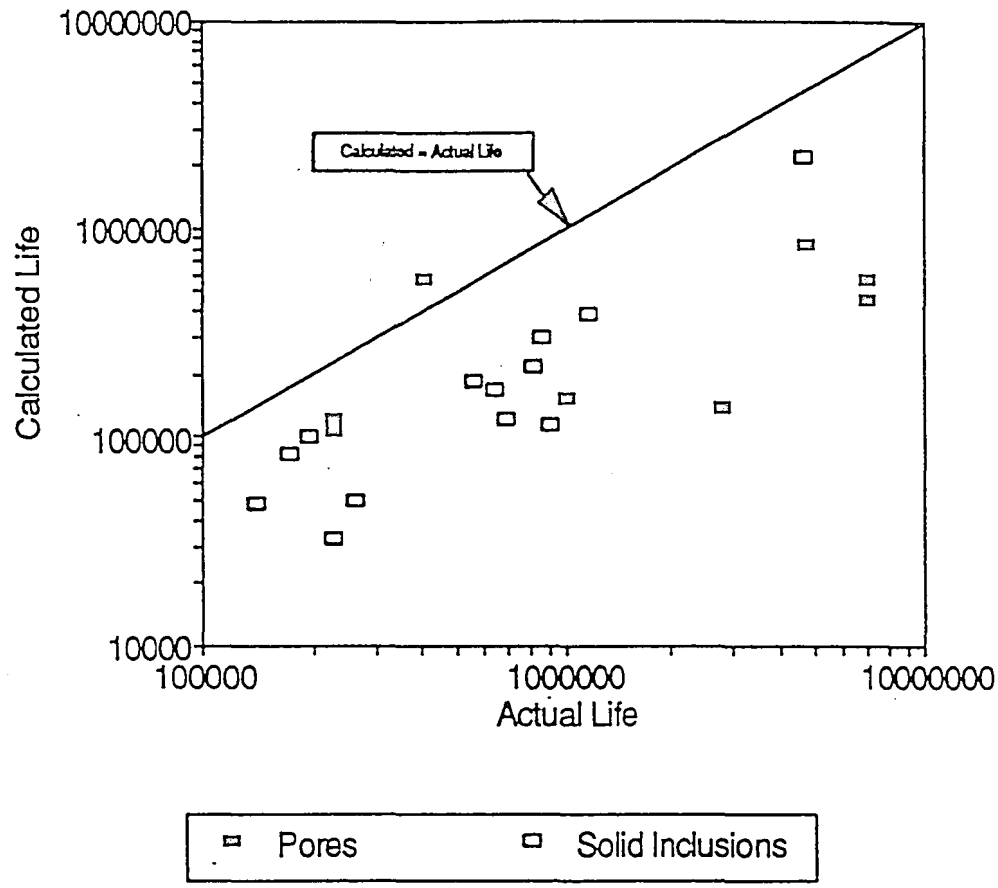


**Figure 20:** Fatigue Life of Longitudinal Fillet Weld Calculated Using the Inscribed Radius Model with Initial Discontinuity Size Determined From Halo Dimensions.

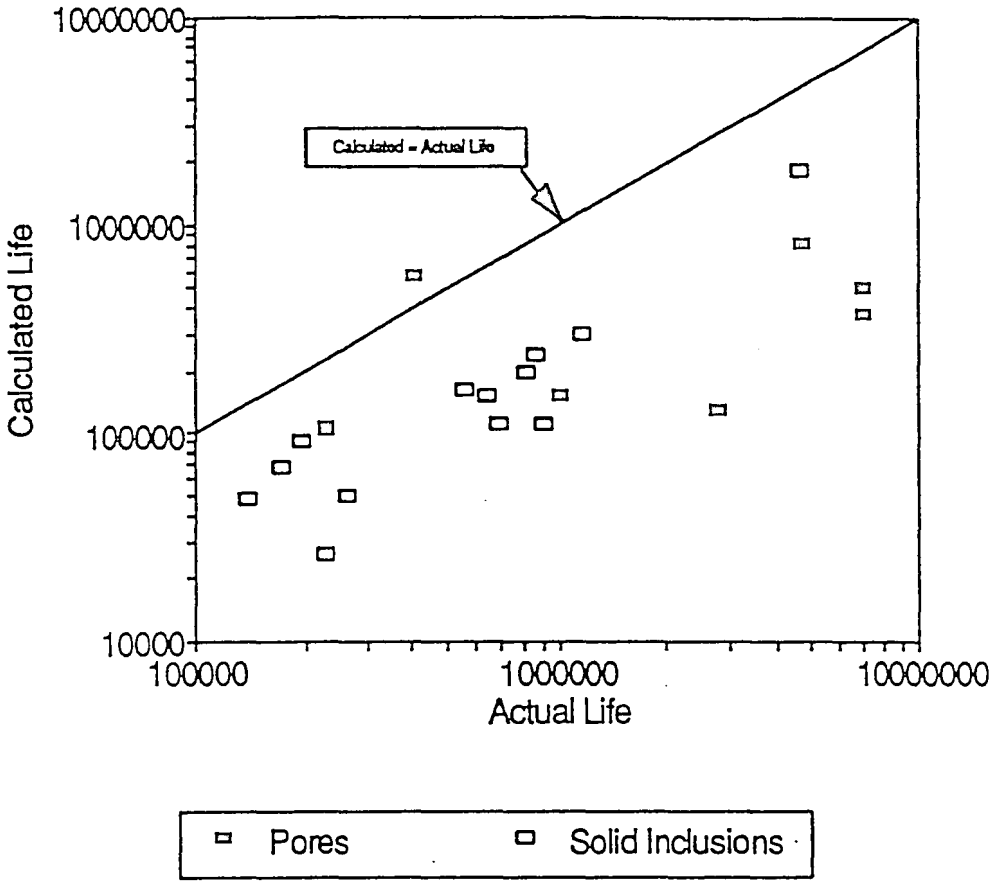


**Figure 21:** Fatigue Life of Longitudinal Fillet Weld Calculated Using the Equivalent Radius Model with Initial Discontinuity Size Determined From Halo Dimensions.

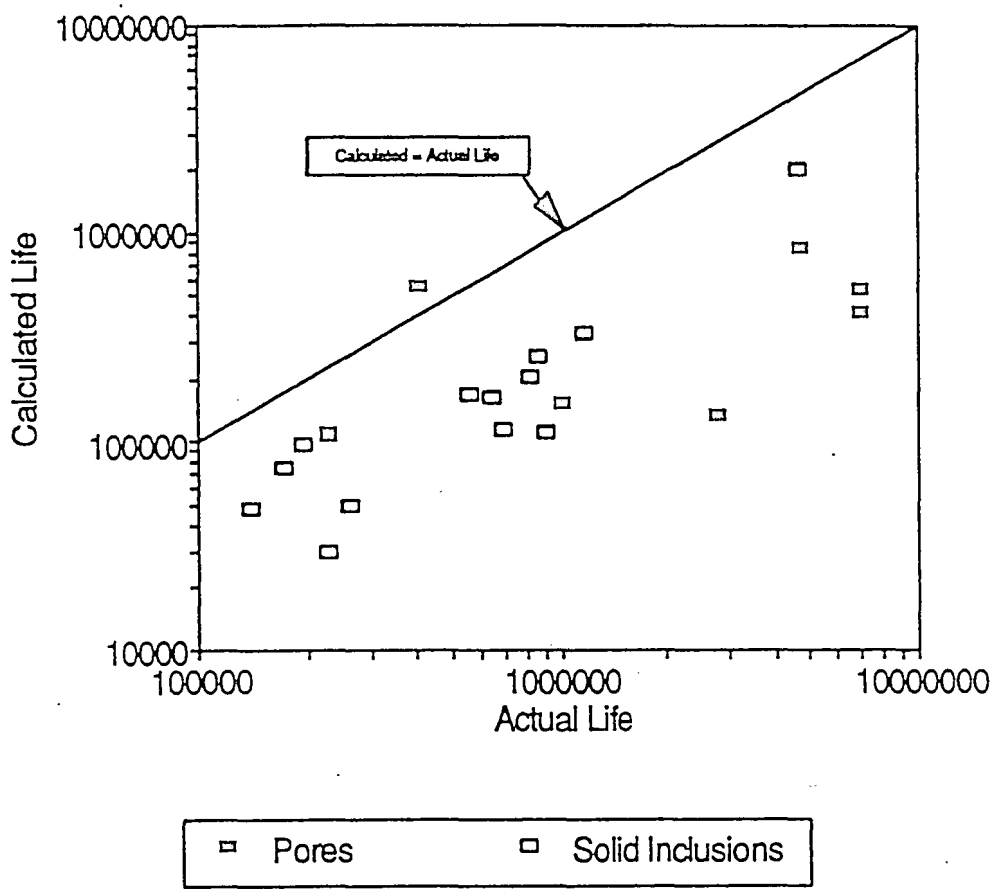


**Figure 22:** Fatigue Life of Longitudinal Fillet Weld Calculated Using the Elliptical Model with Initial Discontinuity Size Determined From Halo Dimensions.

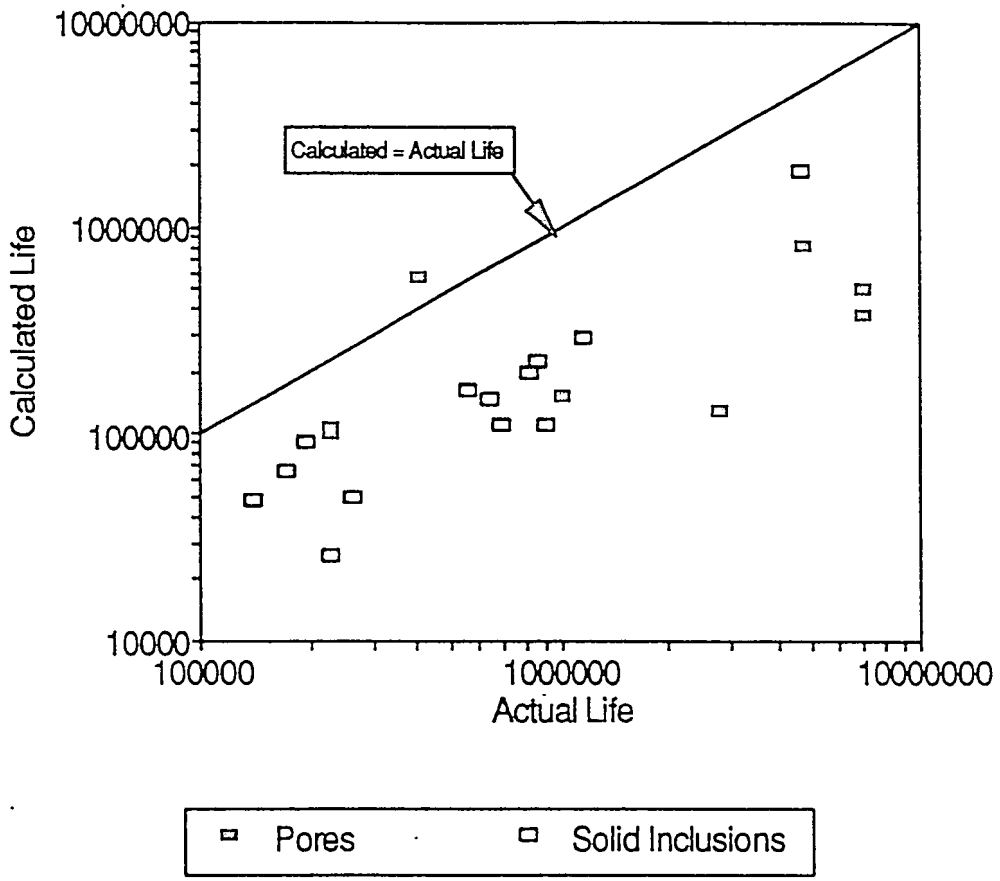


**Figure 23:** Fatigue Life of Longitudinal Fillet Weld Calculated Using the Combination Model with Initial Discontinuity Size Determined From Halo Dimensions.

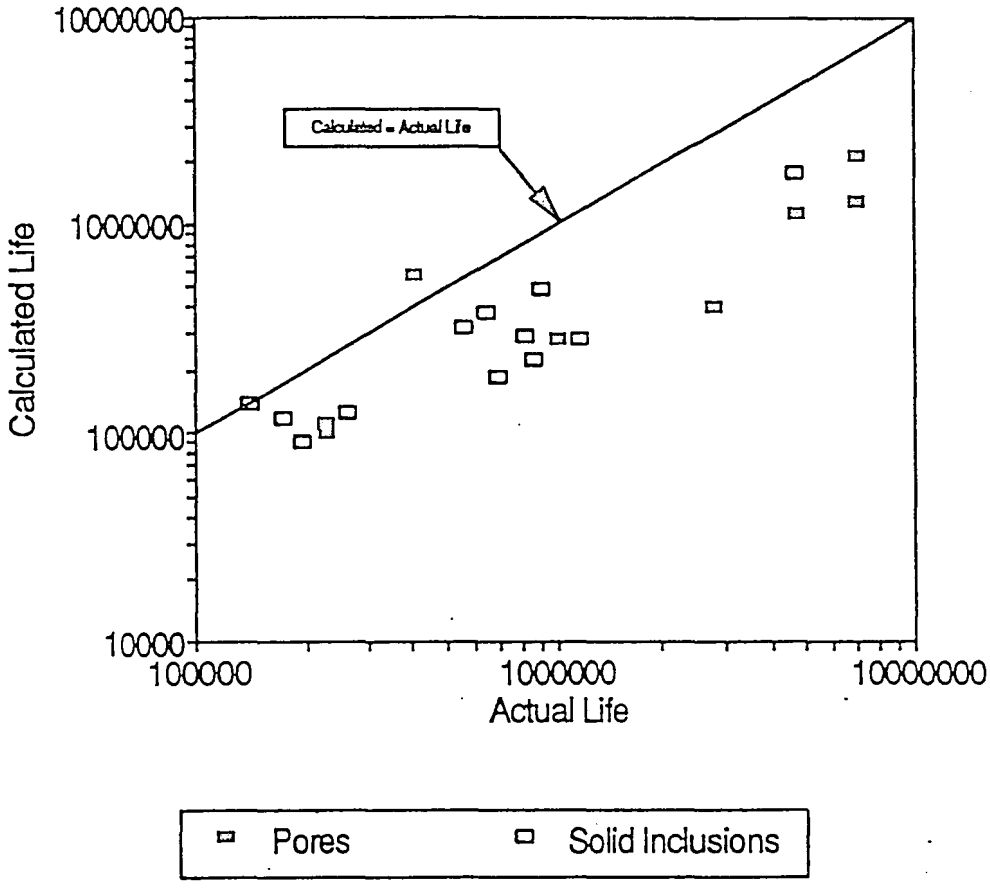


**Figure 24:** Fatigue Life of Longitudinal Fillet Weld Calculated Using the Circumscribed Radius Model with Initial Discontinuity Size Determined From Actual Discontinuity Dimensions.

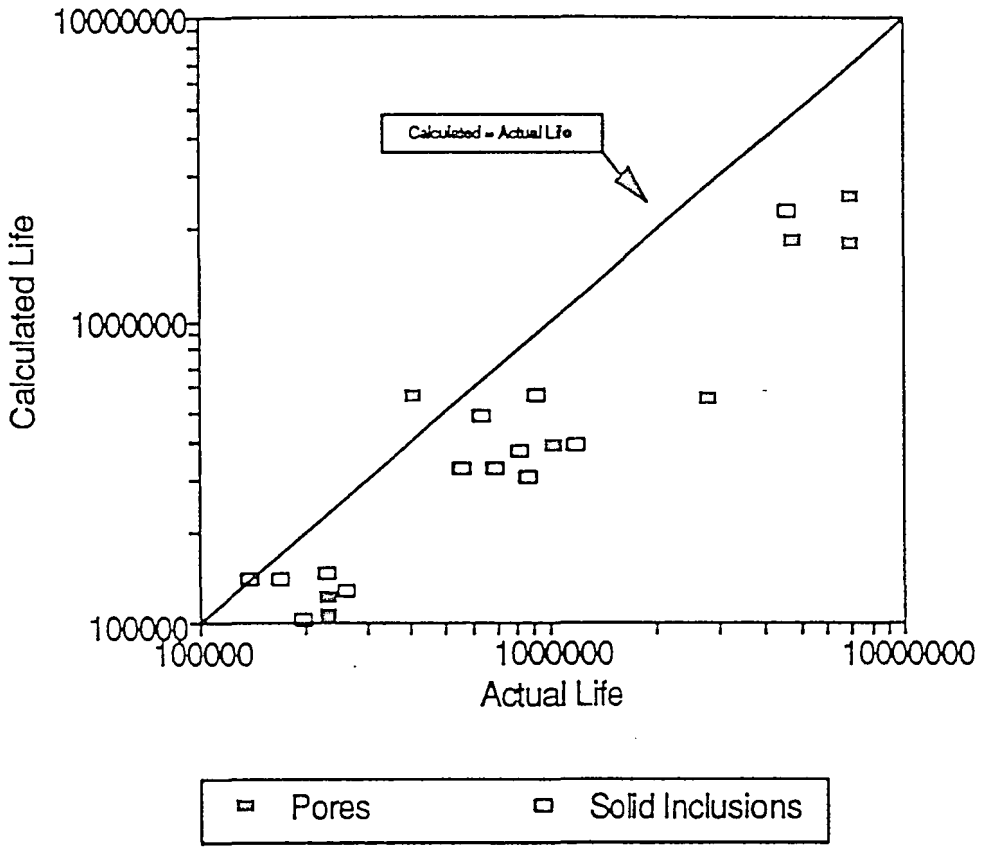


**Figure 25:** Fatigue Life of Longitudinal Fillet Weld Calculated Using the Inscribed Radius Model with Initial Discontinuity Size Determined From Actual Discontinuity Dimensions.

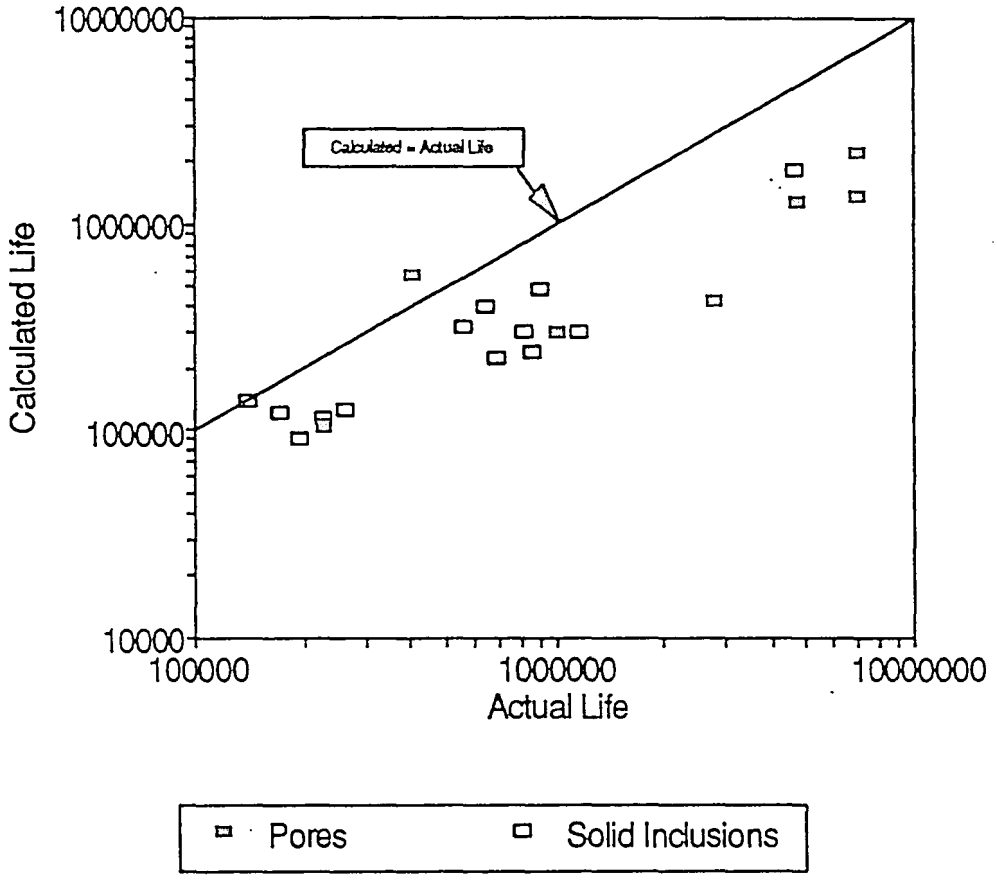


**Figure 26:** Fatigue Life of Longitudinal Fillet Weld Calculated Using the Equivalent Radius Model with Initial Discontinuity Size Determined From Actual Discontinuity Dimensions.

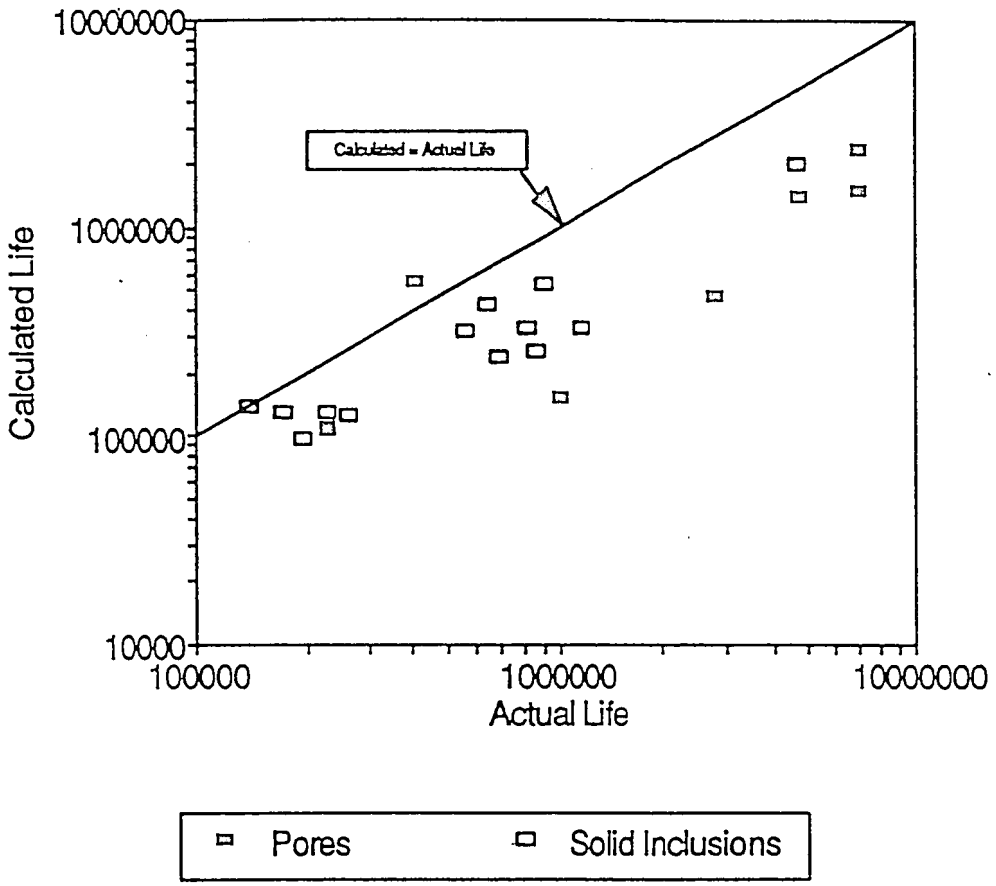


**Figure 27:** Fatigue Life of Longitudinal Fillet Weld Calculated Using the Elliptical Model with Initial Discontinuity Size Determined From Actual Discontinuity Dimensions.

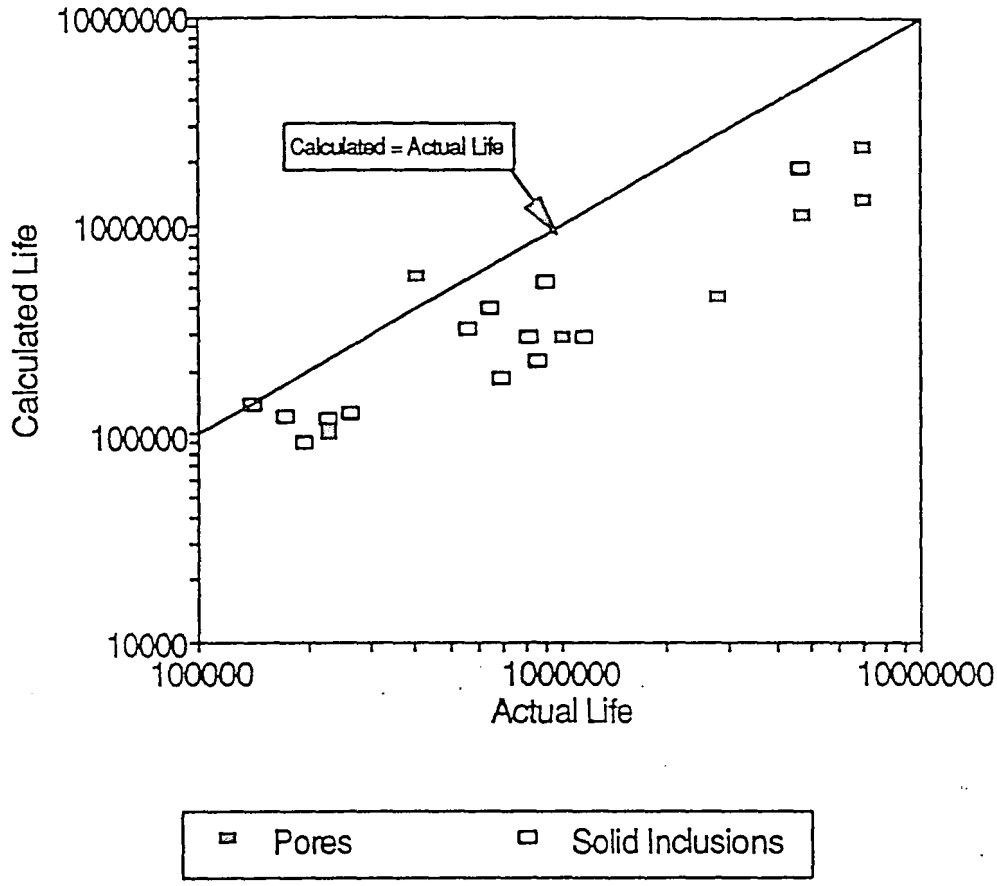


**Figure 28:** Fatigue Life of Longitudinal Fillet Weld Calculated Using the Combination Model with Initial Discontinuity Size Determined From Actual Discontinuity Dimensions.

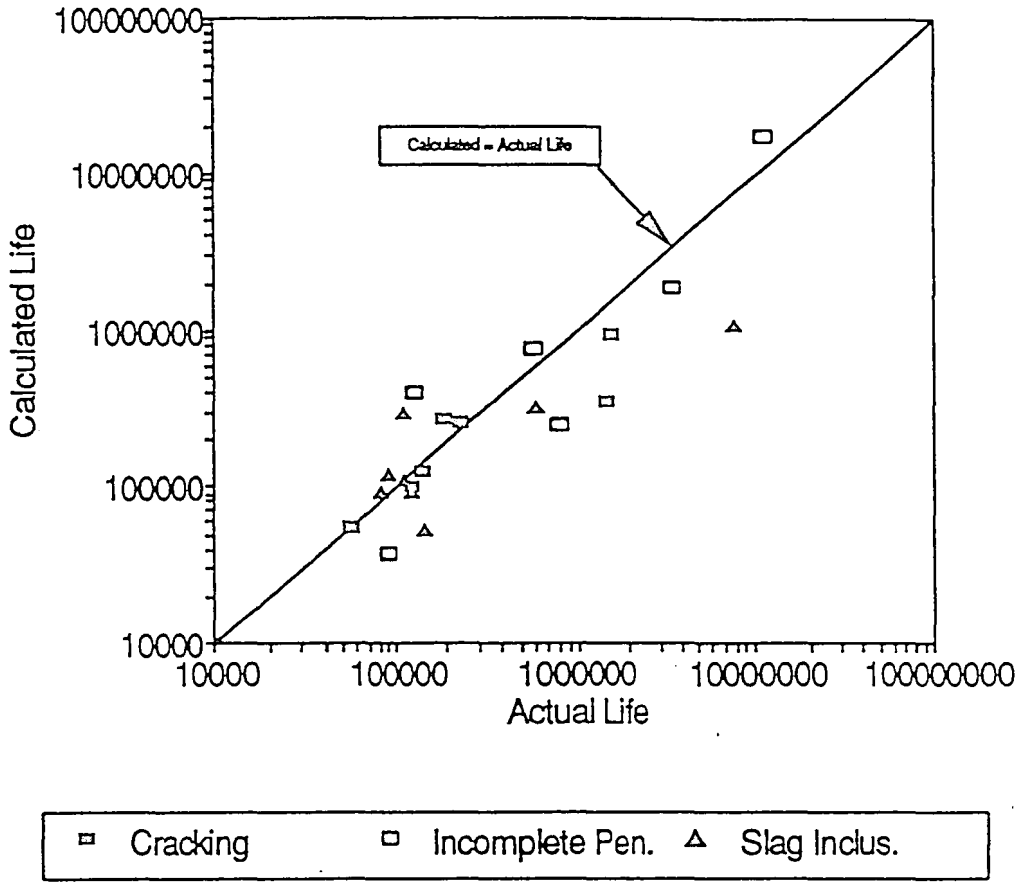


**Figure 29:** Fatigue Life of Transverse Groove Weld Calculated Using the Circumscribed Model with Initial Discontinuity Size Determined From Halo Dimensions.

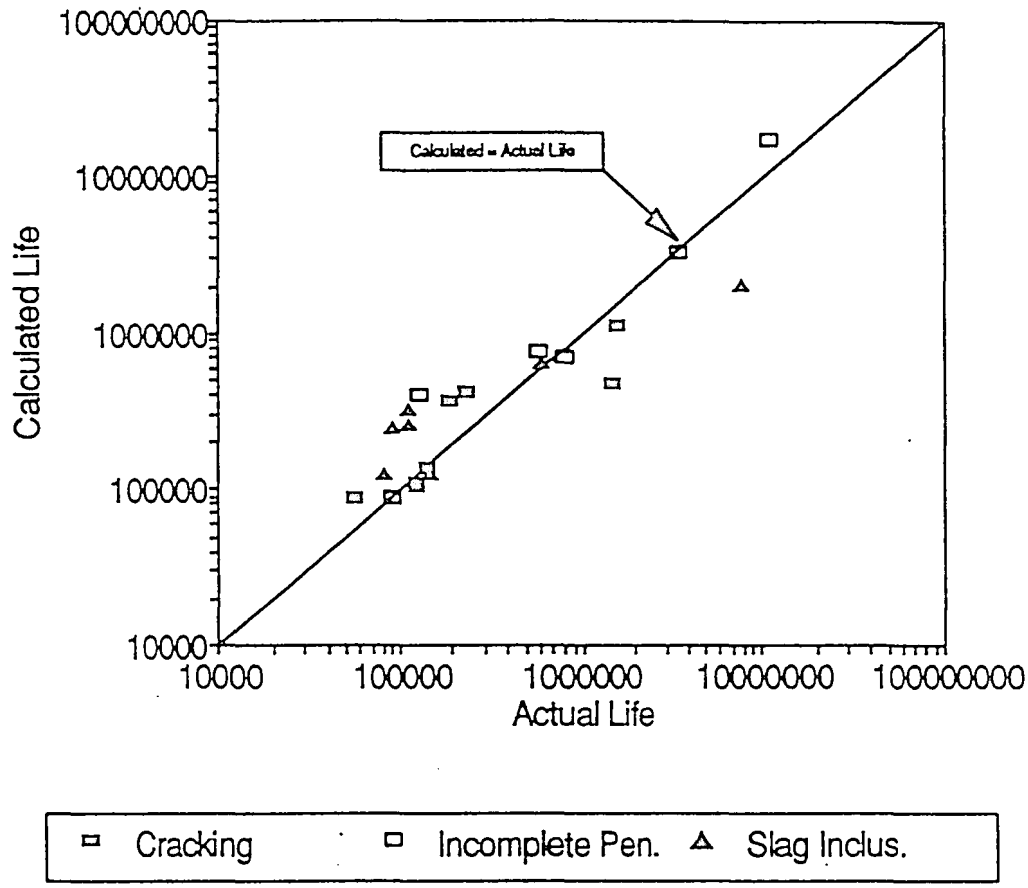


**Figure 30:** Fatigue Life of Transverse Groove Weld Calculated Using the Inscribed Radius Model with Initial Discontinuity Size Determined From Halo Dimensions.

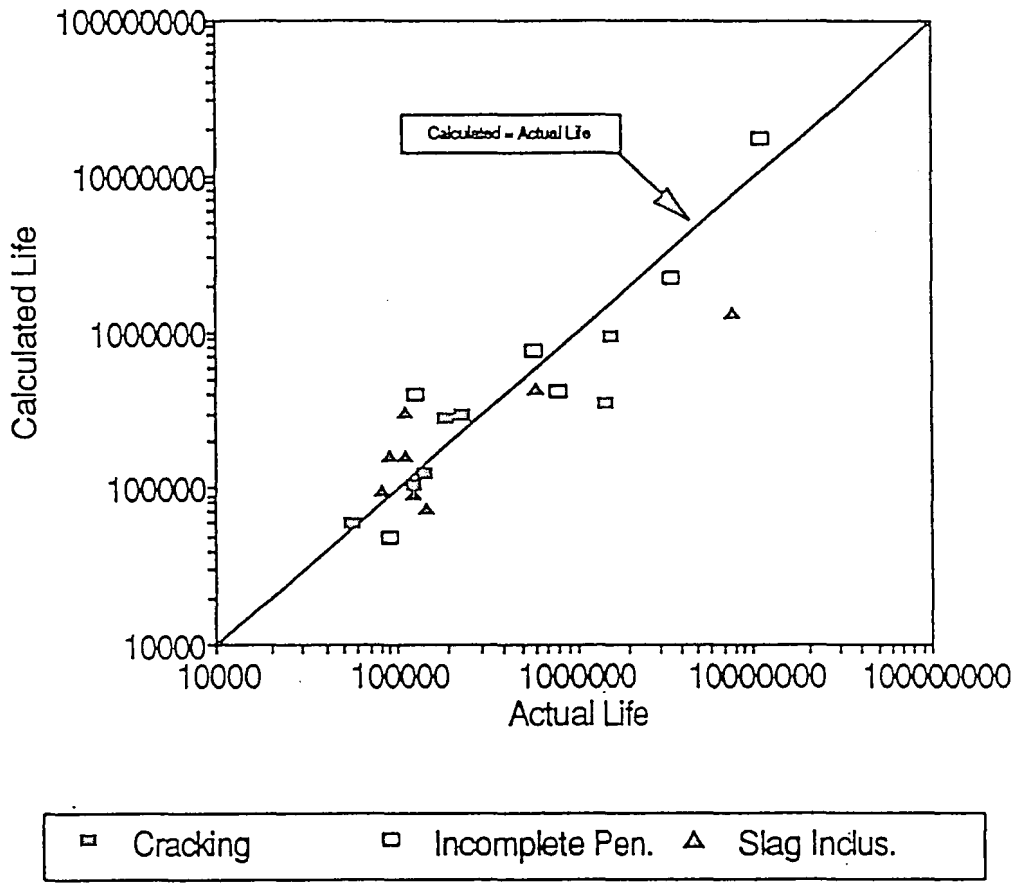


**Figure 31:** Fatigue Life of Transverse Groove Weld Calculated Using the Equivalent Model with Initial Discontinuity Size Determined From Halo Dimensions.

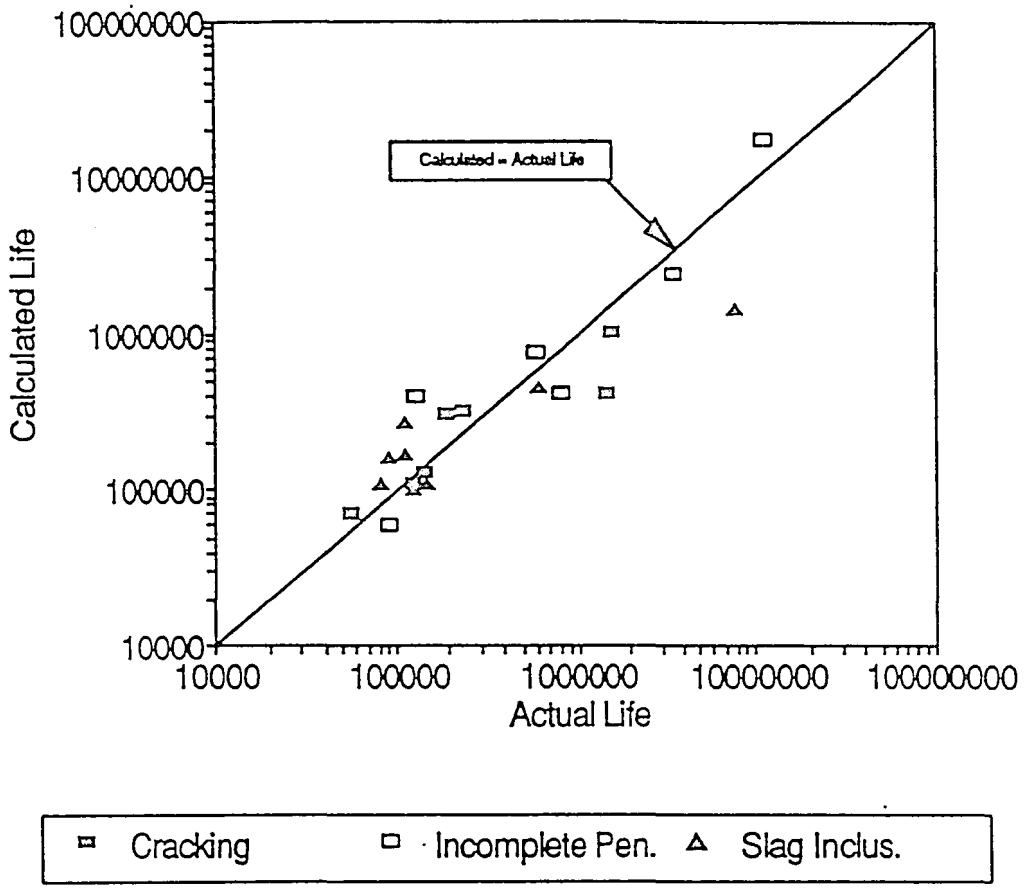


**Figure 32:** Fatigue Life of Transverse Groove Weld Calculated Using the Elliptical Model with Initial Discontinuity Size Determined From Halo Dimensions.

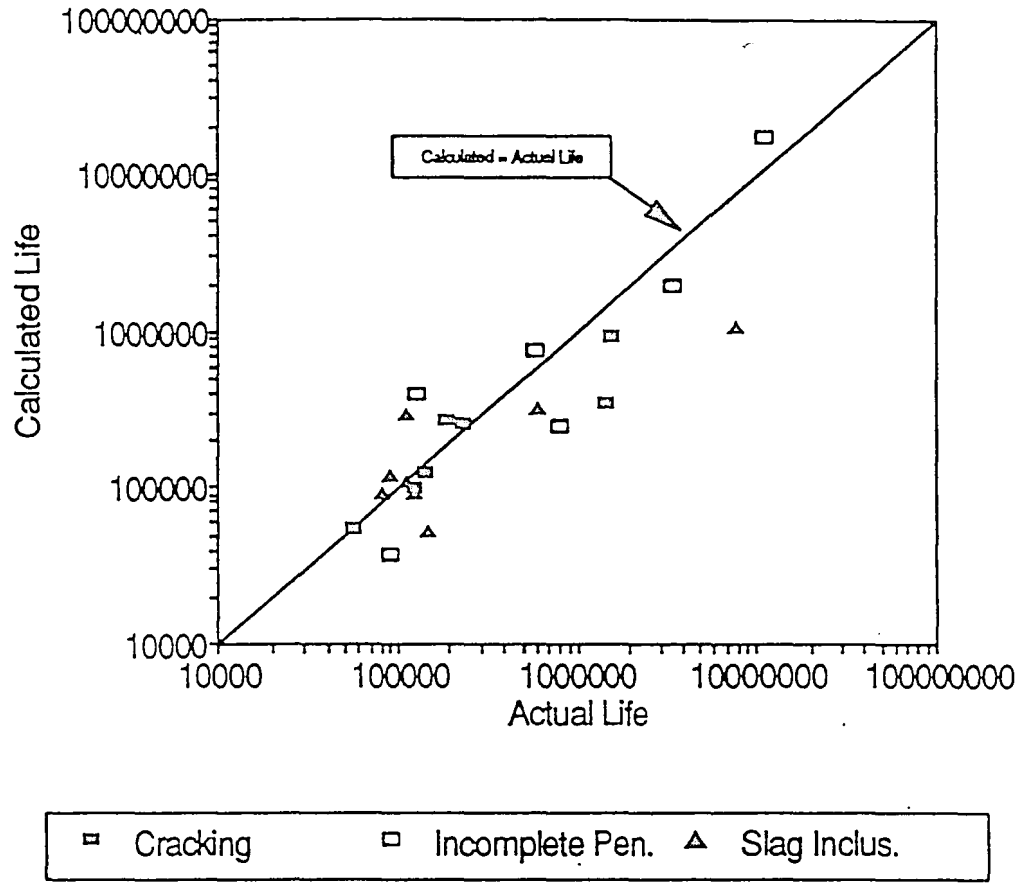


**Figure 33:** Fatigue Life of Transverse Groove Weld Calculated Using the Combination Model with Initial Discontinuity Size Determined From Halo Dimensions.

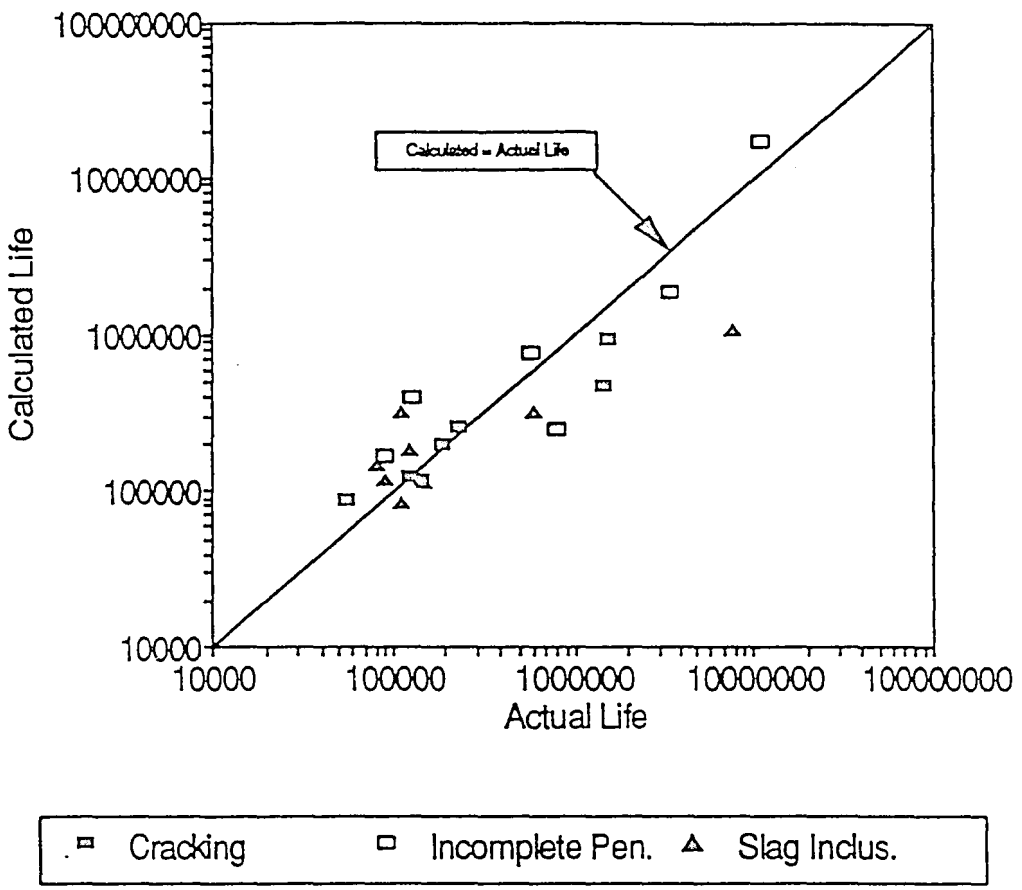


**Figure 34:** Fatigue Life of Transverse Groove Weld Calculated Using the Circumscribed Model with Initial Discontinuity Size Determined From actual Discontinuity Dimensions.

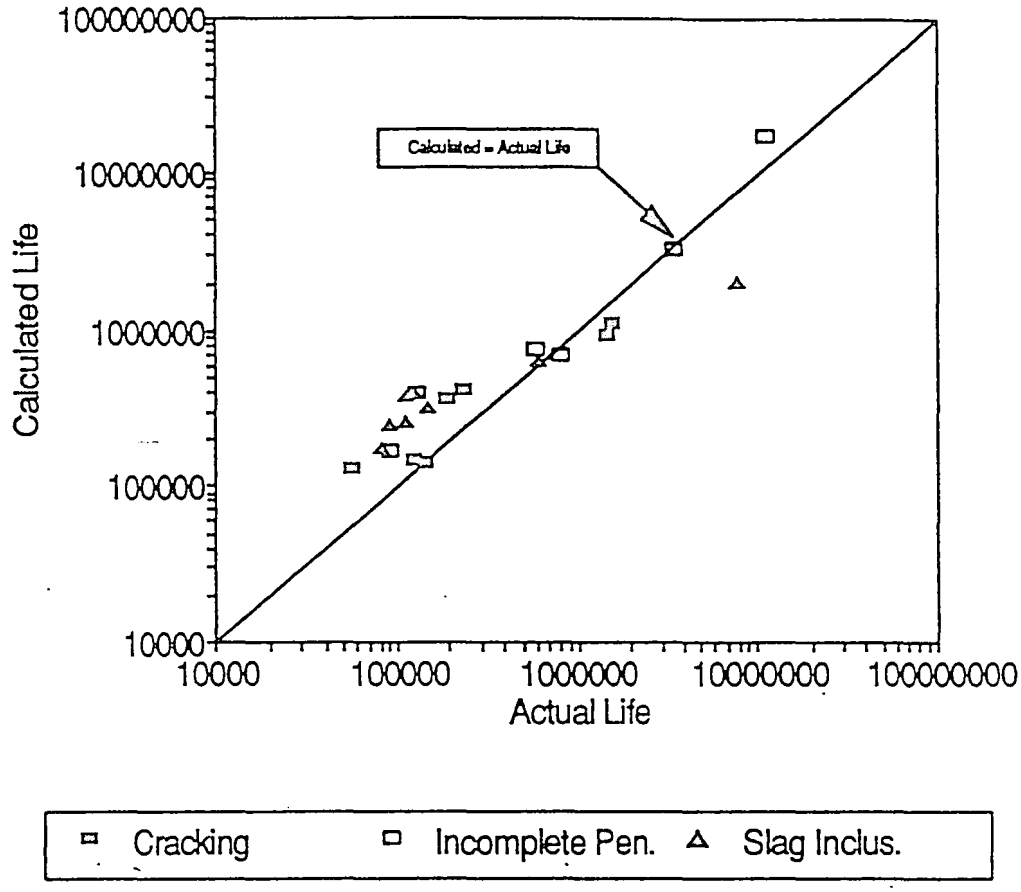


**Figure 35:** Fatigue Life of Transverse Groove Weld Calculated Using the Inscribed Radius Model with Initial Discontinuity Size Determined From Actual Discontinuity Dimensions.

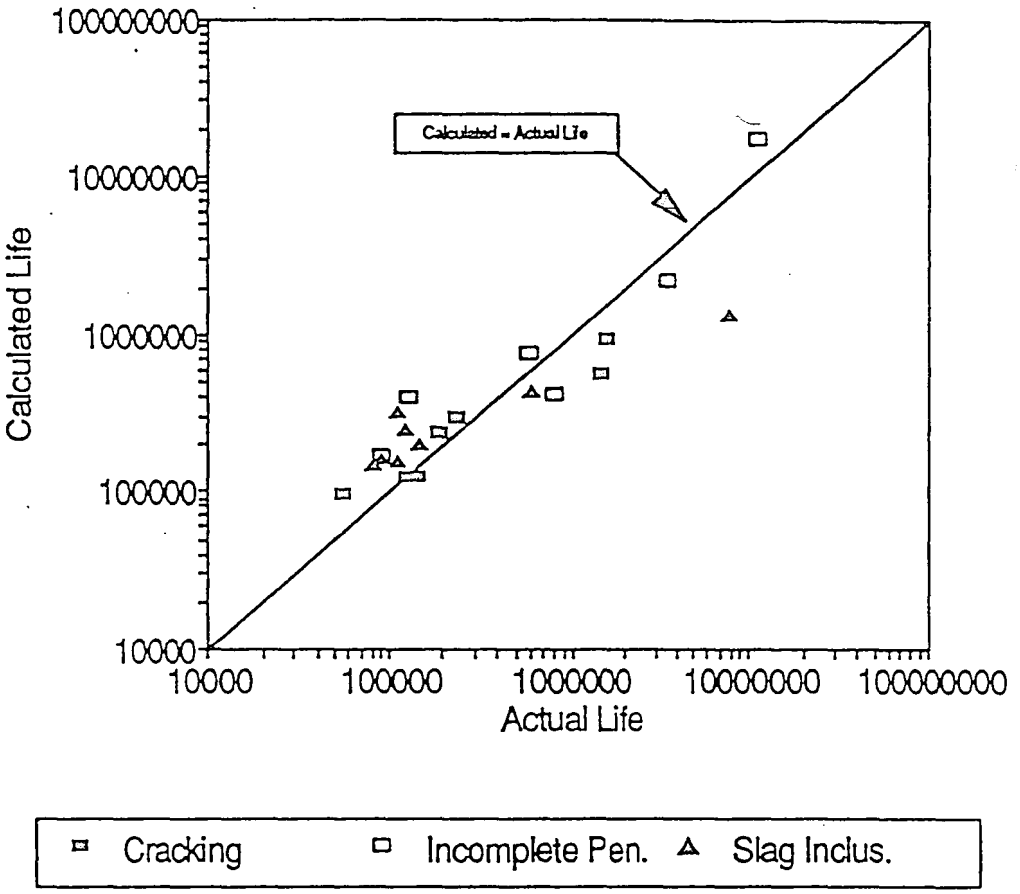


**Figure 36:** Fatigue Life of Transverse Groove Weld Calculated Using the Equivalent Model with Initial Discontinuity Size Determined From Actual Discontinuity Dimensions.

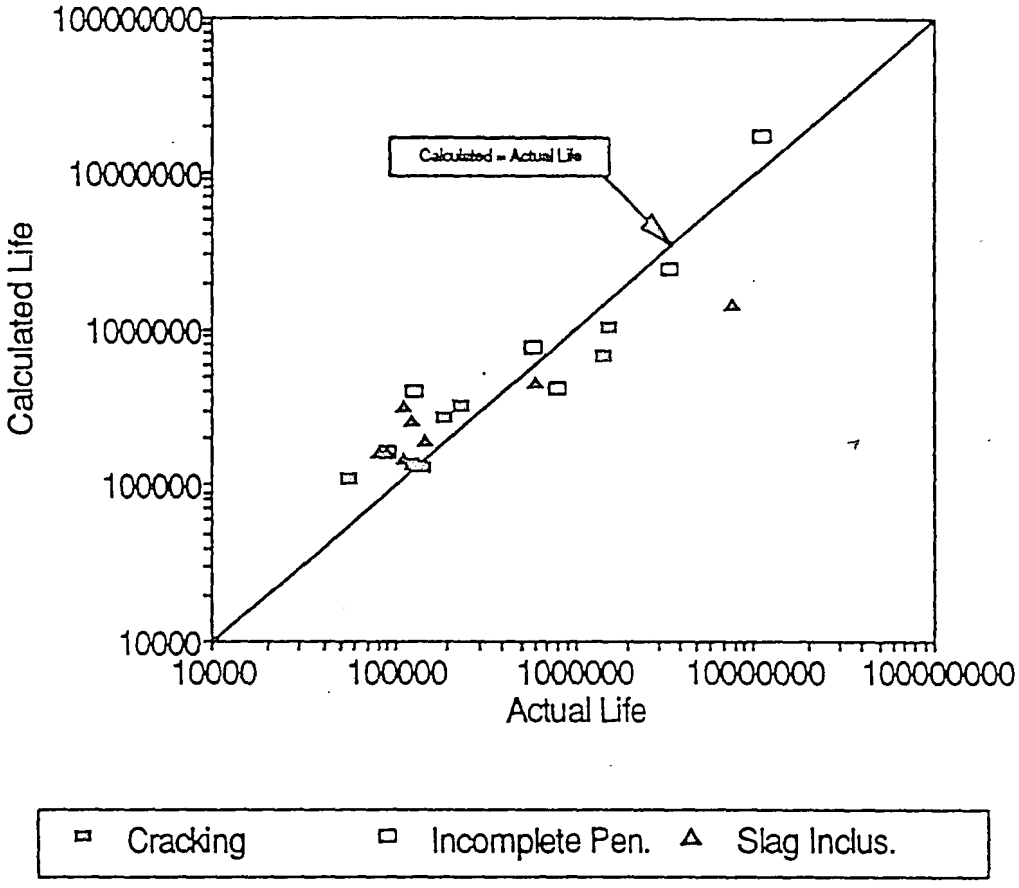


**Figure 37:** Fatigue Life of Transverse Groove Weld Calculated Using the Elliptical Model with Initial Discontinuity Size Determined From Actual Discontinuity Dimensions.

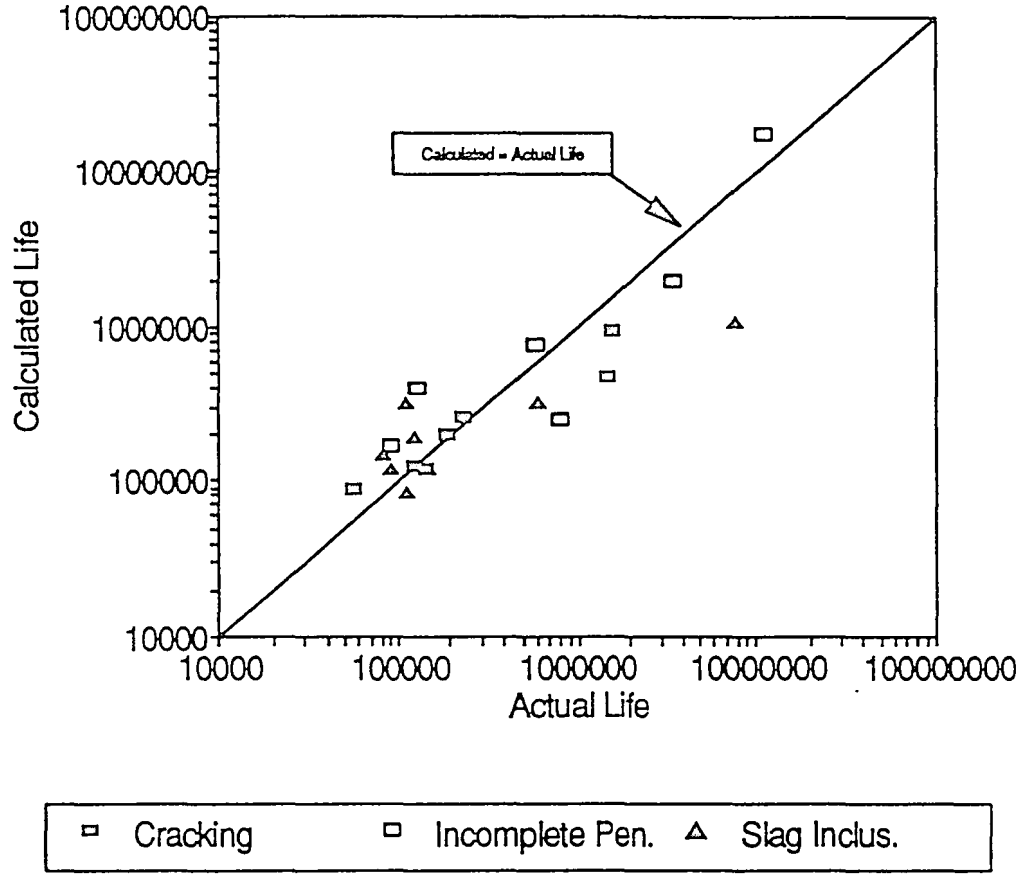


**Figure 38:** Fatigue Life of Transverse Groove Weld Calculated Using the Combination Model with Initial Discontinuity Size Determined From Actual Discontinuity Dimensions.

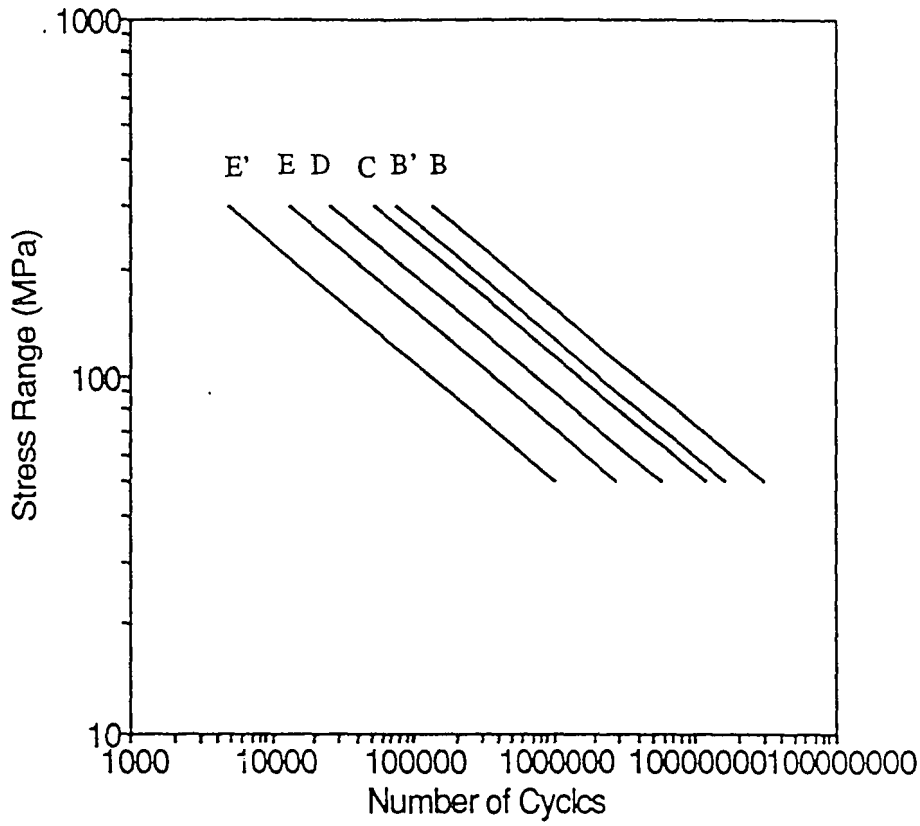


**Figure 39:** Quality Curves Derived Using the Circumscribed Radius Model and Corresponding to AASHTO Design Curves.

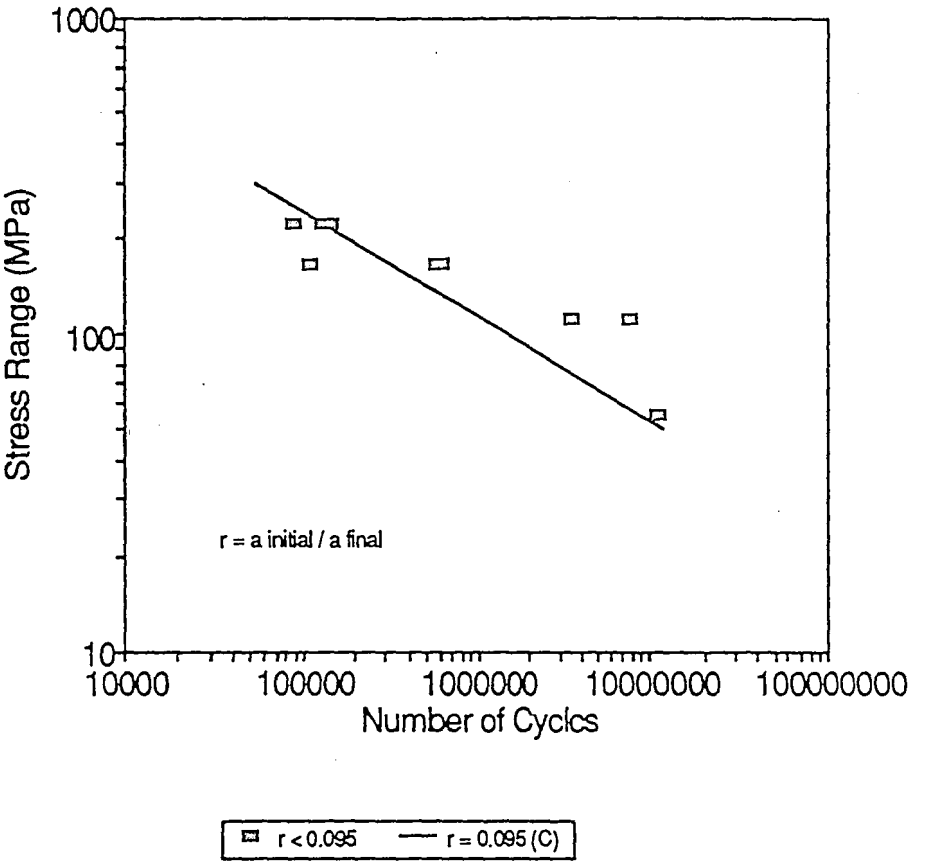


**Figure 40:** S-N Diagram Showing All Transverse Groove Weld Data With r < 0.095 (Quality Category < C) and r = 0.095 (Quality Curve C)

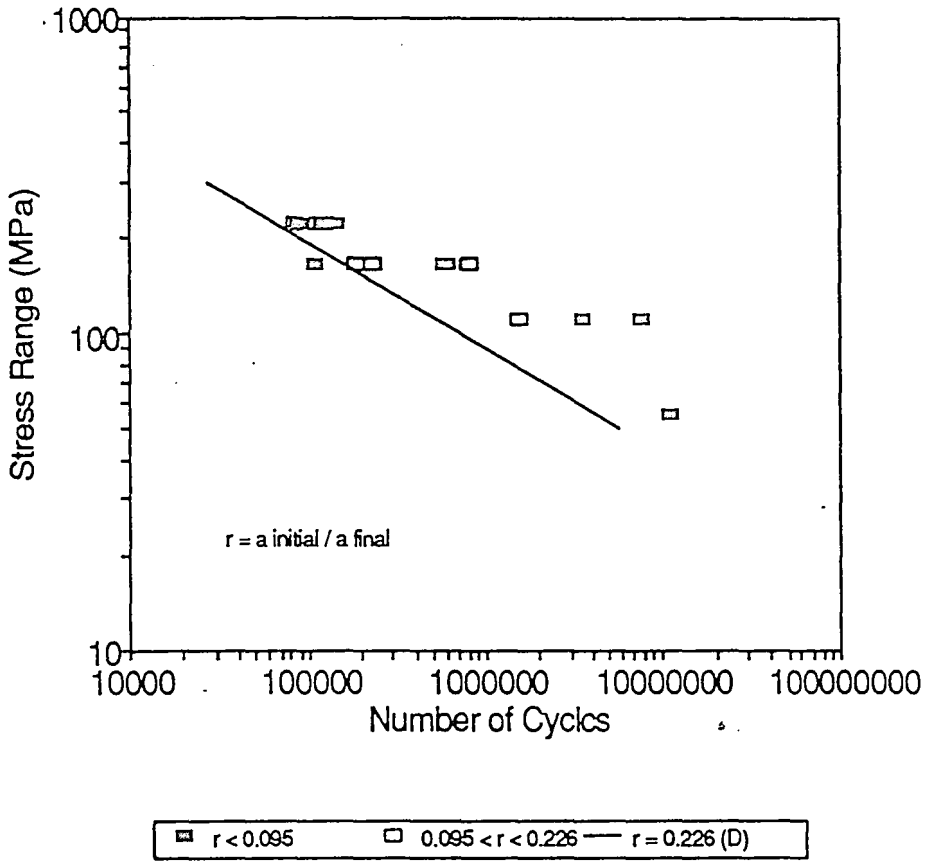


**Figure 41:** S-N Diagram Showing All Transverse Groove Weld Data With r < 0.226 (Quality Category < C and C- D) and r = 0.226 (Quality Curve D)

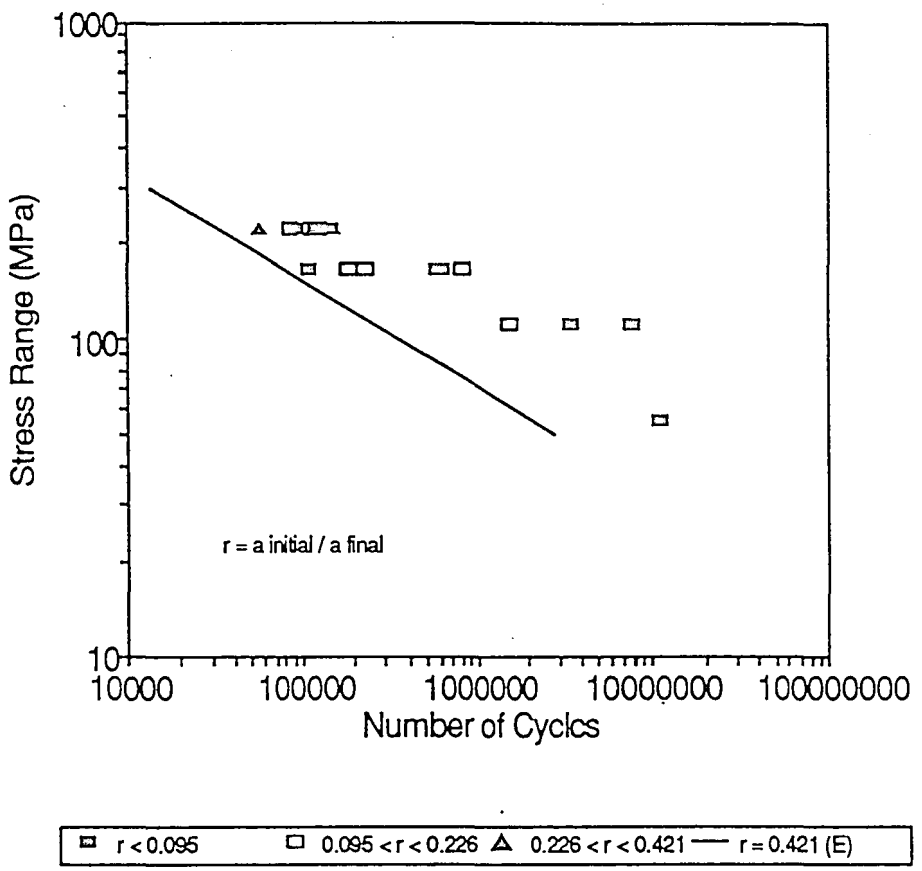


**Figure 42:** S-N Diagram Showing All Transverse Groove weld Data With $r < 0.421$ (Quality Category < C, C - D and D - E) and $r = 0.421$ (Quality Curve E)

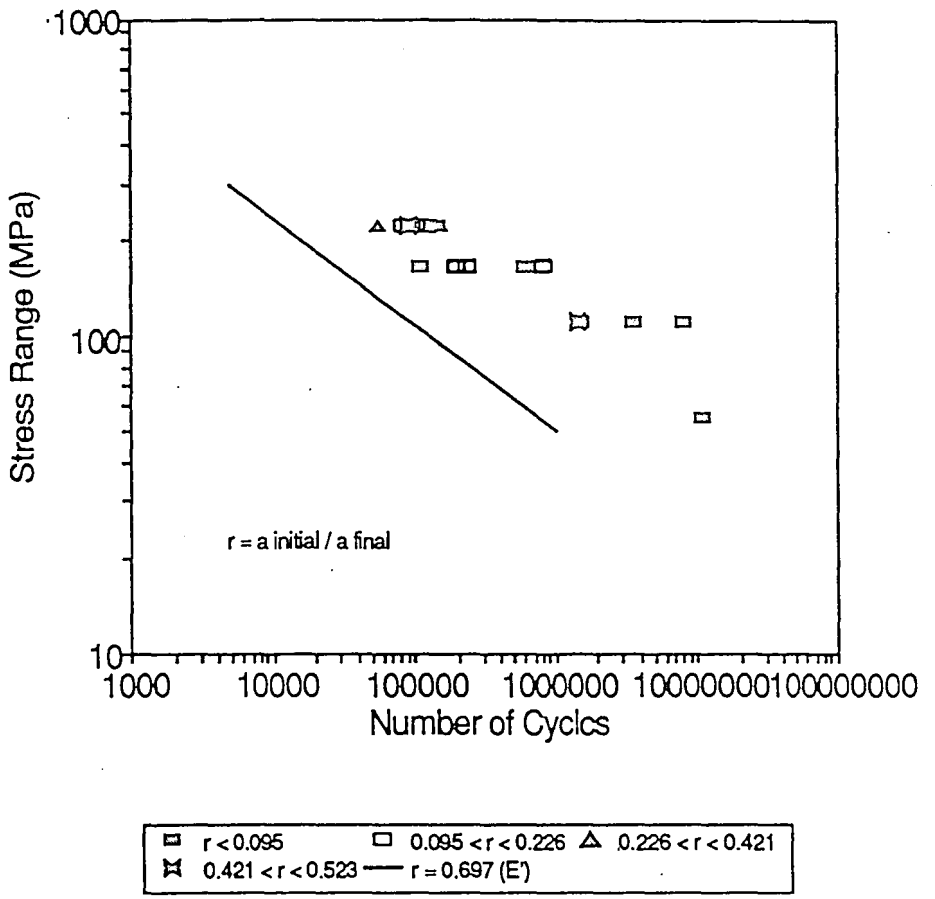


**Figure 43:** S-N Diagram Showing All Transverse Groove Weld Data With r < 0.523 (Quality Category < C, C - D, D - E and E - E') and r =0.697 (Quality Curve E')

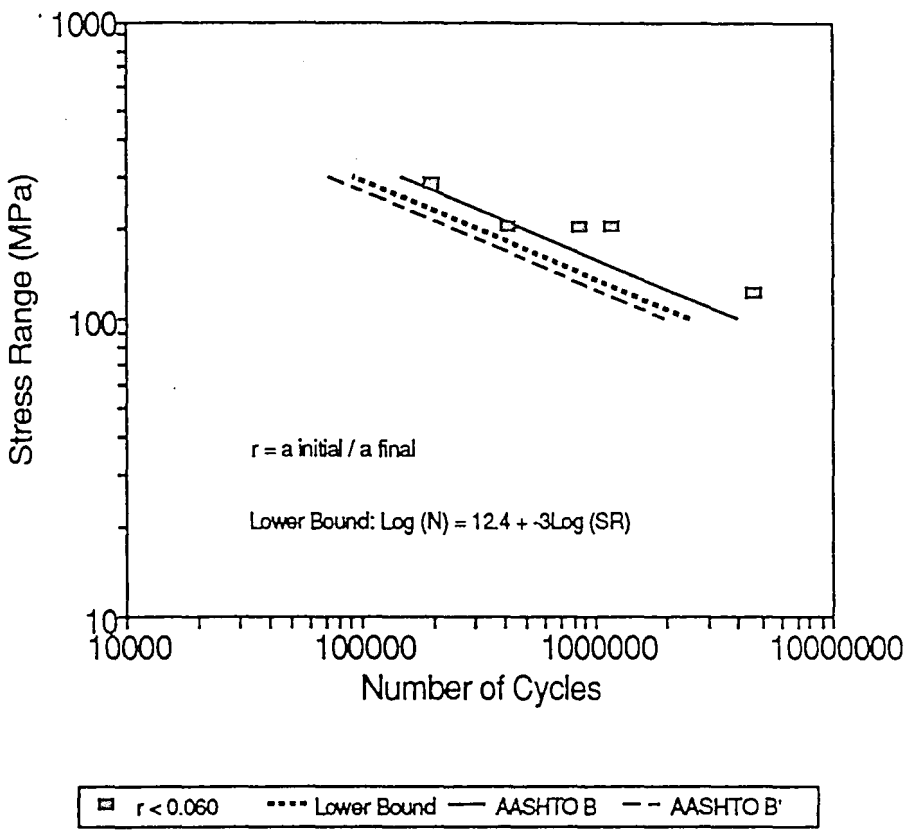


**Figure 44:** S-N Diagram Showing All Longitudinal Fillet Weld Data With r < 0.060 (Quality Category < B'), Lower 95% Confidence Bound and AASHTO Curves B and B'.

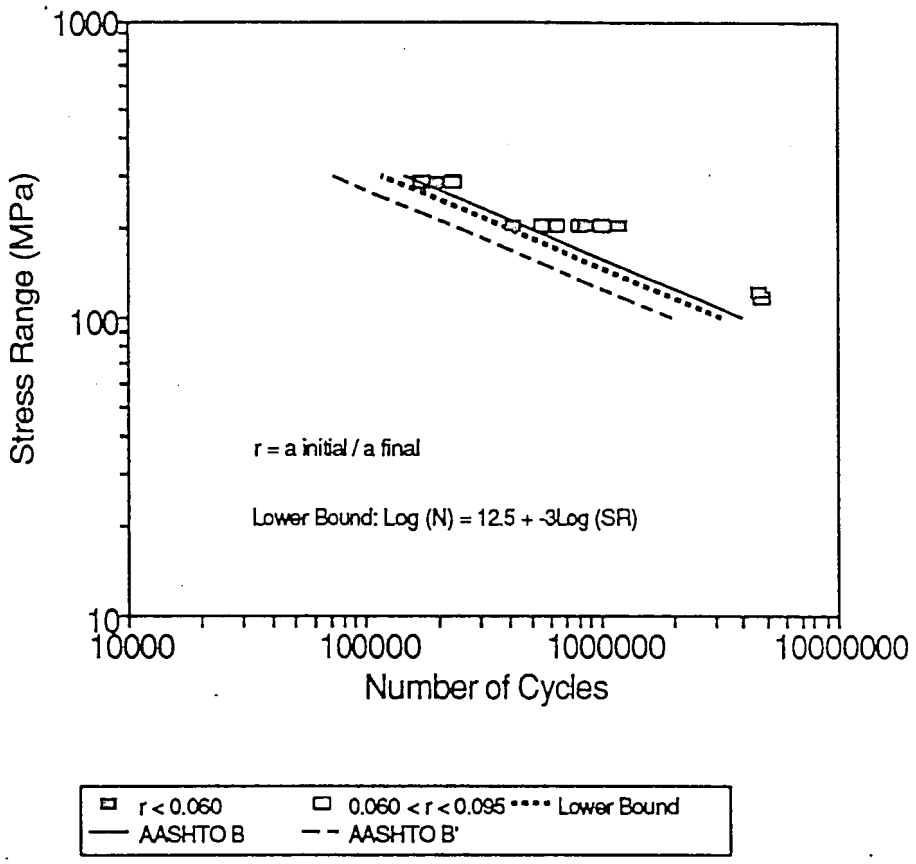


**Figure 45:** S-N Diagram Showing All Longitudinal Fillet Weld Data With r < 0.095 (Quality Category C), Lower 95% Confidence Bound and AASHTO Curves B and B'.

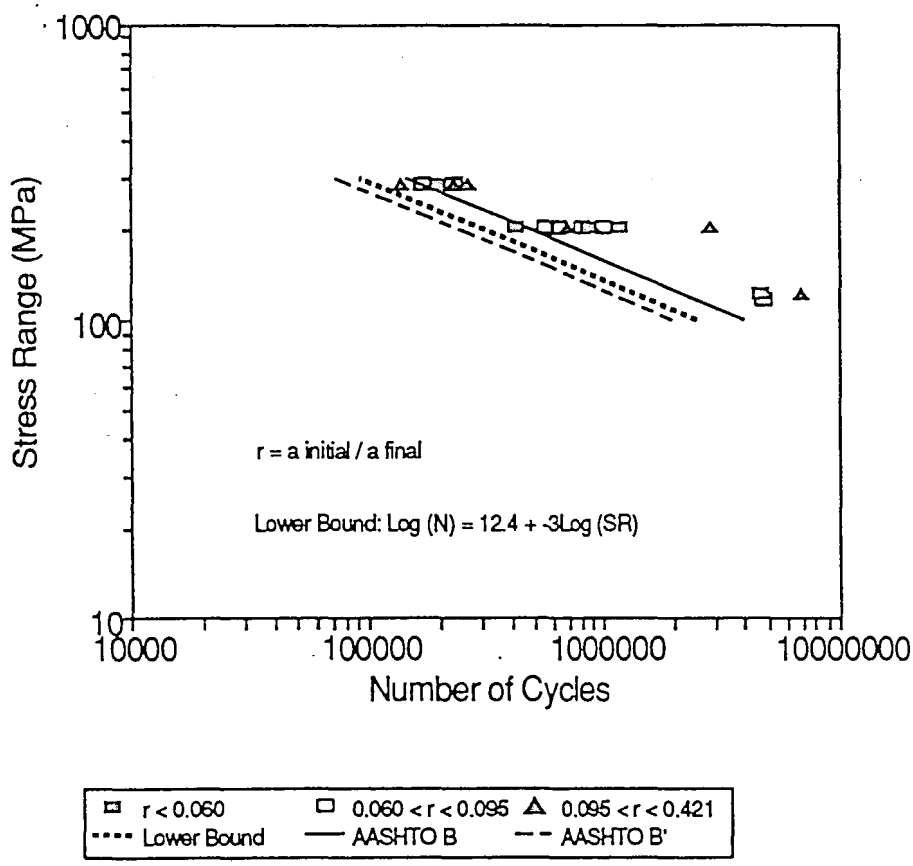


**Figure 46:** S-N Diagram Showing All Longitudinal Fillet Weld Data With r < 0.421 (Quality Category D+), Lower 95% Confidence Bound and AASHTO Curves B and B'.

# Vita

The author was born in Park Ridge, Illinois on August 13, 1969 to the parents of Mary H. and Dale P. Kober. He graduated from Highland Park High School in Highland Park, Illinois in June, 1987, and received a Bachelor of Science degree in Civil Engineering in May, 1991 from Washington University located in St. Louis, Missouri.

The author came to Lehigh in the Fall of 1991 where he presently works as a research assistant on the Fleet of the Future Program of the Engineering Research Center for Advanced Technology for Large Structural Systems (ATLSS).

END

OF

TITLE